Journal of
Materials Chemistry A

Materials for energy and sustainability

Accepted Manuscript

This article can be cited before page numbers have been issued, to do this please use: F. Sher, A. Hayward, A. El Guerraf, I. Ziani, H. Hrnji, E. Boškailo, B. Wang, A. Chupin and M. R. Nemanu, *J. Mater. Chem. A*, 2024, DOI: 10.1039/D4TA03877K.

ROYAL SOCIETY OF CHEMISTRY

rsc.li/materials-a

Advanced metal-organic frameworks for superior carbon capture, high-performance energy storage and environmental photocatalysis – A critical review

Farooq Sher[1,*], Anna Hayward[2], Abdelqader El Guerraf[3,4], Bohong Wang[5], Imane Ziani[4,6], Harun Hrnjić[4,7], Emina Boškailo[4,7], Alexander Chupin[8], Monica R. Nemțanu[9]

[1]*Department of Engineering, School of Science and Technology, Nottingham Trent University, Nottingham NG11 8NS, United Kingdom*

[2]*School of Mechanical, Aerospace and Automotive Engineering, Coventry University, Coventry CV1 5FB, United Kingdom*

[3]*Laboratory of Applied Chemistry and Environment, Faculty of Sciences and Technologies, Hassan First University, Settat 26002, Morocco*

[4]*International Society of Engineering Science and Technology, Nottingham, United Kingdom*

[5]*National and Local Joint Engineering Research Center of Harbor Oil and Gas Storage and Transportation Technology, Zhejiang Key Laboratory of Petrochemical Environmental Pollution Control, Zhejiang Ocean University, No. 1 Haida South Road, 316022, Zhoushan, P.R. China*

[6]*Physical Chemistry of Natural Substances and Process Research Team, Laboratory of Applied Chemistry and Environment (LCAE-CPSUNAP), Faculty of Sciences, Mohammed 1st University, Oujda 60000, Morocco*

[7]*Department of Chemistry, Faculty of Science, University of Sarajevo, Sarajevo 71000, Bosnia and Herzegovina*

[8]*Peoples' Friendship University of Russia (RUDN University), Moscow 117198, Russia*

[9]*Electron Accelerators Laboratory, National Institute for Laser, Plasma and Radiation Physics, 409 Atomiștilor Street, Bucharest-Măgurele, Romania*

***Corresponding author:**

Dr. F. Sher
Assistant Professor
Department of Engineering, School of Science and Technology
Nottingham Trent University
Nottingham
NG11 8NS
UK
E-mail address: Farooq.Sher@ntu.ac.uk
Tel.: +44 (0) 115 84 86679

View Article Online
DOI: 10.1039/D4TA03877K

Contents

View Article Online
DOI: 10.1039/D4TA03877K

Abstract

Metal-organic frameworks (MOFs) have emerged as a transformative class of materials, offering unprecedented versatility in applications ranging from energy storage to environmental remediation and photocatalysis. This groundbreaking review navigates the recent advancements in MOFs, positioning them against traditional materials to underscore their unique strength and potential drawbacks. In the context of energy storage, particularly within the realm of supercapacitors (SCs), MOF-based electrodes are evaluated for their superior specific capacitance (exceeding 1000 F/g), although these benefits are tempered by higher production cost. A comparative analysis with conventional activated carbon (AC) electrodes reveals MOFs' enhanced performance but also highlights cost as a significant barrier to widespread adoption. In carbon capture and storage (CCS), MOFs are contrasted with established liquid-amine technologies, with MOFs demonstrating environmental benefits, including the ability to achieve high-purity CO_2 collection (>99%), despite higher expenses. Similarly, in photocatalysis, while titanium dioxide remains dominant, MOFs are shown to offer competitive performance with a reduced environmental footprint, though cost considerations again play a decisive role. This review not only consolidates the current state of MOF research but also identifies critical gaps, particularly in cost-effectiveness, that must be addressed to enable broader application. The findings advocate for continued innovation in MOF synthesis and production, with an emphasis on achieving a balance between performance and affordability. In summary, this review highlights the pivotal role of MOFs in advancing material science and underscores the need for holistic approaches in material selection, with a forward-looking perspective on sustainable and economical production methods.

Keywords: Metal-organic frameworks; Activated carbon; Energy storage; Environmental remediation; Carbon capture and Photocatalysis.

View Article Online
DOI: 10.1039/D4TA03877K

1. Introduction

The dawn of the 21st century marked the emergence of metal-organic frameworks (MOFs); porous structures consisting of metal ions and organic linkers. Prior to MOFs, zeolites (aluminium silicate crystals) were the world's most porous materials [1]. However, MOFs have overcome zeolites' surface area by more than 100% in some cases. In addition to that, the structure of the cavities and the size of the pore in MOFs can be tailored as a function of metal ions, organic ligands, and synthesis conditions, and hence are thus amenable to engineering for targeted applications [2], which catalyses exponential growth in research on their applications [3]. Due to their unique architectures and chemical or physicochemical properties, MOFs remain in a class apart, with a wide reach of applications. Metal-containing nodes (SBUs) and organic linkers are used to create very porous structures, which typically have surface areas greater than 7000 m^2/g [4]. Control over topology, dimensionality, and stability can be achieved by selecting the right metal centers and organic ligands. For example, functional groups high in nitrogen can enhance CO_2 absorption; certain MOFs can attain up to 40 cc/g [5].

On the other hand, sensitivity to humidity and thermal instability create practical problems, as illustrated by ZIF-8, which swells at low pressure but phase transitions at higher pressures [6]. Synthesis conditions and metal-organic coordination bonds are key to the chemical stability and reactivity of MOFs; high-throughput computational screenings have identified MOFs with high gas adsorption capacities, such as methane storage up to 200 cm^3/cm^3 [4]. However, theoretical predictions do not often match real-world performance, suggesting that somehow models and real applications are detached from one another. It typically focuses on crystallinity and leaves out the other forms, such as amorphous or semi-crystalline forms, which might also hold special properties [7]. All this proves that there is a need to develop better characterization techniques and insight into structure-function interplay to further advance the application of MOFs in

View Article Online
DOI: 10.1039/D4TA03877K

carbon capture, energy storage, and environmental remediation. The historical development of MOFs shows the huge progress made in material science from exclusively inorganic or organic structures to hybrid systems possessing new properties [8]. The necessity of material that shows high porosity but custom architecture of the material developed during the late twentieth century marked the starting point for the development of MOF [9]. Early studies, and mostly those related to Prussian blue analogues, were the basis for the fast-growing interest in MOF research in the late 1980s [10]. The "node-and-spacer" approach, proposed by Richard Robson, enabled design of frameworks with well-defined coordination geometries and complex structures. MOFs, like HKUST-1 and MOF-5, developed in the late 1990s and early 2000s, represent advances in synthesizing large surface area materials that have high porosity and good crystallinity [11].

In response to escalating energy demands and intensifying environmental challenges, the development of advanced materials has become increasingly critical [12]. MOFs have emerged as a highly versatile class of materials, offering exceptional properties that hold the potential to revolutionize energy storage, environmental remediation, and photocatalysis [13]. As the global population continues to grow and conventional energy sources dwindle, innovative approaches to sustainable energy generation and environmental restoration are urgently needed. MOFs present a promising solution due to their structural flexibility, large surface area, and tunable properties. Energy storage, environmental remediation, and photocatalysis are key areas where advanced materials have the potential to drive transformative change. Traditional materials, such as metals, semiconductors, and polymers have historically played significant roles in these applications. However, these materials often face in efficiency, stability, and versatility. MOFs, with their exceptional characteristics, offer a promising alternative that could overcome these limitations. While MOFs are very promising, there are several serious technological problems

View Article Online
DOI: 10.1039/D4TA03877K

to be overcome. Their structural stability is the first and foremost problem. Such interactions of the proton and metal ion can result in degradation, and therefore most MOFs cannot be used for an extended period of time in these environments [14]. Improvement of stability includes high-valent metal ions and proper organic linkers, which generally decrease the diversity of possible MOFs. On the other hand, most MOFs require comparatively high temperature and pressure for synthesis and, therefore, are energy-consuming and expensive. In this regard, the search for alternative synthesis techniques, including the solvothermal and microwave methods, or recently mechanochemical methods, assumes the leading role among researchers to decrease the price of synthesis and increase scalability [15].

Moreover, their generally low electrical conductivity limits the broad use of MOFs in electrochemical applications. Strategies to enhance conductivity include embedding conductive material carbon-based compounds or using highly conjugated organic linkers; however, these add complexity and are more expensive to synthesize. For example, the MOF derivatives, such as TMCs, have been designed to enhance conductivity and improve structural stability [16]. One such example of improvement is the hybrid ZnS/MXene, which was reported to demonstrate improved electron transfer and ion adsorption capabilities due to uniform anchoring of ZnS nanodots onto the MXene nanosheets. The incorporation of a few metals into one MOF structure has also shown some bright prospects in enhancing electrochemical performance but adds more complications in terms of synthesis and scalability. For instance, sequential chemical etching and sulfurization in the preparation of Zn-Co-S rhombic dodecahedral cages showed enhanced specific capacitance because they hold a double-shelled structure [17]. Environmental degradation stands as one of the foremost challenges of the 21st century. Increased awareness of global warming, coupled with concerted efforts by governments and societies, is driving research into environmental pollution mitigation. The United Nations has specified a series of

View Article Online
DOI: 10.1039/D4TA03877K

sustainable development goals, showcasing this assertion [18]. Recent research suggests that MOFs demonstrate tremendous potential in capturing and detoxifying environmental toxins across various media, such as water, air, and soil [19]. The increasing concentration of atmospheric CO_2, primarily driven by the combustion of fossil fuels since the industrial revolution, has been a major contributor to anthropogenic global warming [18]. The atmospheric concentration of CO_2 has increased from 280 ppm in 1962 to 400 ppm in 2015 [20], a concerning trend due to its links to global warming and associated environmental degradation, as well as potential adverse health effects [19]. MOFs have shown significant potential in this regard, particularly in carbon capture and storage (CCS) technologies. Their ability to selectively adsorb CO_2 from the atmosphere makes them a viable candidate for reducing greenhouse gas emissions [21].

In the realm of energy storage, MOFs' are being explored for their application in both supercapacitors (SCs) and metal-ion batteries. MOFs can serve two main roles in these energy storage devices: Primarily, they can function as direct electrode materials with modifiable particle and pore dimensions. Secondly, they can serve as templates and precursors for producing porous carbons and metal oxides. The resulting porous carbons and metal oxides maintain the extensive surface area and highly porous structure of the MOF precursors, making them ideal for implementation in electrical double-layer supercapacitors (EDLCs) and pseudocapacitors [22]. Moreover, MOFs have garnered attention in photocatalysis owing to their distinctive properties. Photocatalysis entails harnessing light energy to propel chemical reactions [23], and MOFs' extensive surface area and porosity provide numerous active sites for catalytic reactions. Researchers have incorporated various photocatalytic components, such as metal nanoparticles or organic dyes, into MOF structures to enhance their photocatalytic performance. MOFs can serve as photocatalysts themselves or as platforms to support other

View Article Online
DOI: 10.1039/D4TA03877K

catalytic materials. The tunable nature of MOFs allows researchers to modify their electronic and optical properties, influencing their efficiency in light absorption and charge separation critical factors in photocatalytic processes.

In this comprehensive and groundbreaking review, the report embarks on a pioneering journey to assess the comparative advantages of MOFs over conventional materials. Delving into the realm of energy storage, it investigates how MOFs can potentially revolutionize energy storage technologies, including supercapacitors and metal-ion batteries, due to their exceptionally high surface area, tunable electronic properties, and facile ion diffusion pathways. This new approach to energy storage could enable previously unattainable levels of efficiency and performance to be achieved. In the context of environmental challenges, the exploration focuses on a remarkable novelty, namely the way MOFs display an unprecedented affinity for carbon dioxide capture. This discovery offers a compelling and revolutionary alternative to conventional adsorbents, with the potential to significantly mitigate greenhouse gas emissions. Furthermore, in the domain of photocatalysis, MOFs have showcased a transformative capacity to harness solar energy for driving chemical reactions with unmatched efficiency, representing a major leap forward in sustainable energy conversion technologies.

This review tackles these issues by providing an in-depth analysis of case studies, experimental results, and theoretical insights to illuminate the merits and limitations of MOFs compared to conventional materials across three key applications: energy storage, carbon capture, and photocatalysis. Tables summarizing the advantages and disadvantages of both conventional and MOF materials are presented for each application, with a focus on performance, environmental impact, and cost-effectiveness. Each broad factor receives a relative percentage weighting based on importance, with the most critical factor assigned the highest percentage. Sub-factors

View Article Online
DOI: 10.1039/D4TA03877K

within each category are also identified based on the literature, assigning them scores out of 3 (3 correlating to high importance). After determining the weightings, both materials are evaluated using a comparison matrix for each factor, using a scale of 1 to 5 (1 very bad, 2 bad, 3 suitable, 4 good, and 5 very good). The resulting scores allow a comparison of MOFs and conventional materials for each of the three applications, helping identify which material offers the most benefits based on the identified factors. Such a systematic approach will ensure that all aspects are covered and that clear, actionable insights into practical benefits of MOFs in addressing technological challenges in energy storage, carbon capture, and photocatalysis are delivered. **Fig. 1** summarizes the methodology followed throughout this groundbreaking literature review.

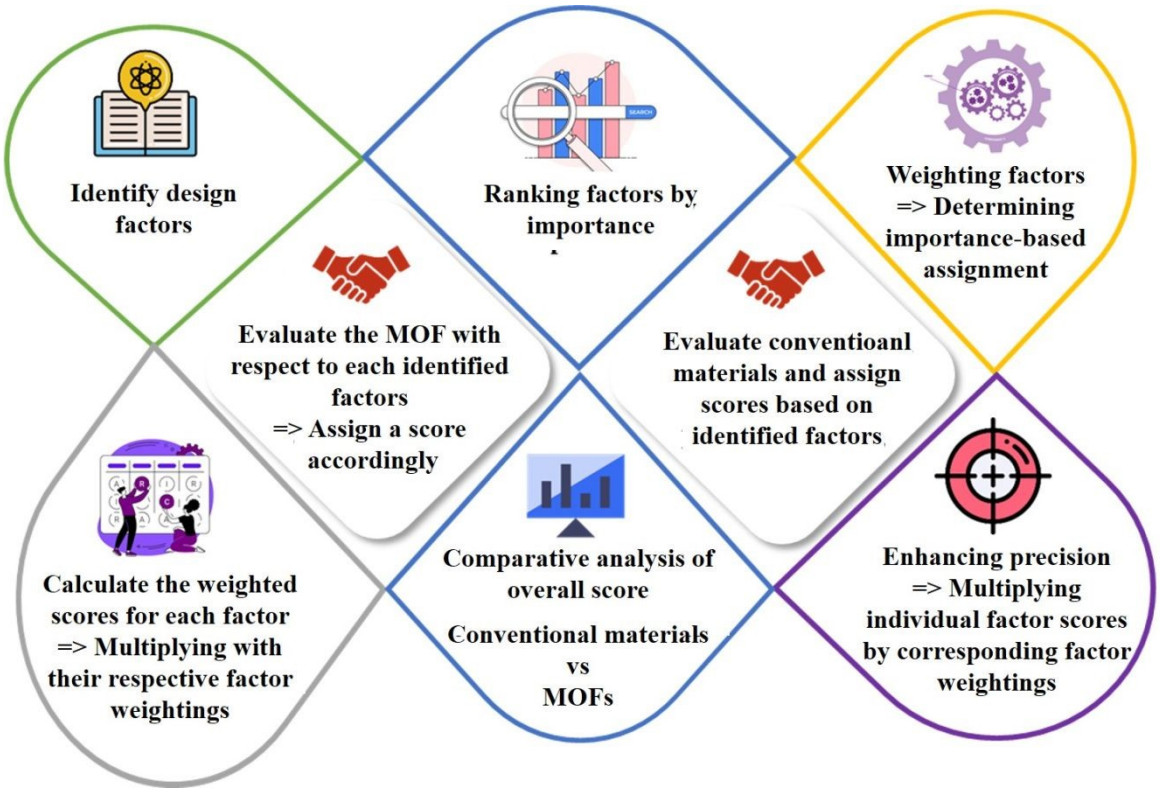

Fig. 1. Diagram explaining the adopted methodology for the present literature review. A systematic comparison matrix is employed to assess the relative benefits of MOFs, offering clear, actionable insights into their potential as a transformative material in critical fields.

View Article Online
DOI: 10.1039/D4TA03877K

2. Porous MOF and conventional materials for carbon capture

The argument presented by Mukherjee et al. [18] emphasizes humanity's reliance on gas as a critical component of energy and industrial processes. They contend that liquid fuels and feedstocks in the chemical industry have been largely replaced by gases. However, this viewpoint is challenged by the research conducted by Furukawa et al. [24] which shows a steady increase in all fossil fuels, both sources agree on the general trend of increasing CO_2 levels and their contribution to global warming and consequential environmental degradation. A sorbent's CO_2 selectivity is determined by comparing how much CO2 it can absorb to another gas while meeting certain predetermined parameters [18]. In the examination of a sorbent employed for post-combustion carbon capture, selectivity versus nitrogen (SCN) holds significant relevance. Selectivity is crucial as it impacts both the purity of the captured CO_2 and the concentration of CO_2 in the effluent gas discharged into the atmosphere. Mukherjee and colleagues [18] also suggest that increasing the SCN of a sorbent by five-fold could significantly reduce the cost of C-capture. Other important factors that influence sorbent selection for C-capture include stability, working capacity, regenerability and feasibility of scale-up.

2.1 Conventional liquid alkanolamine in carbon capture

For over half a century, liquid amine technology has remained at the forefront of carbon capture and storage (CCS) technologies [18]. This method of bulk-scale carbon capture operates through chemisorption, involving chemical reactions between CO_2 and the sorbent material. Originating in the 1930s, these processes were initially developed, and since the 1950s, they have been employed by gas-treating plants for the removal of acid gases like CO_2 and H_2S [19,25]onsequently, liquid amine processes are frequently recognized as the most mature CCS method and boast a high Technology Readiness Level (TRL) of 9 [25,26]. In two commercial-scale facilities housed within coal-fired power plants, post-combustion liquid amine CCS technology had been successfully installed as of 2018 [26]. The post-combustion liquid-amine CCS process

View Article Online
DOI: 10.1039/D4TA03877K

(**Fig. 2**(a)) involves exposing the flue gas stream to an aqueous amine solution, commonly a member of the alkanolamine class, typically a 20–30 wt% aqueous monoethanolamine (MEA) [27]. Subsequently, the amine undergoes a reaction with CO_2 in the flue gases, resulting in the formation of carbamates or bicarbonate products, which can then be separated and removed. The utilization of liquid amines is based on their capacity to achieve significant levels of purification and separation through the chemisorption process [18].

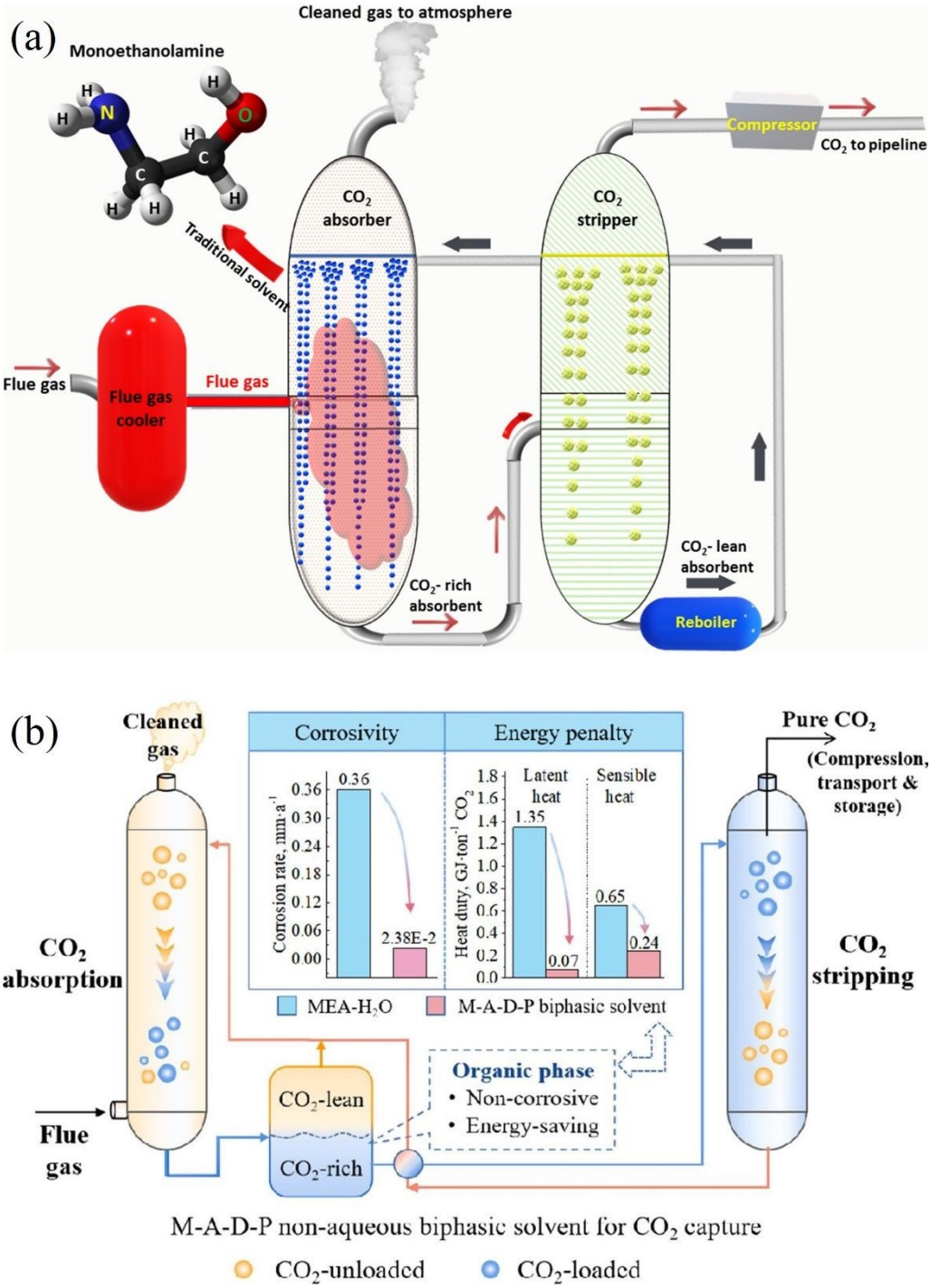

Fig. 2. (a) Post-combustion technology involves cooling hot flue gas before directing it to an absorber unit that typically contains a monoethanolamine solvent as the traditional sorbent. The CO_2-rich absorbent is then sent to a stripper unit to release the CO_2 gas, while the CO_2-lean absorbent is recycled back to the absorber unit. Finally, the pure CO_2 is compressed and dehydrated for transport via pipelines and for storage purposes. Adopted from Ref. [28] with permission. (b) A schematic illustration of a reactor containing a nonaqueous monoethanolamine-based biphasic solvent for reduced energy penalty and corrosion of carbon dioxide capture. Adopted from Ref. [29] with permission.

Monoethanolamine (MEA) offers several advantages, such as a substantial CO_2-carrying capacity, biodegradability, and rapid adsorption rates [26,27]. Additionally, it is well-suited for carbon capture applications with low CO_2 partial pressures. Because of this, MEA has become the industry standard for carbon capture amines despite having modest degrees of toxicity and oxidative and thermal degradation [26]. In the context of standard post-combustion flue gas CO_2 separation, employing a 30 wt% MEA solution at pressures ranging from 10–15 kPa, a temperature of 40 °C, and targeting a 90% CO_2 removal rate, it is typically estimated that a reboiler would necessitate approximately 3.6–4.0 GJ per tonne of captured CO_2 [26]. This value has been verified by a number of small- and medium-sized pilot studies [30]. While it's important to acknowledge that reducing reboiler energy is just one of several performance considerations, it is often regarded as a primary focus in the realm of chemical sorbent research. Liquid amines offer a notable advantage for CCS due to their often-high selectivity. Liquid amine CCS technology does have several disadvantages, though. Chemisorbents form strong covalent connections, in contrast to physisorbents, which work through van der Waals interactions [18]. Consequently, the regeneration of sorbents in the case of chemisorbents demands more energy, resulting in a larger energy footprint. Furthermore, in situations with low CO_2 concentrations, the kinetics of the chemisorption process are likely to be sluggish, which is less than ideal for CCS.

View Article Online
DOI: 10.1039/D4TA03877K

In a study conducted by Li et al. [29], a novel approach to advance CO_2 capture technology aims to reduce energy penalties and mitigate equipment corrosion simultaneously (**Fig. 2**(b)). A new biphasic solvent system was developed for carbon dioxide (CO_2) capture, comprising monoethanolamine (MEA), 2-amino-2-methyl-1-propanol (AMP), dimethyl sulfoxide (DMSO), and N,N,N',N",N"-pentamethyldiethylenetriamine (PMDETA). Performance evaluation revealed that the optimized solvent achieved a high CO_2 loading of 0.88 mol/mol, with 95.3% of absorbed CO_2 stored in the rich phase, occupying only 56.8% of the total volume. Both MEA and AMP could absorb CO_2 to generate mostly carbamic acid species, according to 13C nuclear magnetic resonance (NMR) studies and quantum chemical calculations. Sufficient mutual solubility was guaranteed by hydrogen bonding with the polar DMSO. Only the CO_2-rich phase needed to regenerate since the less polar PMDETA remained isolated and caused phase separation. The M-A-D-P biphasic solvent dramatically reduced sensible heat and vaporisation heat by 63.1% and 94.8%, respectively, when compared to the MEA benchmark. Corrosion tests demonstrated that M-A-D-P exhibited virtually no corrosion to carbon steel, outperforming the MEA solution. Although liquid-amine technologies have proven effective as "wet scrubbers", their industrial-scale deployment has been hindered by several drawbacks. Grande et al. [31], in their report, emphasize the need to advance CCS technology beyond liquid amine approaches to ensure sustainability, primarily due to the substantial regeneration energy requirements associated with liquid amine-based wet scrubbers, which can exceed 140 °C. The increased energy requirements result from the high stability of the carbamate/bicarbonate species generated during the amine-CO_2 reaction [32]. It is worth noting that the energy required to reverse an amine-CO_2 reaction varies depending on the specific amine used. Ghosh et al. [19] elucidate that this discrepancy is a consequence of bicarbonates demanding less energy compared to carbamates when regenerating the constituent amine.

View Article Online
DOI: 10.1039/D4TA03877K

Various additional drawbacks associated with liquid-amine technologies have been also highlighted [31]. Equipment requirements pose limitations as it is prone to corrosion over time, and retrofitting can prove challenging due to its substantial size. This perspective is substantiated by Vega et al. [25], who propose a potential solution to mitigate equipment corrosion through the use of corrosion-resistant materials and inhibitors, albeit at an added cost. Vericella et al. [27]ggest an alternative approach by proposing the microencapsulation of the amine. This approach seeks to avoid direct contact between the amine and the equipment, as well as effluent gases, potentially mitigating equipment corrosion and decreasing evaporative losses. Moreover, it has been reported by several sources that liquid amines are susceptible to deterioration and breakdown when they come into contact with dust, HCL, HF, SOx, NOx, and oxygen, among other contaminants [25]. Concerns have been expressed regarding the elevated volatility and limited stability of liquid amines. As per the findings of Williams and their research team [33], conducting multiple capture-release cycles leads to notable losses of amine sorbent, subsequently causing a decrease in efficiency and performance. The collective impact of these factors can also negatively affect the overall efficiency of a power plant utilizing post-combustion liquid amine carbon capture and storage technology. A recent report attributed a 30–40% reduction in the overall efficiency of power plants to the difficulties associated with implementing CCS technology [19].

Furthermore, an associated cost was estimated to range from €70 to €100 per ton for this reduction in efficiency. Concerns have been also raised regarding the industrial scalability of liquid-amine technology, with certain publications questioning its suitability for large-scale implementation. Vega et al. [25] contend that, until the CO_2 capacity can be expanded from its present 800 tons per day to the necessary 8000 tons per day, the technology may not be suitable for large-scale CO_2 emission mitigation on an industrial level. Additionally, one of the most

View Article Online
DOI: 10.1039/D4TA03877K

significant challenges associated with liquid-amine processes is their restricted scope for performance enhancement [18]. Much of the existing literature underscores the significance of creating novel technologies with enhanced capabilities to supplant current liquid-amine processes. Conversely, the Energy Technologies Institute (ETI) argues that liquid-amine technologies still offer opportunities for future advancements [34]. They cite the development progress of bi-phasic systems as evidence of this potential.

Moreover, the environmental impact of amines has raised significant concerns. Williams et al. [33] argue that, owing to their highly toxic nature, amines are unsuitable for direct air capture (DAC) applications and could potentially pose an environmental threat if employed in such contexts. Vericella et al. [27] corroborate this viewpoint, noting that the commonly used amine for CCS, monoethanolamine (MEA), generates toxic degradation byproducts. Furthermore, there are apprehensions that the decrease in power plant efficiency resulting from the presence of liquid-amine post-combustion technologies may partially offset the technology's advantages [18]. Another foremost issue with liquid-amine CCS is the high cost; with some sources claiming the capture of 1 ton of CO_2 costs around 50–100 USD (as a conservative estimate) [18]. Contrarily, an earlier report from 2015 provided an estimate of the maximum cost of post-combustion amine CCS as \$110/tCO_2 [35]. As a result, numerous sources contend that the technology is not yet commercially feasible for widespread use. Another problem is the extra expense associated with the post-combustion C-capture system because it needs electricity to operate. Liquid-amine CCS (L-A CCS) technology typically causes a large rise in capital costs along with a decrease in power plant efficiency [34].

There are indications that beyond 2030, continuous technological advancements may lead to cost reductions in liquid-amine technology, ultimately enhancing its viability for large-scale implementation. Developers in the US, Canada, and the UK have committed to sharing publicly

View Article Online
DOI: 10.1039/D4TA03877K

all knowledge, data, and designs related to CCS technology, which should foster innovation. According to the ETI, larger projects will enable the exploitation of economies of scale, which will lead to additional cost reductions [34]. One recommended approach is the sequential deployment of existing C-capture technologies in 3 or more full-scale power plants. The ETI suggests that sequential deployments will result in a reduction in risk [34]. Reduced finance costs, larger scale, and infrastructure sharing all work together to potentially cut the cost of output energy by about 45%. Because it might result in more affordable financing solutions, risk minimisation reduces financing costs.

2.2 Metal-organic frameworks in carbon capture

2.2.1 Performance and challenges

Solid sorbents such as MOFs are exciting candidates for low-temperature C-capture [32]. Their intrinsic properties such as their high porosity and their customizable chemistry provide the potential to tune MOFs for improved CO_2 uptake capacity and selectivity [26]. Despite their benefits, MOF sorbents face several hurdles. It is generally agreed that the thermal conductivity of sorbents affects the C-capture operation and regeneration process's cost and cycle time [36]. MOFs, however, tend to have poor thermal conductivities (at T = 25 °C, the thermal conductivity of MOF-5 single crystal stands at a mere 0.32 W/m K) [37]. The enhancement of MOFs' thermal conductivity is presently the subject of relatively few studies, thus perhaps more research in this field is warranted. Opt-UiO-66(Zr)-$(OH)_2$ (2.50 mmol/g) is one of the best-performing pristine MOFs [38]. This MOF is both water-stable and shows a CO_2 uptake higher than that of MEA [38]. Based on their functional characteristics, modified metal oxide fragments (MOFs) for C-capture can be broadly categorised into three groups: MOFs with amine-functionalized sites (AFSs), unsaturated metal centres (UMCs), and saturated metal centres (SMCs)[18]. Reports suggest that, while able to provide a significantly improved working capacity, the UMC-rich MOFs with the highest capacities suffer from modest selectivity versus

View Article Online
DOI: 10.1039/D4TA03877K

nitrogen (SCN) [18]. UMCs can be generated by removing the solvent molecules responsible for the partially coordinated metal atoms in some MOFs. This can be done through heating the material or vacuuming. These UMCs exhibit an excellent CO_2 affinity, and can therefore be used to enhance the capture capacity of a MOF at low pressures [39].

A new bimetallic MOF, functionalized with pyrazine and used in combination with polysulfone (PSf), was employed to create a mixed matrix membrane (**Fig. 3(A)**) [40]. This innovative membrane demonstrated adaptable interfaces facilitated by the incorporation of the interfacial plasticizer, polyethylene glycol (PEG). The inclusion of the MOF filler notably boosted the CO_2 capture capacity of both pristine PSf membranes and PSf/PEG blend membranes. Specifically, with the PSf/PEG/Pyrazine-MOF membrane, the CO_2 permeability rose dramatically from 6.82 Barrer for the pure PSf membrane to 17.13 Barrer [40]. Bhatt et al. [41] detailed the development of a hydrolytically stable fluorinated metal-organic framework (MOF) referred to as NbOFFIVE-1-Ni. Remarkably, this synthesized MOF exhibits significant CO_2 adsorption capacities, measuring approximately 1.3 mmol/g gravimetrically and 51.4 cm^3 (STP) cm^3 volumetrically when exposed to 400 ppm of CO_2 at 298 K (**Fig. 3(B)**). Furthermore, a methyl-functionalized aluminium-based MOF (ZJU-620(Al)) with remarkable chemical-thermal stability and a high specific surface area of 1347 m^2/g has been recently developed [42]. This MOF has emerged as a highly promising candidate for CO_2 capture due to its exceptional recyclability and impressive capacity, reaching up to 4.25 mmol/g at 298 K and 1 atm. CO_2 molecules are primarily captured within two distinct sites. The first site (I) is situated in close proximity to the AlO_6 clusters, while the second site (II) is positioned between two parallel benzene rings, separated by a distance of 6.64 Å (**Fig. 3(C)**). While MOF technology has held great promise to date, the performance data from **Fig. 3(D)** raises some deeply troubling questions about realistic applicability [43]. Specifically, it constructs bond dissociation energy

from the noisy-prone measurements of emulated hardware under two error mitigation schemes: state preparation and measurement (SPAM) error mitigation and post-measurement symmetry verification (PMSV). A variational outcome of up to ±1 mHa based on noise alone illustrates the practical challenges in reliably predicting MOF performance under more realistic conditions [43].

View Article Online
DOI: 10.1039/D4TA03877K

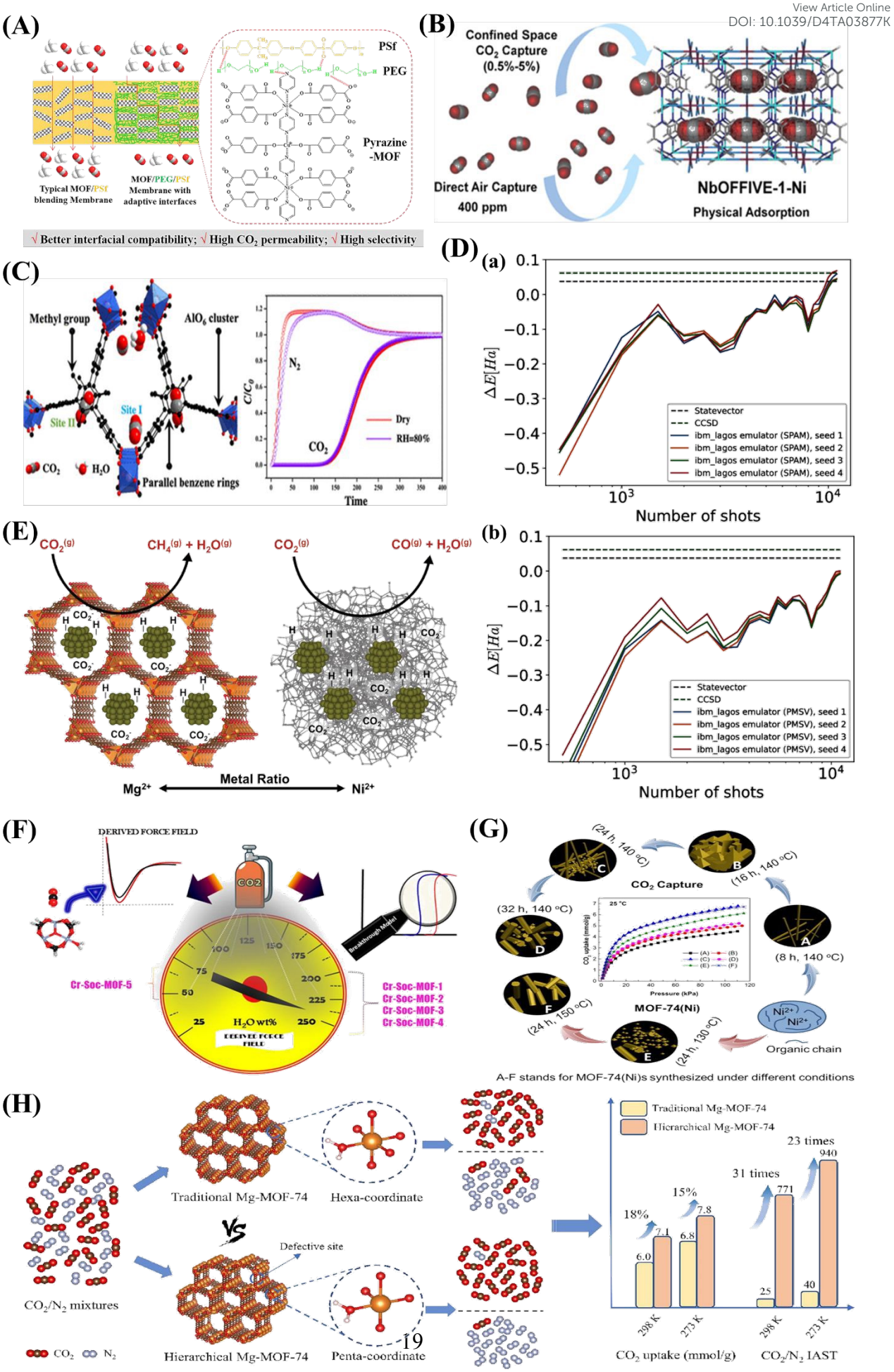

Fig. 3. (A) An illustration of the interactions and interfacial structure of the PEG/PSf mixed matrix membrane with pyrazine-MOF incorporation for the separation of CO_2 from CH_4. Adopted from Ref. [40] with permission. (B) Fluorinated MOF, NbOFFIVE-1-Ni, for trace CO_2 removal and air capture. Adopted from Ref. [41] with permission. (C) Methyl-functionalized Al-based MOF ZJU-620(Al) for CO_2 capture. The two main types of sites where CO_2 molecules are adsorbed are Site I, which is close to the AlO_6 clusters, and Site II, which is between two parallel benzene rings. Adopted from Ref. [42] with permission. (D) Calculate bond dissociation energy using noisy emulated hardware data for 2 noise rates. Demonstrating two error mitigation approaches: (a) state preparation and measurement (SPAM) error mitigation, and (b) post-measurement symmetry verification (PMSV). Both approaches use the same set of 4 randomization seeds results in order of the number of measurement shots. Adopted from Ref. [43] with permission. (E) Catalysts with MOF-74 templating comprising mixed metals for effective carbon dioxide capture and methanation. The resultant support material influences a qualitative CO_2 hydrogenation reaction pathway involving the reverse water-gas shift and Sabatier reactions. Adopted from Ref. [44] with permission. (F) Coordinatively unsaturated MOF with square octahedral (Soc) topology (Cr-Soc-MOF) for super-adsorption of CO_2 under humid conditions. Adopted from Ref. [45] with permission. (G) MOF-74(Ni) synthesized under different conditions for carbon capture and storage. Adopted from Ref. [46] with permission. (H) A schematic diagram showing how defect-rich hierarchical porous Mg-MOF-74 and conventional Mg-MOF-74 are prepared differently and their application in CO_2 adsorption. Adopted from Ref. [47] with permission.

Mg-MOF-74 is often used as a benchmark for other physisorbents, as it has an excellent CO_2 adsorption capacity in dry conditions at low pressures (5.5 mmol/g at 0.15 bar, 313 K [18,48] and up to 8 mmol/g at 1 bar and 298 K [39]). The high density of UMCs is largely responsible for the remarkable CO2 uptake values. It is created by reacting 2,5-dihydroxyterephthalic acid with magnesium metal salts, which produces a large amount of UMCs within the MOFs framework. Bahamon and associates compare a number of MOFs to zeolites in their report [49]. Because Mg-MOF-74 performs well in TSA operating settings, they present it as having good potential for TSA separation. According to their findings, Mg-MOF-74 outperformed zeolite 13X, a zeolite that is frequently utilised [49]. In the same context, a mixed-metal metal-organic framework (MOF) referred to as NiMg-MOF-74 was utilized as a template to achieve the even distribution of small nickel nanoclusters within the native MOF framework [44]. Through the adjustment of the Ni-to-Mg ratio within the initial MOF, it is possible to modulate both the available surface area and crystallinity after thermal treatment (**Fig. 3(E)**). This, in turn, has an impact on the capacity for CO_2 adsorption and the selectivity of hydrogenation.

View Article Online
DOI: 10.1039/D4TA03877K

On the other hand, critics have often pointed out the poor performance of MOFs in gas separation, particularly under humid conditions. Palakkal et al. [45] examined coordinatively unsaturated MOF (CUS-MOF) with square octahedral (Soc) topology. The research encompassed examinations of both co-adsorption (CO_2/N_2) and single-component (CO_2, N_2) adsorption with moisture at 298 K and pressures between 0 and 10 bar. The authors focused on five different Cr-Soc-MOFs, which exhibited experimentally established iso-structural topologies but differed in polynuclear aromatic ring size and N-heteroatom content within their pore walls (**Fig. 3(F)**). Remarkably, Cr-Soc-MOFs with larger pore volumes exhibited CO_2 uptake ranging from 23 to 35% by weight, with selectivity levels ranging from 20 to 50%, even up to 70% relative humidity (RH) [45]. A Ni-based metal–organic framework, MOF-74(Ni), was synthesized using a straightforward condensation reflux method [46]. By adjusting the synthesis duration at different temperatures, both the structure and CO_2 adsorption isosteric heat of MOF-74(Ni) could be customized (**Fig. 3(G)**). After being produced at 140 °C for 24 hours, the optimised MOF-74(Ni)-24-140 demonstrated remarkable CO_2 adsorption capacity, attaining 8.29/6.61 mmol/g at 273/298 K with a pressure of 1 bar. This capacity surpassed that of previously reported MOF-74-Ni, UTSA-16, and DA-CMP-1 under similar conditions by factors of 2.0/2.1, 1.5/1.6, and 3.6/4.9, respectively. An et al. [47] reported the synthesis of a defect-rich hierarchical porous Mg-MOF-74 (**Fig. 3(H)**). The defect-rich hierarchical porous Mg-MOF-74 exhibits an increased adsorption enthalpy of CO_2 at zero load, rising from 36 to 46 kJ/mol compared to conventional Mg-MOF-74. Moreover, the saturated CO_2 adsorption capacity under ambient pressure has seen a significant improvement of 15%.

Despite high performance of Mg-MOF-74, their application is hindered by several factors including its relatively poor CO_2 selectivity over other gases such as O_2, N_2, and CH_4 (all of

View Article Online
DOI: 10.1039/D4TA03877K

490 which are abundant in the flue gas mixture) [18]. Additionally, whereas CO_2 molecules are
491 strongly attracted to UMCs, H_2O molecules would preferentially occupy the open metal sites
492 [50]. As a result, Mg-MOF-74 absorbs substantially less CO_2 when it is exposed to moisture. This
493 is troublesome since there is a significant amount of H_2O(g) (5–7%) in flue gases [50]. Hence, it's
494 crucial to explore and devise methodologies for enhancing the selectivity over nitrogen of the
495 MOF, particularly in the presence of water. An example of the ongoing research into this issue
496 includes the introduction of amines into MOFs in an effort to emulate the chemisorption of CO_2
497 used by conventional liquid-amine technologies [51]. In a recent study conducted by Kim et al.
498 [52], MOFs modified with diamines (nitrogen compounds) were investigated. The modified
499 MOFs can capture and release CO_2 at lower temperatures than those used by existing carbon
500 capture materials [52]. As a result, the CCS process requires far less energy than it does with
501 existing technology, which lowers the process's cost [52]. Amine-modified MOFs are produced
502 by grafting amine functional groups onto MOFs [18]. This can improve the MOF's SCN and
503 operating capacity, but regrettably, there is frequently a significant regeneration energy penalty
504 [53]. Nonetheless, under capture conditions, some alkylamine-modified MOFs have good CO_2
505 working capabilities, SCN, and moderate regeneration [39]. There have been successful reports
506 of functionalizing Mg_2(dobpdc) with N,N'-dimethylethylenediamine (mmen). Coordination
507 bonds form between the amine groups and the unsaturated metal centers (UMCs) on
508 Mg_2(dobpdc). The resultant MOF, mmen-Mg_2(dobpdc), boasts a high density of amine groups,
509 leading to enhanced selectivity versus nitrogen (SCN) even in the presence of water. At 313.15
510 K and 0.15 bar, the CO_2 adsorption capacity reaches 3.5 mmol/g. Moreover, this MOF
511 effectively mitigates the substantial energy requirements for regeneration, further bolstering its
512 potential for carbon capture applications [39]. **Table 1** summarizes adsorption data for a variety
513 of functionalized MOF sorbents at different pressures and temperatures.
514

View Article Online
DOI: 10.1039/D4TA03877K

Table 1. CO_2 adsorption data for a variety of functionalized MOFs at different experimental conditions.

		CO_2 uptake (mmol/g)					
Adsorbent	**Functionality**	**Low pressure (mbar)**	**0.15 bar**	**1bar**	**Temperature (K)**	**Selectivity (S_{CN})**	**References**
Mg-MOF-74	UMC	NA	5.35	8.1	296	182 (IS) (15:85)	[18]
Mg_2(dobpdc)	UMC	NA	4.85	6.42	298	NA	[53]
UiO-66-$(CH_3)_2$	UMC	NA	1.3	4.01	293	58 (IS) (15:75)	[54]
UiO-66	UMC	NA	NA	1.8	298	23 (IAST) (14:57)	[18]
Co-MOF-74	UMC	NA	2.76	6.69	296	NA	[18]
mmen-Mg_2 (dobpdc)	Amine-modified	2.05 at 0.4mbar	3.13	3.86	298	200 (IS) (15:75)	[55]
[Mg_2(dobdc) $(N_2H_4)_{1.8}$]	Amine-modified	3.89 at 0.4mbar	5.18	5.51	298	NA	[56]
UiO-66-NH_2	Amine-modified	NA	1.15	2.6	298	32 (IS)	[18]
MOF-5	Pristine MOF	NA	NA	2.1	298	10.1 (IS)	[57]
MOF-505	Pristine MOF	NA	0.4	1.5	304	NA	[18]

2.2.2 Manufacturability, stability and cost

Mukherjee et al. [18] emphasize the importance of the industrial-scale production of candidate sorbents to meet the quantity demands of later-stage pilot-scale testing and wide-scale rollout. Most MOFs are not yet manufactured on a large scale, and the few that can be, are synthesized as powders [26]. MOFs need to be structured sorbents to be incorporated into the C-capture procedure. Therefore, it is necessary to look for ways to turn MOFs into pellets, beads, fibres, or monoliths. The absence of methods for transforming microcrystalline MOF powders into devices has given rise to numerous problems [18]. Some studies explore the incorporation of

View Article Online
DOI: 10.1039/D4TA03877K

MOFs into support structures (monoliths or pellets) but these are still in the early development stages [58]. Generally, research into the pelletizing MOFs without binders has shown a reduction of approximately 5% in the MOF's CO_2 uptake capacity [59]. Research conducted by Peterson et al. [60] employed octane adsorption experiments to investigate the effect of pelletization pressure on the properties of UiO-66. Results showed that pelletization at 68.94 bar led to an 8% reduction in octane adsorption and pelletization at 689.5 bar led to a larger reduction of 16%. However, results for the pelletization of HKUST-1 reported by Asadi et al. [61] show a 20% decrease in CO_2 uptake capacity. This suggests that sorbents may have varying uptake capacity responses to pelletization. Hu et al. [62] argue that, given the complexity of pelletization, an empirical approach involving practical investigations is necessary.

The current synthesis of MOF powders is typically done via solvothermal batch processes. These processes are time-consuming, require the use of expensive organic solvents, and involve complex purification methods [62]. These problems lead to high manufacturing costs, which may reduce their attractiveness as possible sorbents from an economic standpoint. Although more work needs to be done, some progress has been made recently, such as the utilisation of twin-screw extrusion (TSE) kg per hour-scale MOF synthesis without the use of ore-reduced solvents. When suggesting uses for newly created materials, a variety of considerations, including toxicity, life-cycle assessment studies, and economic implications, must be taken into account in addition to the previously mentioned concerns. On the other hand, one prominent drawback that has hampered the applicability of MOFs in this domain is their stability under the conditions of CCS operation, with many MOFs exhibiting poor hydrolytic stability [18]. This means that when MOFs are exposed to moisture, they are prone to decompose. There have been developments in the field to address this issue and recent research shows promise of progress. Investigated strategies include doping MOFs with alkyl amines (or other chemical functions)

View Article Online
DOI: 10.1039/D4TA03877K

and improving the MOF's hydrophobicity [62]. Studies on doping MOFs with N,N,N′,N′-tetramethylethylenediamine, hydrazine (N_2H_4), and 2,2-dimethyl-1,3-diaminopropane (dmpn) have shown that the CO_2 absorption capability is nearly entirely retained when there is moisture present [63]. However, it is important to note that doped MOFs may still struggle with poor chemical, mechanical, and thermal stability [53]. Research by Dalvi and Rossky [64] showed a marked improvement in hydrophobicity from MOFs decorated with fluoro or alkyl groups, suggesting this could be an alternative solution.

Another method of preparation that has been explored is wet granulation. This method, proposed by Chang and colleagues [65], mixes the MOF with a mesoporous γ-alumina (MRA) binder to produce millimeter-scale spheres (**Fig. 4(a)**). Numerous MOFs, including MIL-101(Cr), UiO-66(Zr)-NH2, MIL-100(Fe), and UiO-66(Zr), have shown effectiveness with this strategy. After shape, the MOF's natural characteristics are preserved with the aid of a binder. Furthermore, tiny businesses like Mosaic Materials and NuMat are making a concerted effort to satisfy these needs [26]. In the research conducted by Das et al. [66], the authors detailed formation of a hydrogen-bonded three-dimensional (3D) framework involves a zinc (II) center, a partially fluorinated elongated dicarboxylate ligand, and an amine-rich melamine co-ligand (**Fig. 4(b)**). Notably, this framework exhibits two distinct types of 1D channels adorned with CO_2-attractive ($-NH_2$ and $-CF_3$) groups that facilitate the framework's exceptional selectivity for CO_2 adsorption (uptake of 49.88 and 31.16 cm^3/g at 273 and 298 K, respectively) [66]. Furthermore, a straightforward and comprehensive room-temperature procedure has been established for the fabrication of (111)-oriented UiO-66 membranes [67]. This method utilizes a ZrO_2 buffer layer-modified porous α-Al_2O_3 substrate and a Zr(n-OPr)$_4$ source (**Fig. 4(c)**). Experimental findings revealed that conducting the reaction at room temperature (RT) increased the number of missing linkers within the UiO-66 framework (1.5 per Zr_6 formula unit). Consequently, this resulted in

View Article Online
DOI: 10.1039/D4TA03877K

enhanced CO_2/N_2 adsorption selectivity due to a stronger affinity interaction between CO_2 and the defective sites in the Zr6-oxo cluster nodes [67].

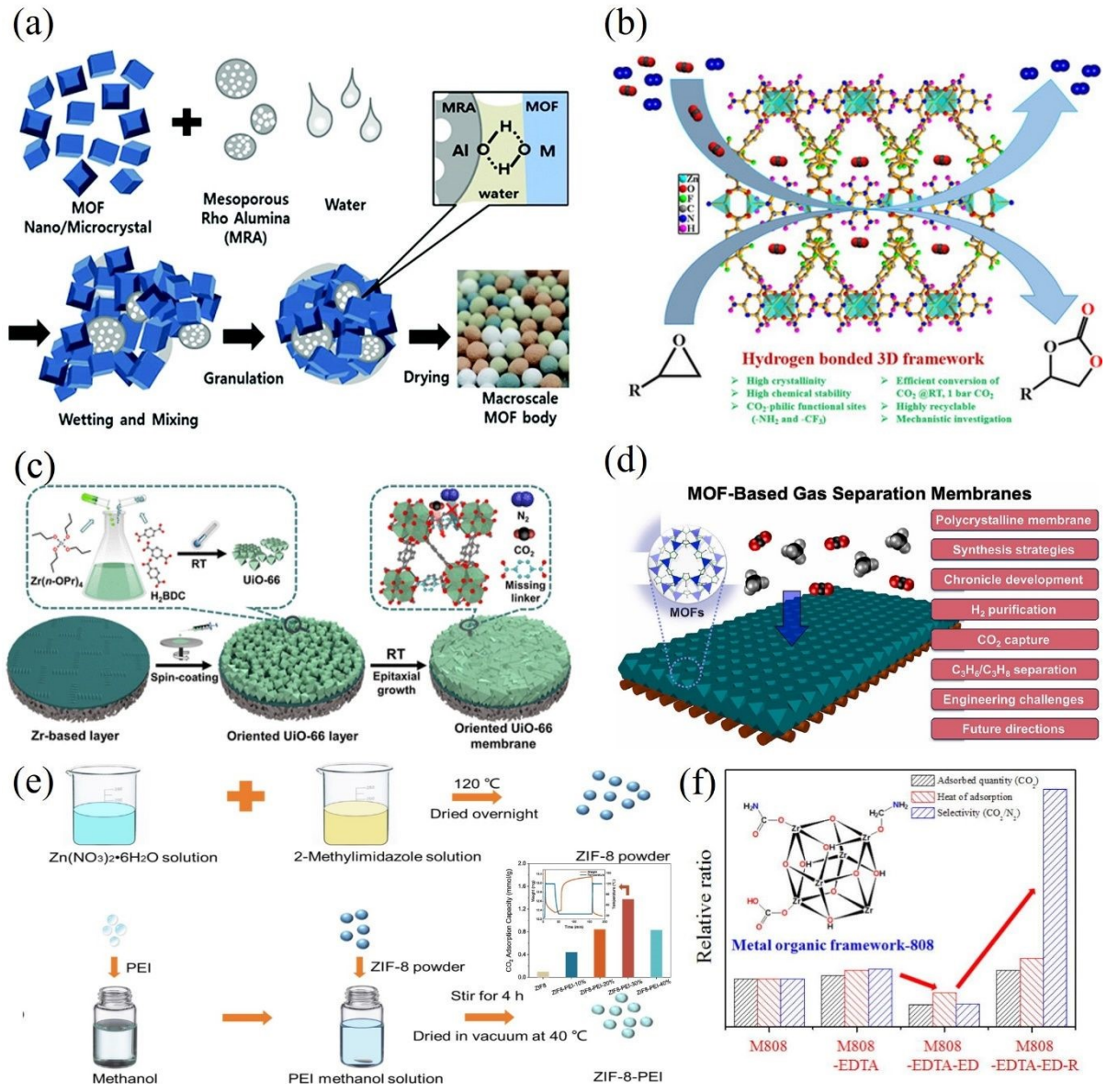

Fig. 4. (a) Creating MOF granules or spheres via the wet granulation process by aggregating MOF and MRA particles. Adopted from Ref. [65] with permission. (b) The rational design of a porous Zn(II)-MOF with several functional sites that can be used, under moderate conditions, for extremely effective CO_2 fixation with internal and terminal epoxides. Adopted from Ref. [66] with permission. (c) A schematic diagram depicting the entire room temperature preparation process for defect-engineered (111)-oriented UiO-66 membranes. A higher CO_2/N_2 adsorption selectivity was demonstrated and attributed to the stronger affinity interactions between CO_2 molecules and the defective sites in the Zr_6-oxo cluster nodes. Adopted from Ref. [67] with permission. (d) Diagram showing the in-situ growth process for homochiral MOF membrane production on nickel net and its use for molecular separations. Adopted from Ref. [68] with permission. (e) A synthesis process of unmodified and PEI-modifed ZIF-8 and the corresponding adsorption capacity at different PEI loadings. Adopted from Ref. [69] with permission. (f) Zr-based MOF functionalized with ethylenediaminetetraacetic acid (MOF-808-

592 EDTA), ethylenediamine (MOF-808-EDTA-ED), and lithium aluminium hydride (MOF-808-
593 EDTA-ED-R) for selective CO_2 adsorption. Adopted from Ref. [70] with permission.

594

595 Conversely, many research endeavours have focused on MOF-based gas separation
596 membranes, with particular attention to ZIF-8 [68] (**Fig. 4(d)**). The exploration of MOF
597 membranes for gas separation traces back to 2009 [71], with the milestone achievement of the
598 first continuous MOF-5 membrane via an in-situ growth method. This milestone marked the
599 beginning of MOF membrane development for gas separations. Other methods include layer-
600 by-layer growth, electrochemical synthesis, vapour phase synthesis, seeding and secondary
601 growth, and contra-diffusion also appeared in the ensuing ten years. Particularly noteworthy is
602 the considerable focus on ZIF-8 in MOF membrane research due to its exceptional C_3H_6/C_3H_8
603 separation capabilities, straightforward synthesis, and the potential for producing high-quality
604 membranes. A recent study involved the synthesis and characterization of ZIF-8 with varying
605 weights of polyethyleneimine (PEI) [69]. The results indicated that ZIF-8 with 30 wt.% PEI
606 achieved the highest CO_2 uptake of 1.4 mmol/g under dry conditions and demonstrated
607 remarkable CO_2/N_2 separation performance (**Fig. 4(e)**). The CO_2 adsorption capacity of ZIF-8-
608 PEI30% notably rose to 1.7 mmol/g when exposed to humid flue gas with 50% relative
609 humidity (RH). Furthermore, even after undergoing 50 adsorption/desorption cycles, only a
610 slight decrease in adsorption capacity was observed. Park et al. [70] have directed their efforts
611 towards improving the efficiency of Zr-based metal-organic framework (MOF-808) for CO_2
612 capture by introducing various functional groups onto the MOF surface. Notably, reducing the
613 MOF-808-EDTA-ED compound with lithium aluminium hydride (LAH) led to a significant
614 enhancement in performance, including higher CO_2 adsorption capacity, CO_2/N_2 selectivity,
615 and isosteric heat of adsorption. For example, under conditions of 298 K and 1 atm, MOF-808,
616 MOF-808-EDTA, MOF-808-EDTA-ED, and MOF-808-EDTA-ED-R demonstrated CO_2/N_2
617 selectivity of 40, 48, 19, and 197, respectively (**Fig. 4(f)**). This significant enhancement is

View Article Online
DOI: 10.1039/D4TA03877K

attributed to the contribution of functional groups and porosity. The introduction of amides during the reaction with ED resulted in decreased MOF porosity, negatively impacting CO_2 capture. However, subsequent reduction of amides to amines improved adsorption effectiveness [70].

Regarding the cost, it can vary widely depending on several factors, including the specific MOF composition, synthesis method, scale of production, and market demand. Generally, MOFs are more expensive to produce compared to traditional adsorbents like activated carbon due to their complex synthesis processes and sometimes costly precursor materials. At present, the production of MOFs typically involves expensive starting materials and specialized synthesis techniques, which contribute to higher production costs. Additionally, the purity and quality of MOF materials also affect their cost, with higher-purity MOFs often commanding a premium price. As was previously said, the creation of MOFs that require less temperature to absorb and release CO_2 will probably lead to lower process costs over time [52]. However, MOF sorbent costs are still considered the limiting factor for their commercial application [62]. Since MOF sorbents for post-combustion C-capture have not been subjected to real-world trials, prices can be estimated in part by considering the price of the substrates or raw sorbent utilised in the preparation [18]. The metal ions or clusters are often inexpensive, consequently, the main factor affecting the cost of a MOF sorbent is the linker cost. Whilst most sorbents use polycarboxylate ligands, there is a variety of inexpensive and commercially available ligands, for example, one of the most common ligands, 4,40 -bipyridine (bipy) [72]. Commercial MOF vendors still charge significantly more than more conventional porous materials like zeolites, even though MOFs are synthesised from comparatively cheap ingredients [62]. This is often attributed to high manufacturing costs which are the result of a shortfall in large-scale production methods.

View Article Online
DOI: 10.1039/D4TA03877K

3. Energy storage devices

Currently, supercapacitors (SCs) are among the most popular energy-storage devices [73], which have already found applications in consumer electronics, memory backup systems as well as industrial-scale power and energy management devices [74]. Although conventional capacitors have a larger energy density, SCs are seen to be better because of their many benefits, including flexible packaging, low weight, minimal heating, and strong device stability [75]. Furthermore, SCs have proven to be both safe and reliable, as Sundriyal et al. [74] highlight in their recent application in the emergency doors of the Airbus A380. In addition, one of the most intriguing uses of SCs is in contemporary transportation systems like electric cars. The sales ban on internal combustion engines (IC) engines will be accelerated from 2040 to 2035 as a result of growing social and governmental pressure to reduce fossil fuel consumption. As a result, the electrical energy storage (EES) devices used in these transportation systems must be able to provide a high enough power density to expedite vehicle charging times [74]. SCs' high-power densities (up to 15 kW/kg) give them the ability to charge and discharge rapidly, which would enable fast charging of electric vehicles and their good cyclic stability would ensure that their performance wouldn't degrade significantly over time. However, their largescale usage is hindered by low energy densities meaning that they are unable to hold large amounts of energy [75].

In the same context, electrodes play a critical role in SC performance, therefore selecting an electrode design and material is key to ensuring effective energy storage. Sundriyal et al. [74] suggest several critical electrode parameters that determine the performance of the SC including specific capacitance, power and energy densities, cycle life, and stability in bending. Forse et al. [76] also offer a range of critical electrode material properties that require consideration, including a large specific surface area, good stability at high temperatures, pores size and distribution, high corrosion resistance, high conductivity, and cost-effectiveness. Research by

View Article Online
DOI: 10.1039/D4TA03877K

Huang et al. [73] supports this but summarises the performance criteria under the broad umbrella of material properties that allow for a short ion or charge transfer channel whilst also providing many active sites.

Many sources discuss the relationship between the specific surface area (SSA) and capacitance as though it were linear, with higher SSAs resulting in a higher capacitance [73]. Whilst this is true for certain SC electrodes, Wu and Cao [77], highlight that in some instances, a higher SSA will not guarantee a greater capacitance. Effective surface area (ESA) is a surface area that is directly utilised for charge absorption and is associated with the distribution of pore sizes. As previously mentioned, the low energy density of SCs is currently impeding their practical deployment [78]. Energy density denotes the quantity of energy that a SC can store per unit volume of SC [74]. On the other hand, power density describes the amount of power transferred per SC volume. The difference between SSA and the attained specific capacitance is a topic covered in a number of studies. Some reports indicate that during charge storage, not all of the pores are used [75]. Consequently, Forouzandeh et al. [75] argue that while SSA is an important performance parameter for EDLC design, other factors such as pore size distribution and ESA will also influence the SC's electrochemical performance. In their research paper, Wu and Cao [77] state that the electrode surface area is the main influencer on the electrochemical properties of the SC.

Phiri et al. [79] highlight the important role played by ion-transport kinetics in SC electrode performance. According to their research, the material's surface area and pore structure affect the electrode's ion kinetics. Consequently, the authors suggest a material that combines a high SSA with a combination of micropores and mesopores (to raise the ESA) while thinking about ways to improve the electrochemical performance of electrodes. They suggest that the

View Article Online
DOI: 10.1039/D4TA03877K

mesopores may serve as a quick pathway for the SC electrolyte to move, boosting the capacitance of the SC and that the micropores offer a sizable SA for quick ion adsorption. Wu and Cao [77] also propose other factors for consideration such as the electrical conductivity of the electrode material and the presence of surface functional groups. Overall, factors such as power and energy densities, cyclability, specific capacitance and morphology require consideration during the material selection process for SC electrode capacitors. Moreover, cyclability pertains to the count of charge and discharge cycles a supercapacitor can undergo before experiencing electrode degradation and notable performance decline. [77]. Often, degradation only becomes evident after prolonged cycling. Consequently, estimating the cyclability can be difficult. Weinstein and Dash [80] warn that laboratory-based testing of cyclability often relies on "beaker tests". During these tests, the SC electrodes are placed in a beaker and submerged in the electrolyte. This kind of approach reduces the effect of contaminants on cyclability by allowing them to diffuse into the huge volume of electrolyte that causes errors. On the other hand, because of the device's real operating circumstances, there is minimal room for diffusion because the electrolyte volume is rather tiny [80]. Therefore, the cycle life obtained through laboratory tests is likely to be different from values obtained from testing the real fabricated SC. Cyclability is an important factor for the assessment of both the performance and the environmental impact of the design. If the electrode degrades quickly, more material will be required over the lifetime of the device or the device will require replacing.

In another context, Forouzandeh et al. [75] highlight a series of considerations for assessing the environmental impact of an electrode including the toxicity, reusability (reformation prospects), and energy requirements for the primary manufacturing (processing raw materials). Furthermore, Weinstein and Dash [80] postulate that, because SCs are often relatively small compared to the device they power, there is little incentive to reduce the size and weight of the

View Article Online
DOI: 10.1039/D4TA03877K

SC if it results in higher costs. Manufacturers of SC are more concerned with controlling costs than with making incremental performance advances. Price is acknowledged as significant, but it is not given more weight than the other factors [75]. Contrarily to Weinstein and Dash, Pongprayoon and Chaimanatsakun [81] argue that the two most important design requirements for SCs are tuning the electrode material morphology (pore shape and size) to optimize the transportation of electrolyte ions and a high SSA to increase the availability of electrochemically active sites. Both are relevant for improving performance rather than reducing cost.

3.1 Porous carbonaceous materials for supercapacitors

Porous carbonaceous materials stand out as highly versatile materials for supercapacitor electrodes, particularly due to their diverse applications in various biomass sources. In recent scientific research, there has been a notable emphasis on synthesizing carbonaceous materials from biowaste, which produces a variety of morphologies and surface textures. The typical synthesis process involves carbonization and activation steps, leading to activated carbon with tunable pore sizes and exceptionally high specific surface area compared to other carbonaceous materials. This renders activated carbon a preferred choice for supercapacitor electrodes. Prior to the rise of MOFs, most studies on supercapacitor electrode materials were concentrated on carbon-based materials [82]. Activated carbon (AC) is used in almost all electrochemical capacitors (ECs), and many producers of SC choose to use coconut shell AC as their active electrode material [80]. Phiri et al. [79] note that while graphene and carbon nanotubes (CNTs) are also common material choices for SC electrodes, their wide-scale deployment has been hindered by their high production costs and disposition to nanoparticle aggregation which limits their effective SSA.

View Article Online
DOI: 10.1039/D4TA03877K

3.1.1 Performance and properties

Carbon SC electrodes usually work via charge adsorption, resulting in large power densities and long cycle life [73]. In addition to this, carbon electrodes often present superb chemical stability and electrical conductivity. An AC fabricated electrode in a study by Li et al. [83] displayed a specific capacitance of 207.5 F/g and a cycle life of over 3000 cycles when tested at a current density of 0.5 A/g. Another study reports an energy storage density of about 28 Wh/kg, but it also mentions that the device's charge supply rate limits the amount of power that can be produced [84]. Research by Ajay and Dinesh [85] yielded a specific capacitance of 107.6 F/g for commercially available AC measured at a 5 mV/s scan rate. However, Phiri et al. [79] argue that biomass-derived ACs also have disadvantages, including discrepancies in the structures of the biomass sources. Because of this, the ideal circumstances for the synthesis of AC from one biomass source might not be appropriate for another. According to their studies, this can also apply to a single biomass source that is used intermittently. As a result, a biomass source needs to have a predictable and consistent structure to be taken into consideration for large-scale practical applications.

AC-based SC electrodes are well suited for this purpose, not only do they have a high thermal and electrochemical stability, but they also benefit from a large SSA. Available values of AC SSA vary with most papers agreeing on a value within the range of 1000–3000 m^2/g [86,87]. Conversely, a study by Weinstein and Dash [80] suggests a theoretical maximum SSA of 2000 m^2/g. Carbon materials have a high SSA in addition to being relatively simple to produce, modify, and optimise [87]. The premium-grade AC utilised for SC electrodes has been refined to guarantee that the ash level is less than 1% and the halogen and iron impurities are fewer than 100 ppm [80]. This purification helps to improve the cycle life of the electrode. Despite this, ACs are still comparatively cheap. ACs also benefit from high pore volumes in the range of 0.5–2

View Article Online
DOI: 10.1039/D4TA03877K

766 cm^3/g [87]. As previously stated, other literature suggests that the SSA is not as important as the
767 pore size and its impact on the effective specific surface area (ESSA) [75]. Research by Arenillas
768 et al. [88] supports this, suggesting that for AC electrodes, the whole SSA is not used for charge
769 storage as the larger electrolyte ions are unable to enter the small micropores. The largest
770 obtainable SSA for AC is estimated at 3000 m^2/g, whilst the obtainable ESSA ranges from 1000
771 to 2000 m^2/g [75]. Forouzandeh et al. [75] also examine the potential drawbacks associated with
772 large specific surface areas (SSAs), noting in their report that, in some scenarios, augmenting
773 the SSA can induce electrolyte decomposition and create dangling bond positions. Additionally,
774 a high pore volume may arise from attempts to raise the SSA through excessive activation. Poor
775 conductivity and low material density, which resulted in low energy and power densities, were
776 among the effects of these huge pore volumes that were investigated [89]. The impact of various
777 electrolytes on the obtained capacitance of AC electrodes has also been studied. It was shown
778 that the capacitive performance of AC electrodes was enhanced when an aqueous electrolyte
779 was used instead of an organic electrolyte.
780
781 The performance and characteristics of activated carbon as electrode materials for
782 supercapacitors are very well presented in **Fig. 5A (a, b)**. The latter presents the CV curves of
783 the electrodes at a scan rate of 50 mV/s and gives an idea about their capacitive behaviour and
784 electrochemical performance. That nearly rectangular shape of the CV curve indicates ideal
785 capacitive properties; among them, better performance is obtained for the AC-HF sample [90].
786 **Fig. 5A(b)** shows the galvanostatic charge-discharge curves of the electrodes at a current
787 density of 1.5 mA/cm^2, which provides the potential for energy storage. The GCD curves are
788 overlapping linearly and symmetrically, which further testifies to the high reversibility and
789 efficiency of the activated carbon electrodes, especially AC-HF, with the longest charging time
790 and discharge time and thus indicative of higher energy storage capacity [90]. A recent

View Article Online
DOI: 10.1039/D4TA03877K

breakthrough introduced a straightforward and cost-effective technique for producing high-performance cellulose-based activated carbon fibre papers (ACFPs), capable of serving as self-supporting supercapacitor electrodes without the need for binders [91]. This innovative approach combines wet papermaking, thermal carbonization, and double activation processes, enabling the on-site conversion of fibrillated pulp fibres into cellulose-derived activated carbon, seamlessly integrated with carbon fibres (CFs) (**Fig. 5(B)**). The electrochemical evaluations demonstrated that the ACFPs exhibited outstanding electric double-layer capacitive behaviour (**Fig. 5(C)**), with coulombic efficiency and capacity retention remaining at 98.58% and 100%, respectively, even after 10,000 cycles (**Fig. 5(D)**). The authors further elucidated the schematic representation of charge transfer and electrolyte ion transfer within ACFP [91]. The configuration presented in **Fig. 5(E)** demonstrates a stable three-dimensional conductive network structure through the close interweaving of CFs within the ACF matrix. This arrangement facilitated swift electron migration along the CFs and enhanced the adsorption of electrolyte ions by the ACFs [91].

View Article Online
DOI: 10.1039/D4TA03877K

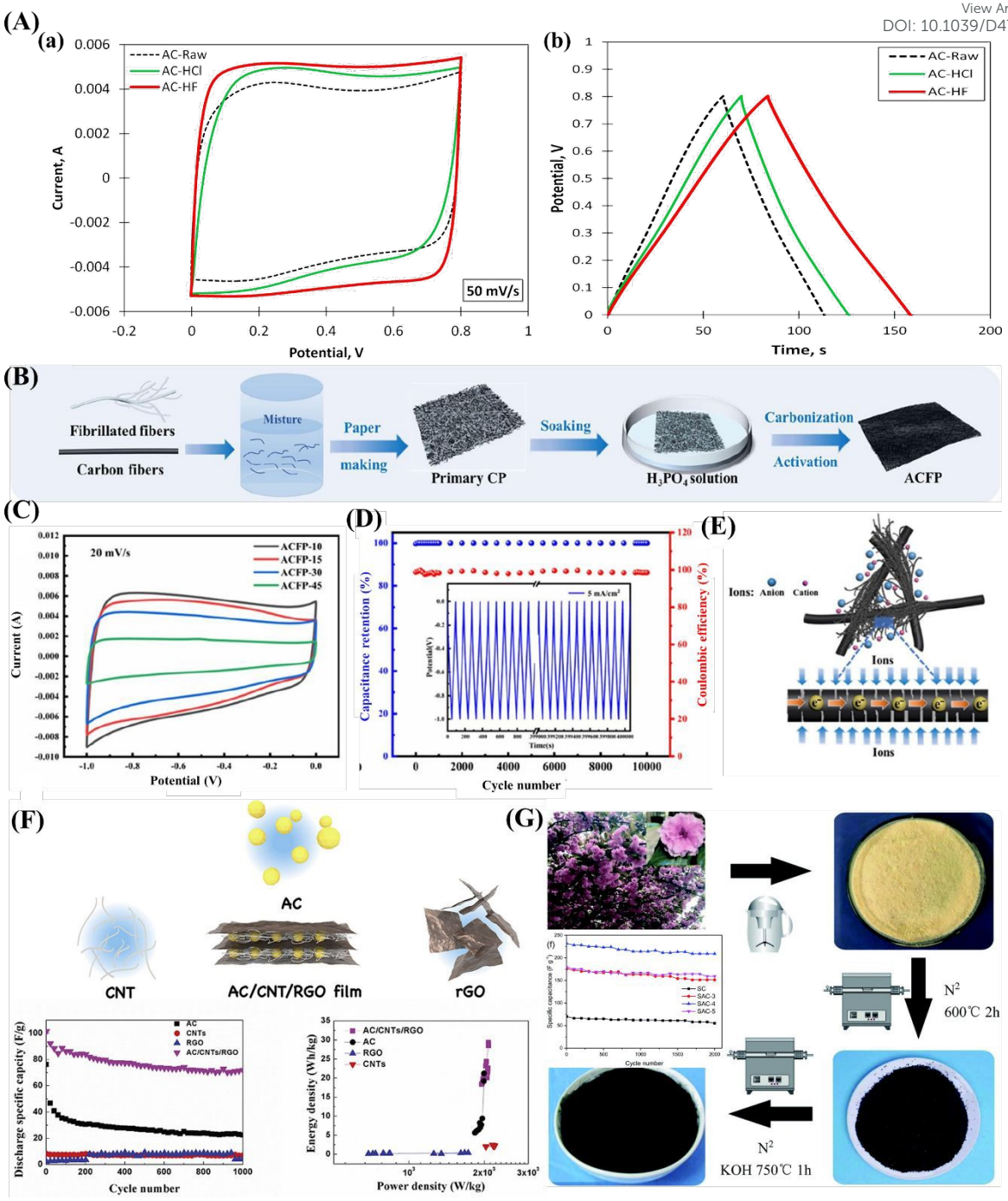

Fig. 5. (A) (a) Cyclic voltammetry curves measured at a scan rate of 50 mV/s; (b) galvanostatic charge discharge curves measured at a current density of 1.5 mA/cm². Adopted from Ref. [90] with permission. (B) Illustration depicting the production process of cellulose-based activated carbon fibre papers (ACEPs), (C) Cyclic voltammetry curves recorded for ACFPs with varying CFs content using a 20 mV/s scan rate, (D) Retention of capacitance and coulombic efficiency measured at a current density of 5 mA/cm^2, and (E) Schematic diagram illustrating the charge transfer and electrolyte ion transfer within the conductive networks in ACFP. Adopted from Ref. [91] with permission. (F) A flexible electrode consisting of self-supporting activated carbon, carbon nanotube, and reduced graphene oxide and its SCs performances show a high specific capacitance of 101 F/g at the current density of 0.2 A/g. Adopted from Ref. [92] with permission. (G) Schematic representation illustrating the production process of porous carbon derived from

View Article Online
DOI: 10.1039/D4TA03877K

sakura, along with its corresponding long-term cycling performances. Adopted from Ref. [93] with permission.

In the work of Li et al. [92], a deliberately engineered self-supporting and flexible film composed of activated carbon, carbon nanotubes, and reduced graphene oxide (AC/CNT/RGO) has been developed (**Fig. 5(F)**). The AC/CNT/RGO electrode demonstrates an impressive specific capacitance of 101 F/g when operated at a current density of 0.2 A/g, resulting in a remarkable maximum energy density of 30 Wh/kg. Conversely, three-dimensional porous carbon materials were synthesized by utilizing sakura petals as the source material and employing a combination of pre-carbonization and KOH activation techniques (**Fig. 5(G)**) [93]. The synthesized porous material exhibited a high specific surface area (up to 1785.41 m^2/g), leading to a maximum specific capacitance of 265.8 F/g at a current density of 0.2 A/g. Additionally, under continuous cycling for 2000 cycles, the capacitance retention rate remains excellent, reaching an impressive 90.2%, demonstrating outstanding cycling stability [93]. Recently, AC was prepared using biochar derived from date seeds via pyrolysis and activated with H_2SO_4 [94]. The elaborated samples demonstrated a specific capacitance of 487.5 F/g at a current density of 1 A/g. Additionally, galvanic charge and discharge trends indicated a higher charge storage capacity with reduced discharge. Another study focuses on converting inexpensive Cilantro plants (C. sativum) into AC aiming to produce a cost-effective AC material that shows promise in supercapacitors for energy storage [95]. The material that was synthesised at 700 °C showed ideal specific surface area (SSA) and surface functionalities, which promoted surface redox processes, electrode wetting, and ion diffusion-induced pseudo-capacitance. At 1 A/g, its specific capacitance was 162.4 F/g. Particularly noteworthy is the remarkable performance of the activated carbon (AC) symmetric supercapacitor, delivering a high-power density of 243.94 W/kg and maintaining minimal capacitance loss over 5000 cycles at 10 A/g, indicative of excellent cycling stability.

View Article Online
DOI: 10.1039/D4TA03877K

3.1.2 Environmental impact

Numerous commercially available ACs are produced from precursors such as coal and polymers, which are fossil fuel-based, making them both expensive and environmentally unfriendly [79]. However, ACs derived from biomass are still promising candidates for SC electrode materials [86]. Large pore volume and surface area (which can surpass graphene's), ease of preparation, and a customised architecture that has been deemed feasible for commercial usage are some of their potential qualities. Gao et al. [96] also draw attention to the other environmental benefits of bio-mass-derived ACs including the renewability and abundance of raw materials that can be used to make ACs. Furthermore, AC-based electrodes show good potential for recyclability. The recycling process for activated carbon was investigated by Jiang and Pickering [97]. The recycling procedure is assumed to be capable of recovering 90% of the electrode's active materials [84]. The measured surface area of the AC that was recovered by this technique is only 95% of its original, pristine value. This indicates a little decline in the content's quality [97].

Considering the environmental impact of recycling/recovering materials, Cossutta et al. [84] suggest using the substitution model. This model's underlying idea is that material recovery reduces the need to generate additional virgin material, which benefits the environment. The quality of the recycled product determines how much virgin material may be substituted (0.95 g of virgin AC can be replaced by 1 g of recovered material) [84]. This is not a 1:1 substitution due to the degradation of material quality/properties. Research by Ke and Wang [98] provides a value for the theoretical specific capacitance for used AC as 200 F/g (this value is based on results for maximum actual SSA). Cossutta et al. [84] highlight that, while the production of AC requires energy, it is not as greenhouse gas (GHG) intensive as other electrode materials (such as graphene). AC production produces around 5 g CO_2 eq./g (compared to ~80 g CO_2 eq./g). Furthermore, since the emissions from the recycling process are lower than the emissions

View Article Online
DOI: 10.1039/D4TA03877K

connected to the sourcing and initial production of ACs, recycling AC supercapacitors can result in a net reduction in GHG emissions. Research by Ntuli and Hapazari [99], also suggests that the use of agricultural by-products or lignocellulosic materials (such as coconut shells) as feedstocks for AC production would further reduce GHG emissions as processing would avoid the emission of GHGs when they rot or burn. However, the lifecycle analysis (LCA) of the AC as electrode materials for supercapacitors manifests a fundamental environmental performance. From here, it is observed that following the ISO framework, 1 kg of AC from coconut shells contains 34.4 MJ of energy use and 5.68 kg of CO_2, char production and activation account for 86% of the CO_2 emissions at 97% [100]. New AC electrodes exhibit competitive environmental performance in comparison with coal-derived AC, reduced graphene oxide, and algae-derived biochar aerogel electrodes, though they have larger impacts on land and water use as a function of the agricultural intensity of coconut production. They have lower impacts in regard to terrestrial ecotoxicity and freshwater eutrophication [101].

The AC production process involves high temperatures and activation agents such as potassium hydroxide, hence is highly energy-intensive with chemical wastes as by-products. The specific surface area for mesophase-derived AC, for example, is 2000 m²/g, reducing to 1600 m²/g when treated thermally but improving its stability by 99% [102]. During usage, AC-based supercapacitors show excellent performance, with thermally treated AC (AC-1000) exhibiting only a 5% reduction in specific capacitance after 10,000 cycles, compared to untreated AC's reductions of 12% and 17% [103]. An asymmetric capacitor using AC and AC-1000 shows a capacitance decrease from 220 F/g to 210 F/g after 10,000 cycles, and to 198 F/g after 20,000 cycles [104]. These efficiencies translate into reduced energy losses and extended lifetimes for devices. However, some of the challenges are in disposal and recycling, wherein exposure to residual chemicals from AC materials may contaminate the environment. Overall, AC materials

View Article Online
DOI: 10.1039/D4TA03877K

enjoy huge technical advantages, but their lifecycle environmental impact implores that the production methods used should be as clean and green as possible, the usage as efficient as can be, and the disposable or recyclable end-of-life-time processes as innocuous as can be to avoid adverse impacts on the environment.

3.1.3 Recent developments in AC electrodes

Recent literature provides a range of strategies for the improvement of AC electrochemical performance. In their 2020 research paper, Grishchenko and colleagues [105] explored modifying the surface of the AC electrodes through oxidation, and while there was a significant reduction in the SSA of oxidized material, they achieved a 1.4 times higher specific capacitance in a symmetric SC electrode compared to a pure AC electrode. Another example of the continuing improvement of AC electrodes can be seen in the work by Cheng et al. [106]. To create a new class of nanocomposite electrodes, the scientists examined the synergistic effects of combining ACs and carbon black (CB) with other species such as carbon nanofibers (CNFs) and carbon nanotubes (CNTs). The study demonstrated that, in comparison to pure AC electrodes, the electrochemical performance was significantly improved by mixing the species employed in the SC electrode. The weight percentage composition of the optimised nanocomposite electrode was 1.25% CB, 3.75% CNT, 1.25% CNF, and 88.75% AC. The completed SC demonstrated good cyclability (capacitance retention of 91.4% over 30000 cycles) and volumetric performance (high capacitance of 66.1 F/cm^3, power density of 101.7 kW/L, and energy density of 29.6 W h/L).

The improved performance is the result of the obtained morphology, as the added CB particles fit into the voids between AC particles and it was found that the flexible CNTs wrap tightly and uniformly around the AC particles. The CNFs were added, which helped to lessen the CB particles' tendency to aggregate. By acting as a bridge between CB and CNT-wrapped AC

View Article Online
DOI: 10.1039/D4TA03877K

particles, CNFs' relative stiffness (as compared to CNTs) enhances the structural stability of the nanocomposite. The final electrode featured a three-dimensional electrical conduction network that enhanced capacitive behaviour and packing density. Furthermore, the nanocompositing approach employed by Cheng et al. [106] utilizes readily available materials to synthesize the nanocomposites. These can then be used to mass-produce large-scale high-performance SC electrodes via the cost-effective industrial slurry process. A recent study focuses on synthesizing graphene oxide (GO) using a modified version of the Hummers' method [107]. The produced GO is then incorporated into an activated carbon slurry to create electrodes for supercapacitors. The addition of an appropriate amount of graphene oxide (GO) into the electrode renders it hydrophilic, thereby enhancing the interfacial contact between the electrode and the hydrogel electrolyte. The oxygen-containing functional groups present on GO attract cations and facilitate ion dissociation, thereby improving ion mobility. However, as an insulator, GO affects electrode conductivity. Remarkably, utilizing GO with weight ratios of 5% achieves a balance, providing a sufficient free ion ratio for good ion conductivity while maintaining acceptable electronic conductivity. Supercapacitors incorporating GO5 exhibit minimal equivalent series resistance (ESR) of 4 Ω and a maximum specific capacitance of 117.7 F/g. In a similar context, biowaste from litchi seeds was utilized to synthesize 3D activated carbon (3D-AC), which was further combined with reduced graphene oxide (rGO) and multi-walled carbon nanotubes (MWCNT) to create a multidimensional carbonaceous material [108]. This composite exhibited a specific capacitance of 320 F/g at 1 A/g. Additionally, 3D-AC served as a supporting matrix for the growth of zinc cobalt sulfide nanoparticles, leading to promising electrochemical performance in both asymmetric and symmetric devices.

Other recently explored strategies include using ultrasonic radiation for Fermi-level position modification of the activated carbon [109], sulphur and oxygen functionality doping of the porous

View Article Online
DOI: 10.1039/D4TA03877K

AC [110], and the formation of composite electrodes via the insertion of polymers into the AC substrate [111]. The price of AC has decreased dramatically over time, and this has been ascribed to the SC carbon market's strong price sensitivity relative to performance. Suppliers such as Kuraray, whose prices have dropped from $150–200 USD per kilogramme to $15 USD per kg, are an example of this price reduction [80]. More recent works provide a lower value of $4.15 USD per kg and also emphasize the manufacturing economic benefits of coconut shell AC by highlighting their abundant supply [87,112]. Activated carbon, while a popular material in supercapacitors, has several limitations that impact its performance. One of the main issues is its broad and irregular pore size distribution that is predominantly microporous (<2 nm). These small pores can limit the accessibility of electrolyte ions, particularly larger ions in organic electrolytes, resulting in reduced capacitance and inefficient ion transport. Despite its high surface area, activated carbon often exhibits low specific capacitance because not all of its surface area is effectively utilized due to the presence of micropores that are too small for ion penetration. Additionally, the properties of activated carbon are less tuneable compared to materials MOFs. This lack of tunability restricts the ability to optimize its surface chemistry, pore structure, and functional groups for specific applications.

3.2 Metal organic frameworks as supercapacitors

Table 2 presents a selection of functionalized MOFs investigated for their suitability as supercapacitor electrodes and compared to activated carbon. The table demonstrates a wide range of potential specific capacitances, with some MOFs showing values higher than those of AC, indicated at the bottom of the table. Additionally, MOFs exhibit the potential for enhanced cyclability compared to ACs, highlighting their promise for supercapacitor applications.

Table 2. Supercapacitor's performance of functionalized MOF compared to AC electrodes.

View Article Online
DOI: 10.1039/D4TA03877K

Electrode material	Cycle life	Specific surface area m^2/g	Current density /scan rate	Specific capacitance F/g	Reference
ZIF-8 (HNC) MOF derived porous carbon	20000	1215	536 mA/hg 1 mV/s	253.6	73
ZIF-8 (NPCF) MOF derived porous carbon	5000	NA	1 mV/s (rate)	332	22
ZIF-8 (NCF) MOF derived porous carbon	10000	NA	5 mV/s (rate)	264	22
Co-MOF MOF directly used	NA	2900	0.6 A/g	206.76	74
Zr-MOF (1) MOF directly used	NA	1047	5 mV/s	1144	22
ZIF-8 (NPC) MOF derived porous carbon	NA	1523	5 mV/s	251	22
MOF-5 (NPC) MOF derived porous carbon	NA	2872	1 mV/s	312	22
Ni-MOF	49.1% (5000)	295.7	1 A/g	1024.4	74
NiOx@NP 3-electrode system. From waste PET	(91.5% retention after 5000 cycles	1523	5 mV/s	581.30	113
3D) Ni-MOF	5000	NA	1 A/g	2150	114

View Article Online
DOI: 10.1039/D4TA03877K

Fe-MOF@AC	10000	180.7	1 A/g 1 mV/s	470.05	[115]
NiO@Ni-MOF	3000	433	1 A/g 1 mA/cm^2	144	[116]
Cu-MOF and Co-MOF	1000	NA	3 mV/s	451 and 103 C/g	[117]
Activated carbon	> 3000	NA	0.5 A/g	207.5	[83]

3.2.1 Pristine MOFs and their composites

From the available literature, it can be observed that the use of pristine MOFs for electrochemical applications, such as SC electrodes, is rare [118]. As previously mentioned, this is predominantly due to their inherent insulating properties which result in low capacitance, often regarded as insufficient for most electrochemical applications [119]. One report explores the use of Fe-MOF and its variants (MIL-88B, MIL100, and MIL-53) as SC electrodes coupled with an aqueous and neutral electrolyte [120]. The device's performance is significantly impacted by the material properties of the electrode, such as the size of the pellet and the pore diameters. Using an aqueous 0.1M Na_2SO_4 electrolyte, it was discovered that the MIL-100 sample only produced a specific capacitance of 34 F/g. The irritating nature of the Fe-MOF and insufficient mixing between the conductive and non-conductive phases of the Fe metal centres were the authors' explanations for this very low specific capacitance. This stops the material's electrons from moving through it in the best possible way when the iron centre is being reduced or

View Article Online
DOI: 10.1039/D4TA03877K

oxidised. The Fe-MOF was deemed unsuitable for use as an electrode due to the limited quantity of redox-active Fe ions in the structure. The use of bare Fe-MOF electrodes has also proven problematic, as experiments have shown that during the reduction cycle, the electrode is subject to some degree of dissolution.

Despite their limitations, MOFs exhibit a rapid diffusion of electrolyte ions into the pores of electrode materials. Consequently, research into utilizing pristine MOFs as SC electrodes has experienced a noticeable uptick. These MOFs often work as pseudocapacitors via faradaic redox reactions between the electrodes and the electrolyte. As the work by Wang et al. [121] shows, these fabricated electrodes yield theoretical values for capacitance as high as 2000 F/g [121]. However, Ramachandran et al. [122] argue that these benefits come at the cost of the electrode's cycle life. In their investigation, they discovered that the cyclic stability of pseudocapacitive MOFs was weakened by frequent charging and discharging cycles. This results from the occasional dissolving of MOF electrode material during the reduction reactions, as well as incompatibility between the electrode and electrolyte. A prominent example of the use of pristine MOFs as SC electrodes is the work done by Lee et al. [123] in their paper. During their experiments with a Co-based MOF electrode in an aqueous electrolyte of 1 M LiOH, the authors were able to achieve a specific capacitance of 206.76 F/g with a current density of 0.6 A/g. After the electrode's cycle life was examined, it was discovered that, after 1000 cycles of testing, its capacitance retention could reach 98.5%. However, the Co-based MOF electrode's performance significantly decreased and was ultimately declared unsatisfactory when tested in different electrolytes (such as KOH and KCl). An investigation was conducted into how the temperature of the synthesis reaction affected the performance, degree of crystallisation, and particle size of a zirconium-based MOF (UiO-66) [124]. It was observed that a sample with the smallest particle size and a synthesis reaction temperature of 50 ^{o}C achieved the highest specific

capacitance (1144 F/g at a 5 mV/s scan rate). However, the cost may prove to be a limiting factor as 1 kg of UiO-66 has been priced at around $25000 USD [125].

Other research into altering MOF morphology to improve SC performance includes the synthesis of a superstructure electrode from "accordion-like Ni-MOF" [126]. Whilst being tested at current densities of 1.4 and 7 A/g, the electrode achieved enhanced specific capacitances (988 F/g and 823 F/g respectively). Additionally, after 5000 cycles, the capacitance retention was 96.5%, which was a respectable retention rate. Highly elevated specific capacitances have also been seen with Ni-MOF electrodes in combination with a 6 M aqueous KOH electrolyte. Yang et al. [127] report that, with current densities of 0.5 A/g and 10 A/g, specific capacitances of 1127 F/g and 668 F/g respectively could be achieved. The high specific capacitances were explained by the authors as the result of the electrode's pseudocapacitive nature. Additionally, it was discovered that this electrode had improved cyclic stability, demonstrating 90% after 3000 cycles. The MOF's layered structure and sizable open facets were both credited with its cyclic stability and quick surface redox reactions.

Rahmanifar et al. [128] reported a one-pot co-synthesis method for creating a novel, water-stable Ni-MOF in combination with a Co-MOF. They also developed a dual Ni/Co-MOF-reduced graphene oxide (rGO) nanocomposite (**Fig. 6(a)**). The asymmetric device comprising activated carbon//Ni/Co-MOF-rGO demonstrated impressive performance, delivering a specific energy of 72.8 Wh/kg at 850 W/kg and maintaining a capacity of 15.1 Wh/kg even under the high specific power of 42.5 kW/kg. Furthermore, it exhibited exceptional cycle life, retaining 91.6% capacitance after 6000 charge-discharge cycles at 1 A/g [128]. In the work of Li et al. [129], a controlled and straightforward two-step method was introduced for cultivating Ni-MOF arrays on the surface of NiCo2O4 nanowires by regulating the MOFs' formation reaction (**Fig. 6(b)**).

View Article Online
DOI: 10.1039/D4TA03877K

The NiCo2O4@Ni-MOF hybrid electrode, after optimization, demonstrates improved electrochemical performance. It presents a notable specific capacity of 208.8 mA h/g at a current density of 2 mA/cm^2, alongside exceptional rate capability [129].

Recent research focused also on the potential of using waste polyethylene terephthalate (PET) derived Ni-MOFs in the synthesis of NiOx@NPC nanocomposite (NiOx nanoparticles with nitrogenous porous carbon) [113]. The simple solvothermal route used to synthesize this porous carbon composite has been described as cost-efficient. A schematic of the process can be seen in **Fig. 6(c)**. The BDC (benzene-1,4-dicarboxylic acid) utilised in this report's synthesis of the NiOx@NPC came from discarded PET bottles. The final product showed good specific capacitance, cyclic stability, and a high specific surface area (1523 m^2/g). But nothing about whether it's appropriate for widespread implementation is mentioned [113]. In another context, a novel electrode material comprising MOFs (Zr-TAA, where TAA stands for trans-aconitic acid) and multi-walled carbon nanotubes (MWCNTs) was easily synthesized using a one-pot reflux method and subsequently employed in a high-performance supercapacitor (**Fig. 6(d)**). Due to its improved conductivity and even distribution of pore sizes, this composite material exhibits outstanding electrochemical performance, achieving a specific capacitance of 562.06 F/g. Moreover, it retains nearly all of its initial capacitance even after undergoing 1000 cycles of testing with a 6 M KOH electrolyte [130].

View Article Online
DOI: 10.1039/D4TA03877K

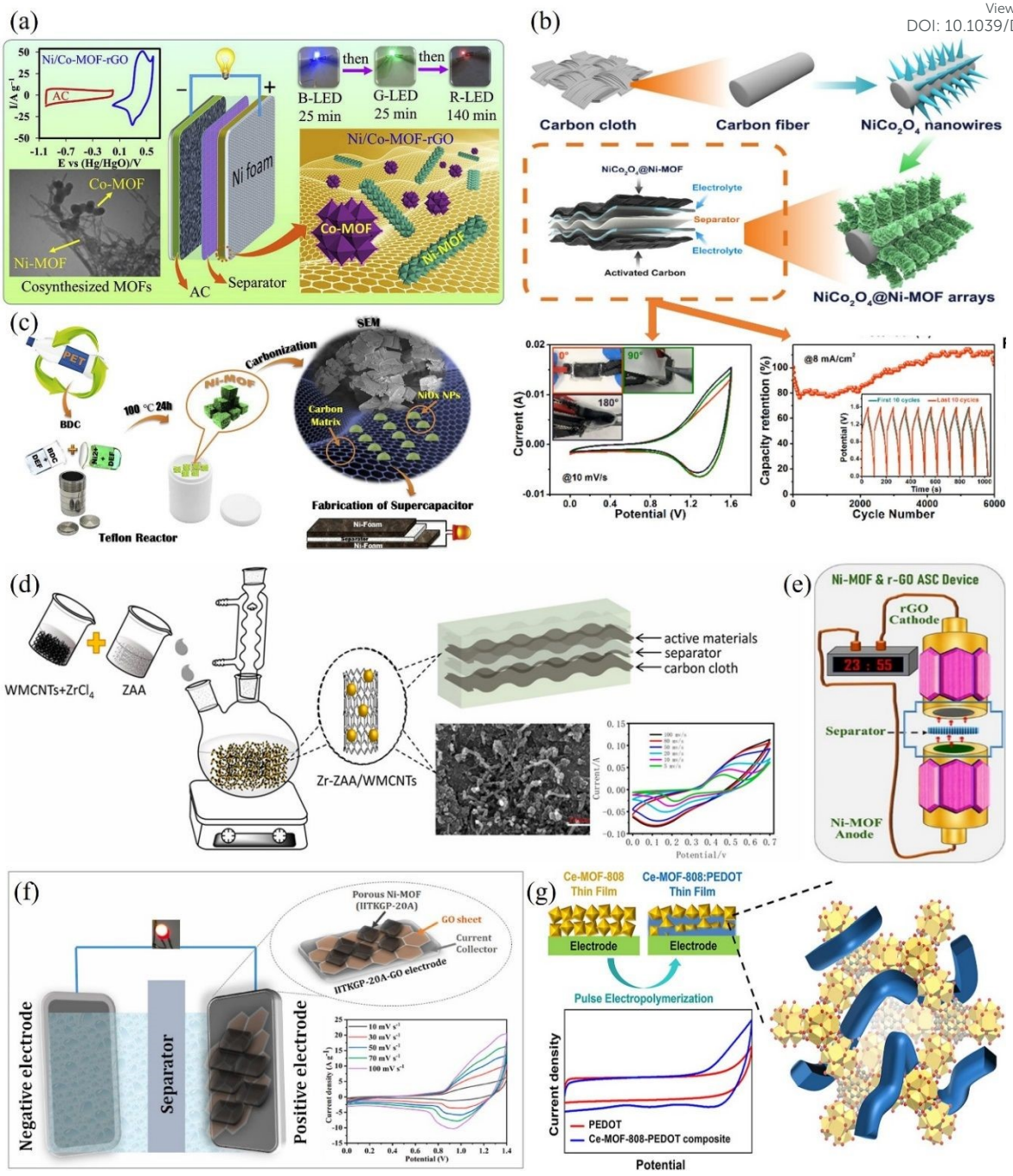

Fig. 6. (a) An asymmetric AC//Ni/Co-MOF-rGO device showing a capacitance of 860 F/g@1.0 A/g in a 3E cell setup. Adopted from Ref. [128] with permission. (b) A schematic depiction of the synthetic method employed to create core/shell hybrid arrays of $NiCo_2O_4$@Ni-MOF on a carbon cloth substrate and the corresponding CV curves, and cycling stability tested at 8 mA/cm^2. Adopted from Ref. [129] with permission. (c) Schematic diagram of the proposed method of synthesizing NiOx@NPC nanocomposites using waste PET with enhanced electrical conductivity and stability and improved charge relocation operation for a better performance of supercapacitor devices. Adopted from Ref. [113] with permission. (d) A novel electrode material, composed of MOFs (Zr-TAA, where TAA is trans-aconitic acid) and MWCNTs synthesized using a simple one-pot reflux method and applied to high-performance supercapacitors. Adopted from Ref. [130] with permission. (e) A three-dimensional Ni-MOF used as an anode electrode in a two-electrode asymmetric supercapacitor device setup. Adopted from Ref. [114]

with permission. (f) Highly scalable and pH stable 2D Ni-MOF-based composites (IITKGP-20A-GO) for high-performance supercapacitors exhibiting a specific capacitance of ~ 840 F/g at 2 A/g current density. Adopted from Ref. [131] with permission. (g) A cerium-based MOF@conducting polymer (PEDOT) nanocomposites for supercapacitors. Adopted from Ref. [132] with permission.

A recent study has concentrated on developing a 3D Ni-MOF with an outstanding capacitance of 2150 F/g at a current density of 1A/g [114]. Subsequently, the synthesized Ni-MOF and reduced graphene oxide were utilized as the anode and cathode electrode materials, respectively, in a two-electrode asymmetric supercapacitor device (ASC) setup (**Fig. 6(e)**). This ASC manifested a specific capacitance of 125 F/g (at 0.2 A/g) and showcased a high energy density of 50.17 Wh/kg at a power density of 335.1 W/kg. Furthermore, the ASC demonstrated excellent reversibility (97.9% Coulombic efficiency) and cyclic stability (94%) after 5000 constant charge-discharge cycles. In the investigation by Sahoo et al. [131], a microporous 2D Ni-MOF was elaborated, demonstrating high scalability and thermodynamic stability across a wide pH range (2–10). Upon introducing GO with a weight percentage of 3%, a specific capacitance value of approximately 840 F/g at 2 A/g was achieved, ranking among the highest within the category of bare MOFs and their composites/derived materials. Subsequently, when used as the electrode material in an asymmetric supercapacitor (**Fig. 6(f)**), it displayed a specific capacitance of 111.4 F/g at a current density of 2 A/g and exhibited excellent retention of 84% cycle life over 7000 cycles [131].

The study by Wechsler et al. [133] reported the fabrication of supercapacitor electrodes using pristine nickel hexaaminobenzene ($Ni_3(HAB)_2$) metal-organic framework (MOF) via electrophoretic deposition (EPD). The symmetric supercapacitor employing the MOF showcases remarkable electrochemical capacitive performance within a potential range of 0–1 V, demonstrating an areal capacitance of 13.64 mF/cm^2 and exceptional ultra-high cycling

stability, maintaining 81% of its capacity over 50,000 cycles. The superior performance of the supercapacitor is attributed to the binder-free electrophoretic deposition (EPD) process and the distinctive structure of 2D MOF nanosheets, which promote ion diffusion throughout the electrodes. Additionally, the literature review explored the utilization of a combination of MOFs and conducting polymers. Nanocomposites were fabricated by combining a cerium-based MOF (Ce-MOF-808) with poly(3,4-ethylene dioxythiophene) (PEDOT) through pulse electrodeposition of PEDOT within thin films of Ce-MOF-808 [132]. he highly porous Ce-MOF-808 displays reversible electrochemical reactivity, offering pseudocapacitance, while electronically conducting PEDOT contributes to a notable double-layer capacitance and enhances electronic conduction between the redox-active cerium sites in the MOF (**Fig. 6(g)**). As a result, the composite demonstrates superior performance compared to both pristine MOF and pristine electrodeposited PEDOT as active materials for supercapacitors [132].

3.2.2 Nanocrystalline MOFs

Research has also advanced in the field of nanocrystalline MOFs (nMOFs) and coin-type cell SCs, this is another example of altering the morphologies of pristine MOFs to enhance their supercapacitive properties. Gu et al. [119] posit that decreasing the particle size of MOFs into nanometre dimensions is an effective method for increasing their achievable capacitance. Particle size reduction improves the material's electrochemical performance significantly by lowering the electrolyte ion diffusion distance and raising the material's ESA [134]. These nMOFs were not commonly reported until recently. Only a few well-known MOFs, like MOF-5, ZIF-8, and ZIF-67, attracted attention because of their composition, which made downscaling simple. A variety of brand-new nMOFs have been developed and tested as part of recent research. Gu et al. [119] begin by synthesizing two MOF crystals via the adoption of the redox-organic linker from 3,30 5,50 -oxybenzobenzenetetracarboxylic acid (H_4L) and metal centres of Ni2þ/Cu2þ (**Fig. 7(a)**). An in-situ solvothermal procedure was used in a single step to obtain

View Article Online
DOI: 10.1039/D4TA03877K

the appropriate nanomaterials. One significant finding was that, with careful choice of solvent and surfactant, the different morphologies attained during material production could be efficiently controlled. When evaluated at current densities of 1 A/g and 5 A/g, respectively, one sample of the as-synthesised nano-NiMOF electrode produced capacitances of 1024.4 F/g and 648.9 F/g, demonstrating exceptional SC performance [119].

Work by Choi et al. [135] explores the synthesis of a range of nMOF structures including HKUST-1, Zr-MOF, nMOF-867, and MOF-5. The nMOF-867 sample exhibited very good supercapacitive behaviour, achieving a capacitance of 5.085 mF/cm^2, almost 6 times higher than the achievable capacitance from a fabricated electrode using commercially available AC (**Fig. 7(b)**). After 10,000 charge-discharge cycles, the nMOF-867 electrode continued to show exceptionally good cyclic stability, with a retention of over 90%. With a capacitance of 5.085 mF/cm2, the Zr-MOF sample under evaluation demonstrated exceptional supercapacitive qualities. This is nearly a 6-fold increase above the capacitance provided by an AC electrode made from commercially available AC. Additionally, the Zr-MOF electrode demonstrated exceptionally high cyclic stability (greater than 90%, which is considered ultrahigh) even after 10,000 cycles [135].

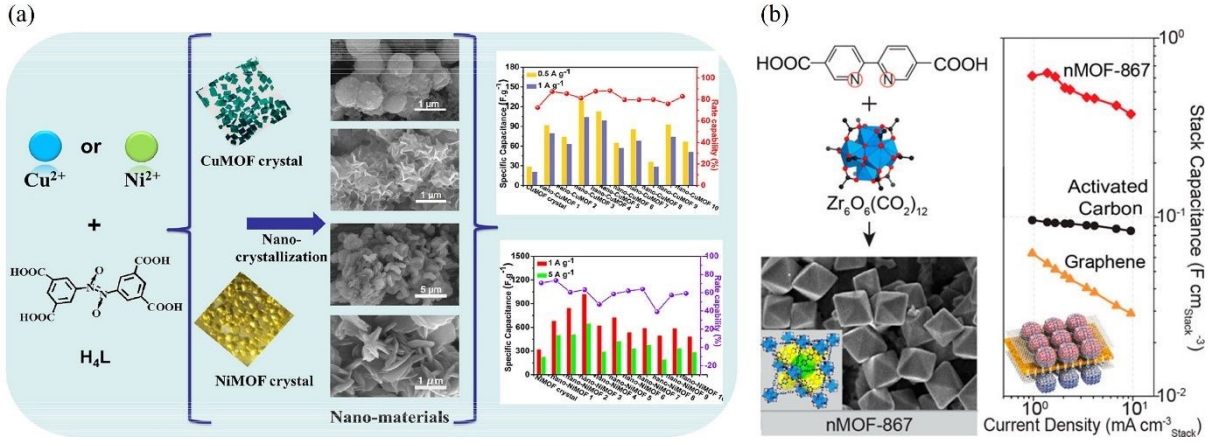

Fig. 7. (a) *In-situ* solvothermal synthesis of nanoscale CuMOF and NiMOF crystals and their specific capacitance (1024.44 F/g and 128.82 F/g for nano-NiMOF and nano-CuMOF respectively) and rate capacitance. Adopted from Ref. [119] with permission. (b) Nanocrystals

View Article Online
DOI: 10.1039/D4TA03877K

nMOF-867 with exceptionally high capacitance showing a stack and areal capacitance of 0.64 and 5.09 mF cm², respectively, with performance maintained over at least 10,000 charge/discharge cycles. Adopted from Ref. [135] with permission.

Some 2-dimensional (2D) MOFs with a high SSA and tuneable porosity have been discovered recently. In their pure state, these MOFs can give sufficiently high electrical conductivity for SC applications [136]. Charge delocalisation inside the material's planes and prolonged pi-conjugation provide this electrical conductivity [137]. Sheberla et al. [136] observed MOF $Ni_3(HITP)_2$'s high bulk electrical conductivity (over 5000 S/m), a value that exceeds those achieved by AC and porous graphite. The first non-carbon-based EDLC symmetric SC was fabricated using Ni3(HITP)2 electrodes after this discovery. After 10,000 cycles, the supercapacitor showed an extremely high areal capacitance of 18 mF/cm^2, and 90% capacity retention [136]. Another 2D MOF that has been investigated for high-performing SC electrodes is hexaaminobenzene (HAB)-derived MOF. Feng et al. [138] reported both a high volumetric and areal capacitance (760 F/cm^3 and 20 F/cm^2 respectively). The cycle life data were similarly encouraging, demonstrating that capacitance retention could only be increased by a factor of 10 after 12000 charging-discharging cycles. Research indicates that selecting the right electrolyte is essential for optimal SC performance. In one experiment, a 1 M LiOH aqueous electrolyte and a Co-based MOF electrode operated at a current density of 0.6 A/g produced a specific capacitance of 206.76 F/g [123]. Furthermore, retention of this capacitance was good (up to 98.5%) over 1000 test cycles. Although, when the electrolyte was changed to KCl or KOH, the performance of the electrode was not satisfactory.

3.2.3 Environmental impacts

Literature focusing on MOF toxicity is limited, and the topic is generally poorly understood [125]. If a MOF is toxic, this is likely the result of the organic ligand metal ions or functional groups [139]. The metal ions in MOFs are in the form of nanoparticles that are nonbiodegradable [125].

View Article Online
DOI: 10.1039/D4TA03877K

Kumar et al. [125], have suggested that out of the most common metal ions in MOFs, zinc and iron are likely to be the least toxic as they are used in the human body. While the toxicity of MOFs may not be fully known, some sources suggest that when MOFs decompose, they may exhibit the same toxicity levels as constituent raw materials from which they are generated. In summary, when considering the environmental impact of MOFs, several factors come into play: (1) Synthesis process: The synthesis of MOFs often involves solvents and energy-intensive processes. Depending on the specific synthesis route, this could contribute to environmental impacts such as greenhouse gas emissions and resource depletion. However, efforts are being made to develop more sustainable synthesis methods, such as using green solvents or employing energy-efficient techniques. (2) Resource utilization: The materials used in MOF synthesis, such as metal ions and organic ligands, can have environmental implications depending on their sources and extraction methods. For example, if the extraction of metal ions involves environmentally damaging processes or if rare or toxic elements are used, it could pose environmental concerns. (3) End-of-life disposal: Consideration should be given to the disposal of MOF-based supercapacitors at the end of their lifespan. While MOFs themselves are generally stable materials, the electrodes and other components of supercapacitors may contain metals or other materials that could pose environmental risks if not properly managed through recycling or safe disposal methods. (4) Performance and durability are key considerations for MOF-based supercapacitors. These devices have inherent advantages such as high surface area and customizable pore structures, which can significantly improve their performance. If MOFs can facilitate the development of supercapacitors with greater energy density and prolonged cycle life compared to conventional materials, it could have a positive impact on the environment. By extending the lifespan of electronic devices and minimizing the frequency of replacements, this advancement has the potential to reduce environmental impacts. (5) Scale of production: As with any technology, the environmental impact of MOF-based supercapacitors

View Article Online
DOI: 10.1039/D4TA03877K

will depend on the scale of production and deployment. Large-scale production could lead to increased energy consumption, waste generation, and resource depletion if not managed properly. The environmental impact and sustainability of Metal-Organic Frameworks (MOFs) used in supercapacitors necessitate a thorough examination, particularly when compared to traditional materials. MOFs like nMOF-867 exhibit superior electrochemical properties, with a stack capacitance of 0.644 F cm^3 and an areal capacitance of 5.085 mF cm^2, far surpassing commercial activated carbon supercapacitors [140].

However, most of the methods for MOF synthesis incorporate eco-toxic solvents, such as N,N-dimethylformamide, coupled with high energy requirements, which may pose a serious environmental impact. Therefore, an in-depth LCA is needed in estimating these materials. For instance, high carbon footprint and energy use can be associated with the production of MOFs; for instance, nMOF-867 is associated with high environmental cost despite its high performance and long lifetime, maintaining activity beyond 10,000 cycles [141]. Moreover, the environmental advantages of MOFs like UiO-66-NH_2, which can be synthesized using aqueous methods reducing environmental impacts by up to 91%, must be weighed against challenges such as degradation and scalability. These methods yield a cradle-to-gate carbon footprint of 43 kg CO_2 eq/kg and a lower production cost of $15.8/kg compared to solvothermal processes [142]. On the long-term sustainability front, MOFs still hold much promise because green synthesis methods using either water or ethanol as solvents have already been developed, and biodegradable MOFs that can minimize their impact on the environment are under construction. Although this might be the case, there is a clear lack of long-term data relating to MOF recyclability and degradation, and their high initial production costs underline the necessity for performing holistic LCA with respect to end-of-life disposal and possible environmental release to make such next-generation materials more environmentally and economically feasible against traditional ones [143].

View Article Online
DOI: 10.1039/D4TA03877K

3.3 Metal-organic frameworks for battery technologies

MOFs and their derivatives have accommodated much interest and proved rather promising to improve sodium-ion batteries (SIBs), and lithium-ion batteries (LIBs) performance. The work by Zhao et al. [144] proved the potential of Prussian blue analogues (PBAs) as SIB cathode material through effective etching. Specifically, etching $Na_2NiFe(CN)_6$ (NaNiHCF) into a dice shape increased its specific surface area, enhancing sodium storage sites and accelerating Na^+ diffusion. The etched NaNiHCF-3 showed a large reversible capacity of 83.5 mAh/g that accounted for about 98.2 % relative to the theoretical capacity, while the unetched counterpart precursor only delivered 76.8 mAh/g. Moreover, NaNiHCF-3 exhibited 71.2 mAh/g at 10 C with a rate capability far beyond that of other electrodes and maintained a very stable life with 94% capacity retention over 1,000 cycles at 1 C. These results further underline the role of morphological control in the electrochemical performance of MOFs with respect to capacity use and cycling stability. Indeed, the tunable porosity and high surface area of MOFs enable theoretically improved ion transport and storage capabilities. For example, nitrogen-doped amorphous Zn-carbon multichannel fibers have exhibited a Coulombic efficiency above 99% for more than 500 cycles at current densities from 1 to 5 mA cm², demonstrating major improvements in lithium metal anode performance. Symmetric cells based on these materials achieve stable cycling for over 2,000 hours, which is the potential for long-term applications [145]. However, the synthesis process is complex due to electrospinning and MOF coating, and this complicates large-scale production. The specific capacity of 104 mAh/g during the high rate of 5 C in the full-cell tests with $LiFePO_4$ cathodes is quite encouraging, but its broader compatibility with various cathode materials remains to be explored. While these MOF-derived materials could effectively reduce dendrite formation and issues regarding local current density, the long-term stability in a range of environmental conditions remains to be evaluated.

View Article Online
DOI: 10.1039/D4TA03877K

Always in the context of LIBs, the study of Du et al. [146] presents an efficient synthesis of 2D layered Mo-MOF@PPy via reflux heating and coating methods, aimed at improving the performance of anode materials in LIBs. Serving as a precursor during the electrochemical reaction, the high-valence Mo within the Mo-MOF effectively binds with Li^+, thereby contributing to the superior electrochemical performance of the material. Additionally, the polypyrrole (PPy) coating significantly enhances the electrical conductivity of the composite by promoting electron transfer. As a result of these synergistic effects, Mo-MOF@ppy achieves a specific capacity of 930 mAh/g at a current density of 100 mA/g and retains a capacity of 750 mAh/g at 500 mA/g after 200 cycles. In a similar study, Zhao et al. [147] utilized stannous sulfate ($SnSO_4$) and graphene to synthesize Sn-MOFs/G nanorods, which were evaluated as anode materials for LIBs. The resulting material exhibited a high specific capacity of 462 mAh/g after 500 cycles at 1 A/g and demonstrated remarkable rate performance, achieving 265 mAh/g at 2 A/g.

In detail, recent progress involving MOFs and MOF-derived materials has unveiled their huge potential towards enhancing the performance of batteries. For example, the synthesis of copper-substituted CoS_2@CuxS DSNBs by a multistep MOF-based templating strategy possessed very impressive electrochemical properties, such as high capacity (535 mAh/g at 0.1 A/g), better rate capability (333 mAh/g at 5 A/g), and extended cycling stability (76% capacity retention over 300 cycles) [148]. The improvements may be attributed to their complex nanostructure, which provided enhanced ionic and electronic conductivity, improved electrochemical reactivity, and mechanical stability. In this respect, this approach can overcome the poor conductivity and fast capacity fading of sulfur metal through the combination of different active materials with hierarchical hollow structures, which can reduce ion diffusion paths and strain accommodation during cycling. Rational design and controlled composition, as emphasized in the present work, are preliminary steps for the development of high-performance anode materials, and this work

View Article Online
DOI: 10.1039/D4TA03877K

further confirms the bright application of MOF-derived materials in next-generation batteries. Although these results are very promising, problems like intrinsic instability of MOFs in electrolyte environments and scalability issues, coupled with generally low electrical conductivity, have to be resolved before their full potential is tapped. Therefore, future studies should address the issues of scalability and stability if the full potential of MOFs in battery applications is to be exploited, ensuring technological advancement with sustainability.

The main advantage of MOFs over activated carbon in energy storage devices lies in their highly tunable structure and functional versatility. MOFs are composed of metal nodes connected by organic linkers, allowing precise control over pore size, shape, and surface chemistry. This tunability enables the design of materials with optimized ion transport and storage, potentially leading to higher capacitance and energy density. Unlike activated carbon, which often has a broad and irregular pore size distribution, MOFs can be synthesized with uniform and well-defined pores, ensuring consistent ion diffusion and reducing resistance during charge-discharge cycles. Additionally, the organic linkers in MOFs can be chemically modified to introduce specific functional groups that enhance interactions with electrolyte ions, while the metal centers can be selected or doped to introduce redox activity, contributing additional pseudocapacitance. MOFs can also encapsulate or host other functional materials, further enhancing their electrochemical performance by providing additional active sites or improving electrical conductivity. This versatility in synthesis and integration with conductive materials makes MOFs a promising material for next-generation supercapacitors, offering the potential for higher energy densities, improved ion transport, and customizable electrochemical properties. However, challenges such as low conductivity, stability, and cost still need to be addressed for MOFs to become a widely adopted alternative in commercial applications.

View Article Online
DOI: 10.1039/D4TA03877K

3.4 MOF metal nodes, ligand architecture and synthesis strategies

In MOFs, the metal nodes, also known as metal clusters or secondary building units (SBUs), play a pivotal role in determining the structure and properties of these materials. These nodes form the inorganic backbone of the MOF and are interconnected by organic ligands to create an extended porous network. The composition of these nodes can vary widely, ranging from simple single metal ions like Zn^{2+}, Cu^{2+}, or Fe^{3+}, which can coordinate with multiple ligands, to more complex metal clusters such as $Zr_6O_4(OH)_4$ or Cr_3O, which involve multiple metal ions linked together, contributing to the stability and diversity of the MOF structure [149]. The coordination environment of the metal nodes, defined by the number of ligands or atoms bonded to the metal ion, is crucial in determining the geometry of the node, which in turn influences the overall topology and dimensionality of the MOF. For example, a metal node with a high coordination number can lead to the formation of highly connected, three-dimensional frameworks, whereas lower coordination numbers might result in simpler, two-dimensional or even one-dimensional structures.

The metal nodes not only shape the structural framework but also impart distinct chemical properties to the MOF. The choice of metal can significantly influence attributes such as thermal stability, chemical reactivity, and catalytic activity. Transition metals like chromium (Cr), zirconium (Zr), or titanium (Ti) are known for imparting higher stability and robustness to the MOF, making them suitable for applications that require durability. On the other hand, metals like copper (Cu) or zinc (Zn) offer tunable reactivity, which can be advantageous in catalytic processes. Metal nodes also play a critical role in the functionality of MOFs. For instance, they can act as active sites for catalysis, with MOFs containing iron (Fe) or cobalt (Co) nodes being explored for oxidation reactions [150,151]. Additionally, the type of metal used in the nodes affects the adsorption characteristics of the MOF, particularly in gas adsorption

View Article Online
DOI: 10.1039/D4TA03877K

applications. MOFs with unsaturated metal sites, such as those with open metal sites, can strongly adsorb gases like CO_2 or H_2, making them valuable for gas storage and separation technologies.

Moreover, the electrical properties of MOFs are influenced by the metal nodes, which is particularly important in applications such as supercapacitors and batteries, where conductivity is essential. Metal nodes can also be tuned through post-synthetic modifications, allowing for the enhancement or alteration of the MOF's properties. This can be achieved through metal exchange or doping, introducing new functionalities or improving stability. For example, in MOFs like HKUST-1, which utilizes Cu^{2+} ions as the metal node, the resulting structure is a robust three-dimensional framework that has been widely studied for gas storage [152]. Similarly, MIL-101, which contains Cr^{3+} ions, is renowned for its exceptional thermal and chemical stability, making it suitable for various industrial applications [153]. Another notable example is UiO-66, where Zr^{4+} ions provide high stability, making it a popular choice for gas storage and separation [154]. Overall, metal nodes are a crucial design element in MOFs, as they not only determine the structural framework but also significantly influence the functional properties, making them central to the development of advanced materials for a wide range of applications.

On the other hand, ligand architecture in MOFs is a crucial determinant of their structural integrity, topology, and functional properties. Organic ligands, or linkers, connect metal nodes or clusters to form the extended porous networks characteristic of MOFs. The size and shape of these ligands significantly influence the MOF's pore dimensions and overall framework [155,156]. For instance, longer ligands typically create larger pores, which can be advantageous for applications like gas storage or catalysis, while the geometric arrangement of the ligands whether linear, angular, or branched affects the dimensionality and complexity of the MOF

View Article Online
DOI: 10.1039/D4TA03877K

structure. Functional groups on the ligands, such as carboxylates, phosphonates, imidazolates, or sulfonates, play a pivotal role in determining the strength and nature of the coordination bonds with metal nodes, impacting the MOF's stability and reactivity. For example, carboxylate groups form strong bonds with metal ions, leading to highly stable frameworks like those in UiO-66, while functional groups such as amines or hydroxyls can enhance adsorption properties by introducing sites for hydrogen bonding [154]. The connectivity of the ligands how many coordination sites they offer affects the density of the network and the robustness of the resulting MOF. Ligands with higher connectivity can create more intricate and stable 3D frameworks, as seen in HKUST-1, where the bidentate trimesic acid ligand coordinates with multiple metal ions [157]. Additionally, the coordination mode of the ligand, whether monodentate, bidentate, or multidentate, influences the rigidity and stability of the framework. Ligand architecture can also be tuned through post-synthetic modifications, allowing for the introduction of new functionalities or enhancements, such as improved CO_2 capture capacities through the addition of amine groups. Examples of MOFs that showcase the importance of ligand architecture include the IRMOF series, which utilizes terephthalic acid ligands to form various frameworks with different properties, and ZIFs (Zeolitic Imidazolate Frameworks), where the imidazolate ligands create highly stable, zeolite-like structures [158,159]

Regarding the synthesis of MOFs, it encompasses a variety of methods, each tailored to achieve specific structural, compositional, and functional characteristics in the final material [160]. Hydrothermal synthesis involves dissolving metal salts and organic ligands in water, followed by heating the solution in a sealed container under high temperature and pressure. This method, widely used for its simplicity, produces high-quality MOF crystals, as seen in the synthesis of UiO-66, where zirconium chloride reacts with terephthalic acid [161]. Solvothermal synthesis, a variant that uses organic solvents instead of water, allows for the formation of MOFs that are

View Article Online
DOI: 10.1039/D4TA03877K

sensitive to water or require particular solvents for solubility, such as HKUST-1, which is synthesized using a solvent system involving alcohols and acetic acid [162]. Ligand-assisted synthesis leverages pre-formed metal-organic complexes to guide the growth of MOFs, enhancing uniformity and control over the final product's properties.

Microwave-assisted synthesis of MOFs is grounded in the principle of using electromagnetic radiation to interact with removable electronic components, such as electrons, ions, or polar molecules in solids, or ions and electrons in liquids. This method typically operates at temperatures above 100°C and within reaction times of no more than 60 minutes. Improvements in reaction conditions can be achieved by optimizing various factors, including the choice of solvent, duration of radiation exposure, temperature, intensity of microwave radiation, and the quantities of reactants. Adjusting these variables helps to enhance the efficiency and quality of the MOF synthesis process [163]. Electrochemical synthesis utilizes an electric current to drive the formation of MOFs from metal salts and ligands, allowing precise control and the creation of MOFs with unique properties, including thin films or coatings on conductive substrates. Moreover, solvothermal-hydrothermal hybrid synthesis combines aspects of both methods, using a solvent system that interacts with both water and organic components, useful for synthesizing MOFs with specific property balances. Post-synthetic modification, though not a primary synthesis method, involves altering the MOF framework after its initial formation through techniques like ligand exchange or metal ion substitution, tuning the MOF's functionality and stability for specialized applications. Direct synthesis from metal oxides uses metal oxides or salts directly to form MOFs in the presence of organic ligands under controlled conditions, advantageous for creating highly stable frameworks. Each of these methods offers unique advantages depending on the desired MOF properties, such as crystal size, pore

View Article Online
DOI: 10.1039/D4TA03877K

structure, stability, and functional capabilities, making them crucial for tailoring MOFs to specific applications [164,165].

4. Photocatalysis

In 1972, Fujishima and Honda's pioneering work saw the creation of the first photocatalytic system using TiO_2 and ultraviolet light irradiation [166]. Since then, a variety of materials have been investigated for photocatalysis applications. As noted by Djurišić et al. [167], there have been few advancements or breakthroughs in photocatalyst concepts and designs. The majority of current research shows only modest advancements, and if photocatalytic technologies are to ever be used on an industrial scale, a significant amount of research and development will be needed. The standards for an effective photocatalyst are generally agreed upon in the literature. The material's characteristics should, in general, permit well-visible light absorption, sufficient degree of resistance to photo corrosion and ideally should inhibit the recombination of electron-hole pairs [168]. Work by Dhakshinamoorthy et al. [169] further stresses the importance of responsiveness to visible light to ensure the efficient use of solar energy, by emphasizing that visible light makes up 43% of total solar energy. Shanmugham et al. [168] provide a range of ideal photocatalyst material properties to help achieve these goals, including a high surface area, narrow band gap, and thermal stability. In addition, several papers agree on the importance of photocatalyst morphology and structure for performance as it influence the surface area and the availability of active sites.

4.1 Conventional photocatalytic materials

Photocatalysis is a transformative technology that leverages light to drive chemical reactions, offering innovative solutions in various fields including environmental remediation, energy production, and chemical synthesis. At the heart of this technology are photocatalyst materials, which absorb photons and use this energy to facilitate or accelerate chemical processes. Among

View Article Online
DOI: 10.1039/D4TA03877K

conventional photocatalyst materials are titanium dioxide (TiO_2), zinc oxide (ZnO), and carbon-based materials such as graphene oxide (GO), and reduced graphene oxide (rGO). Each of these materials has its strengths and limitations, so the choice of photocatalyst often depends on the specific application and the desired properties. Pawar et al. [170] hail titanium dioxide (TiO_2) nanoparticles as being among the most promising photocatalyst materials for commercial use. This is due to their superb optical and electronic characteristics, excellent chemical stability, high photoactivity, low cost, and reusability. Various morphologies of titania photocatalysts, spanning from nano to macrostructures, have been documented in the literature [171]. These encompass spherical particles, rod-like structures, tubular forms, fibrous configurations, and sheet-like arrangements at the nanoscale (**Fig. 8(a)**). These diverse morphologies have been meticulously designed to achieve distinct photocatalytic capabilities by fine-tuning factors such as particle size, specific surface area, pore structure and volume [171]. Research by Zhao et al. [172], however, emphasizes the disadvantages of semiconductor nanoparticles (NPs) such as TiO_2 including a complex separation process from reaction systems, and a high rate of recombination of photogenerated electron-hole pairs. TiO_2 is also prone to aggregation in reactions which reduces its effective surface area and therefore performance.

In their work, Moma and Baloyi [173] postulate that the main issue with TiO_2 photocatalysts is the bandgap (3.2 eV). As a result, only 5% of the solar spectrum of the UV light region can be used for photocatalysis. TiO_2 has a low photocatalytic efficiency as a result. Research by Zhao et al. [172] supports this view, by arguing that this disadvantage is the primary hindrance preventing the use of TiO_2 in isolation for photocatalysis. To increase TiO_2's efficiency, current research also attempts to enhance its photocatalytic activity under visible light irradiation [174] . One method investigated is nitrogen-doped TiO_2, results of such studies show enhanced photocatalytic activity compared to pure TiO_2 [173]. Recent studies suggest also that modifying the defects in

View Article Online
DOI: 10.1039/D4TA03877K

TiO_2 can expand the range of light absorption and enhance the efficiency of charge separation. Various methods, including hydrogenation, plasma treatment, chemical reduction, electrochemical reduction, and oxidation (**Fig. 8(b)**) [175], are employed to produce defective TiO_2 photocatalysts. These catalysts exhibit different types of defects, encompassing bulk and surface defects, and their relevance in photocatalytic applications is documented [175]. Notably, oxygen vacancies and Ti^{3+} defects are identified as pivotal factors in augmenting photocatalytic performance.

Due to the wide band gap of TiO_2, its application in visible photocatalysis is limited. To address this issue, several studies propose introducing oxygen vacancies and carbon quantum dots (CQDs) with up-conversion properties to enhance photocatalytic activity. Li et al. [176] prepared various configurations, including one-dimensional TiO_2 nanotubes (TNs), TNs with oxygen vacancies (OVTNs), TNs embedded with composite CQDs (CQD-TNs), and OVTNs embedded with composite CQDs (CQD-OVTNs). The impact of oxygen vacancies and CQDs on NOx removal through photocatalysis was investigated. Results show that CQD-OVTNs exhibit a significant synergistic effect between CQDs and oxygen vacancies, enhancing visible photocatalytic NO removal efficiency by approximately 12, 2, and 2.6 times compared to TNs, OVTNs, and CQD-TNs, respectively (**Fig. 8(c)**) [176]. Similarly, nitrogen-doped carbon quantum dots (NCQDs) were utilized to enhance TiO_2 through a simple hydrothermal-calcination synthesis method [177]. The incorporation of NCQDs enhances visible light absorption and facilitates electron transfer, thereby improving the separation of photo-generated electron-hole pairs. Even with a low NCQDs content of 3 wt%, the photodegradation rate for methylene blue was 2.25 times faster compared to pristine TiO_2.

A plausible mechanism for the photocatalytic degradation of methylene blue (MB) by

View Article Online
DOI: 10.1039/D4TA03877K

NCQDs/TiO_2 is depicted in **Fig. 8(d)** [177]. When exposed to sunlight, electrons within the valence band (VB) of TiO_2 absorb photon energy from solar radiation, generating electron (e−) hole (h+) pairs in the conduction band (CB) and VB, respectively. The e− can readily combine with dissolved oxygen in water to form •O_2-. Furthermore, the h+ can oxidize OH^- and H_2O molecules adsorbed on the TiO_2 surface to produce •OH radicals. However, e− and h+ often recombine with low efficiency, limiting photocatalytic activity. The introduction of nitrogen-doped carbon quantum dots (NCQDs) serves to enhance visible light absorption and promote charge transfer. Consequently, more photocarriers are generated, and their recombination is substantially suppressed, resulting in a notable increase in efficient active radicals. Consequently, with the combined action of h+, •O_2-, and •OH radicals, methylene blue (MB) molecules undergo mineralization to yield CO_2 and H_2O [177].

In a comprehensive photocatalytic process employing a TiO_2-based photocatalyst, three primary stages are involved: (1) absorption of light and the generation of photogenerated electron-hole pairs by TiO_2, (2) separation and transfer of these photogenerated electron-hole pairs, and (3) redox reactions occurring on the surface of TiO_2 and cocatalysts (as depicted in **Fig. 8(e)**). These consecutive steps collectively govern the overall photocatalytic effectiveness of TiO_2-based photocatalysts [178]. On the other hand, to utilize semiconductor photocatalysts for water treatment, several requirements must be met: the process should be feasible at room temperature and pressure, ensuring complete mineralization without generating secondary pollution [179]. In addition, it should enable repetitive cycles and maintain low operational costs. TiO_2 photocatalysis embodies a photo-induced charge separation process occurring on the TiO_2 surface, which generates highly reactive oxygen species capable of microbial inactivation and organic mineralization without producing secondary pollutants.

View Article Online
DOI: 10.1039/D4TA03877K

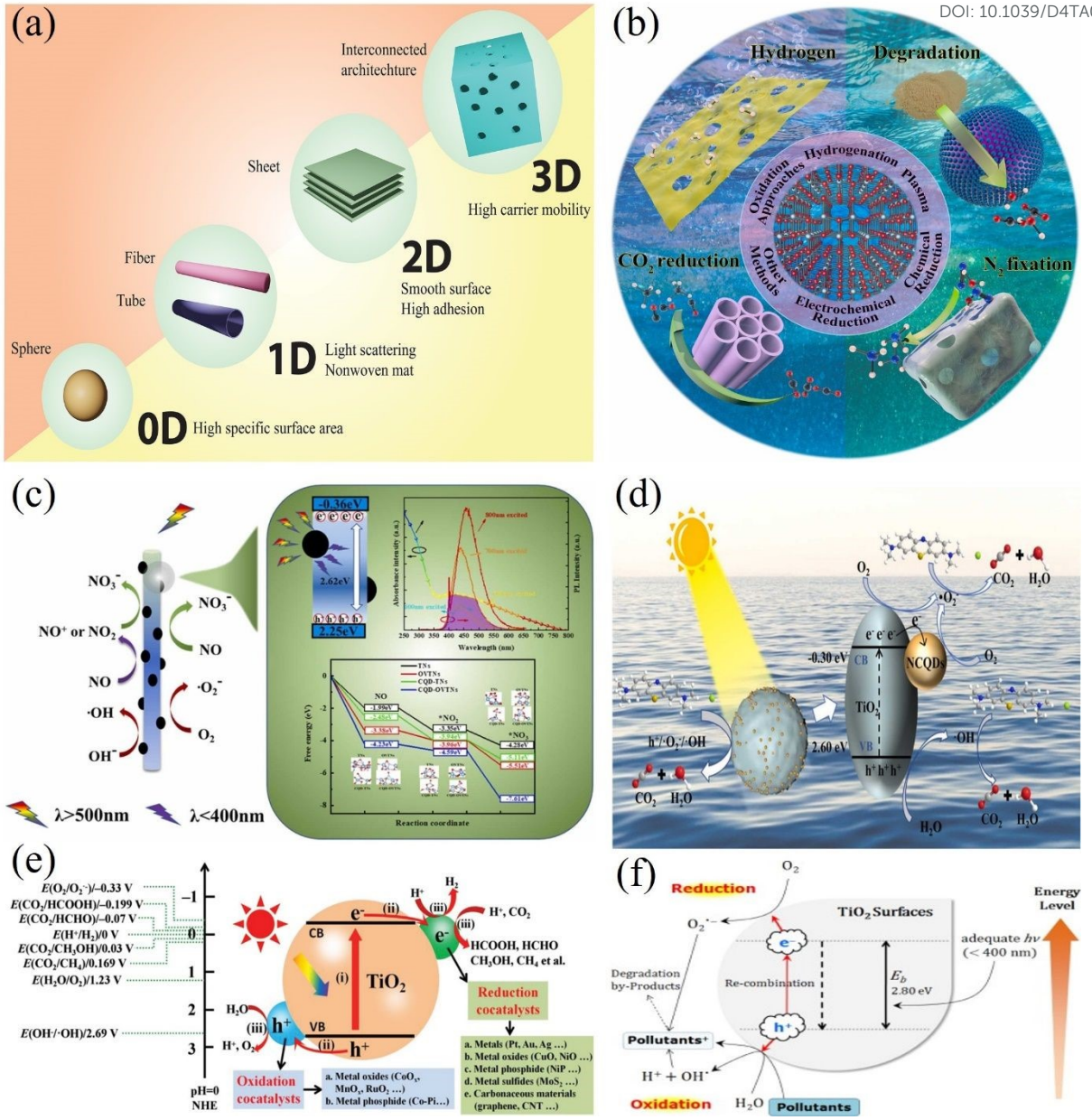

Fig. 8. (a) Various structural configurations of TiO_2 at both the nano and macro scales. Adopted from Ref. [171] with permission. (b) A schematic diagram depicting the utilization of defective TiO_2 materials in photocatalytic applications. TiO_2 photocatalysts are fabricated using various methods such as hydrogenation, plasma treatment, chemical reduction, electrochemical reduction, and oxidation. Adopted from Ref. [175] with permission. (c) Oxygen vacancies and carbon quantum dots (CQDs) with up-conversion properties for enhanced photocatalytic activity of TiO_2 for NO removal under visible light irradiation. Adopted from Ref. [176] with permission. (d) Mechanism for the degradation of methylene blue using NCQDs/TiO_2 under solar irradiation. Adopted from Ref. [177] with permission. (e) Illustration of the photocatalytic reactions occurring on TiO_2-based photocatalysts, enhanced with reduction and oxidation cocatalysts. The redox potentials of various species at pH = 0, referenced to the NHE, are also depicted. Adopted from Ref. [178] with permission. (f) Pollutant removal through the generation of photoinduced charge carriers (e−/h+) on the surfaces of semiconductor TiO_2 particles. Adopted from Ref. [179] with permission.

View Article Online
DOI: 10.1039/D4TA03877K

The schematic representation depicted in **Fig. 8(f)**, illustrates the elimination of pollutants through the generation of photoinduced charge carriers (e−/h+) on the surfaces of semiconductor TiO_2 particles [179]. Upon exposure to UV light, the surface of TiO_2 catalysts suspended in water triggers photo-induced electrons in the conduction band to participate actively in reduction processes. Typically, they interact with dissolved oxygen in the air, resulting in the generation of superoxide radical anions. Meanwhile, the photo-induced holes in the valence band migrate to the surface of TiO_2 and react with adsorbed water molecules, leading to the formation of hydroxyl radicals [179]. It is worth noting that hydroxyl radicals (OH•) play a crucial role as primary active species in the photocatalytic oxidation reaction.

Regarding the environmental impact, TiO_2 has been described as eco-friendly as not only is it reusable (for photocatalysis) but it is also non-toxic [170,180], with Chen et al. [181] claiming it's "the most efficient and environmentally benign photocatalyst". However, there is concern over the potential effects of TiO_2 nanoparticles on humans and animals [182]. Although the shape and magnitude of TiO_2 nanoparticle effects are mostly determined by the physical and chemical properties of the particles, research on the mechanistic toxicology of these particles indicates that they may induce genotoxicity, inflammation, and cell destruction. TiO_2 nanoparticles have been identified by the National Institute for Occupational Safety and Health as potentially carcinogenic to humans as a result [182]. In their life cycle assessment (LCA), Wu et al. [183] evaluated the impact of nano-TiO_2 based on a range of synthesis routes. They discovered that physical synthesis approaches produced a greater environmental impact since they needed large amounts of supporting gas and substantial energy inputs. Chemical routes have a fair amount of impact, with upstream precursor production accounting for a large share of that impact. Because of the bacteria culture media utilised, biological channels also posed a significant environmental impact. Because organic precursors required large amounts of organic solvents,

View Article Online
DOI: 10.1039/D4TA03877K

they performed especially poorly. The LCA model included a freshwater ecotoxicity evaluation factor to account for the possibility of nano-TiO_2 leakage into water sources. It is crucial to remember that while appropriate modelling assumptions have been made and some TiO_2 production pathways are not covered by this LCA, total correctness cannot be guaranteed [183].

On the other hand, TiO_2 is generally considered cost-effective for photocatalytic uses [180]. Furthermore, novel cost-effective production methods are still being developed. An example is the facile sequential calcination and ball milling strategy [184]. It was stated that a post-treatment procedure was developed for less expensive TiO_2 photocatalysts with lower photocatalytic activity. The straightforward and affordable method seeks to raise the less expensive TiO_2 photocatalysts' photocatalytic activity to the same degree as more expensive commercial counterparts with higher photoactivities. This procedure about ninety-fold improves the performance of inexpensive KA100 in lab testing. In addition to TiO_2, zinc oxide (ZnO) and carbon-based materials have garnered significant attention as photocatalysts due to their excellent transport properties, affordability, and versatile morphological structures. In the work of Sansenya et al. [185], photocatalyst based on ZnO with a specific surface area of about 10.6 m^2/g were prepared. The materials have demonstrated high photodegradation capacity of reactive red 141 (R141), Congo red (CR), and Ofloxacin after 20, 60, and 180 minutes of solar light irradiation, respectively. The stability of the photocatalyst was confirmed after three cycles of use, maintaining high performance even after the third cycle, indicating its promising reusability. In similar context, silver was incorporated into ZnO photocatalysts at varying concentrations, exhibited a hexagonal phase with notable performance under visible light and improved anti-photocorrosion properties [186]. Complete removal of reactive red dye and ofloxacin antibiotic was achieved after 25 and 80 minutes of irradiation, respectively. The enhanced photocatalytic activity is attributed to the efficient separation of electron-hole pairs

View Article Online
DOI: 10.1039/D4TA03877K

at the photocatalyst interface. The introduction of metallic silver onto the ZnO photocatalyst creates a Schottky barrier at the silver/ZnO interface, which enhances quantum efficiency and photocatalytic activity.

Kim et al. [187] introduced a novel, high-efficiency catalyst based on a boron-doped C3N4/ZnO composite. This composite demonstrated a significantly enhanced photocatalytic hydrogen evolution rate, approximately 2.9 times greater than that of undoped C3N4/ZnO. This is a straightforward and effective approach for designing highly efficient heterojunction photocatalysts by utilizing charge transfer switching via doping. Recently, it has been found that decorating the Rh co-catalyst of the benchmark GaN–ZnO photocatalyst with Al_2O_3 species via atomic layer deposition significantly mitigates reverse reactions [188]. This modification enhances photocatalytic oxygen water splitting (OWS) activity by more than an order of magnitude, with an apparent quantum efficiency increasing from 0.3 to 7.1% at 420 nm. The partial coverage of Rh surface sites with inert Al_2O_3 effectively suppresses reverse reactions by obstructing the reduction/oxidation cycle of Rh atoms during the photocatalytic OWS process. Moreover, combining ZnO with carbon-based materials, such as graphene oxide, can further enhance its photocatalytic properties. Indeed, an efficient photocatalyst was successfully synthesized using GO/ZnO nanocomposites with embedded metal nanoparticles through a simple one-pot method [189]. A catalytic activity of 84% for the degradation of methylene blue (MB) dyes was achieved with a nanocomposite containing 3.125% GO after 90 minutes of sunlight irradiation. Thus, the GO–ZnO–Ag nanocomposite demonstrates significant potential as an efficient and adaptable photocatalyst for the photodegradation of organic dyes in industrial wastewater. In another work, the photocatalytic degradation of Rhodamine B (RhB) and MB by a material comprising sol-gel synthesized ZnO nanochips, GO and RGO was discussed [190]. Results indicated that ZnO nanochips integrated onto graphene sheets exhibited enhanced

View Article Online
DOI: 10.1039/D4TA03877K

photocatalytic activity, achieving approximately 76.5–98.9% degradation of RhB and MB within 90 minutes of visible light irradiation. Furthermore, ZnO@RGO demonstrated superior photocatalytic performance compared to ZnO@GO, with approximately 2.4 and 2 times higher kinetic rates for the removal of RhB and MB, respectively.

Common materials like TiO_2, ZnO, and GO are popular photocatalysts, but they have notable limitations compared. TiO_2 and ZnO both have wide band gaps (~3.0-3.2 eV and ~3.2 eV, respectively), restricting their activity to UV light, which limits their effectiveness under visible light. Both materials also suffer from rapid recombination of electron-hole pairs, reducing their photocatalytic efficiency. Additionally, TiO_2 and ZnO have lower surface areas, limiting the number of active sites, and ZnO is further hampered by photo corrosion under UV light. GO, while possessing a high surface area, offers limited photocatalytic activity on its own and primarily functions as a support material. Its variable band gap and the complexity of reducing GO to rGO for enhanced activity also pose challenges. In contrast, MOFs offer greater flexibility with tunable band gaps, higher surface areas, and versatile functionalization options, making them superior photocatalysts for a wide range of applications.

4.2 Metal organic frameworks as photocatalysts

Heterogeneous photocatalysis (HP) stands as an advanced oxidation method that has surfaced as a promising alternative with a broad spectrum of applications. These applications include treating effluents for decontamination and disinfection, addressing environmental challenges related to pollutants like CO_2 and NO_x in the atmosphere, and facilitating energy conversion. These are among the most prevalent and widespread uses of this technology. In this context, metal-organic frameworks (MOFs) have been developed to enhance the characteristics and photocatalytic capabilities of conventional semiconductors. MOFs have emerged as innovative photocatalysts due to their intrinsic structural features, which include vast surface area,

organised porous structure, and structural diversity. This application is especially well-suited for MOFs since they can combine photosensitiser and catalytic functions into a single structure [191]. The high porosity of MOFs (macropores larger than 50 nm in some cases) enables rapid substrate and product transport/diffusion from the catalytic sites [22]. Additionally, organic ligands have the ability to absorb photons and transfer electrons from the ligand to the metal centre, thereby generating an excited state in the process. Thus, the utilization of MOFs as photocatalysts encompasses a diverse and extensive range of applications (**Fig. 9(a)**) [192].

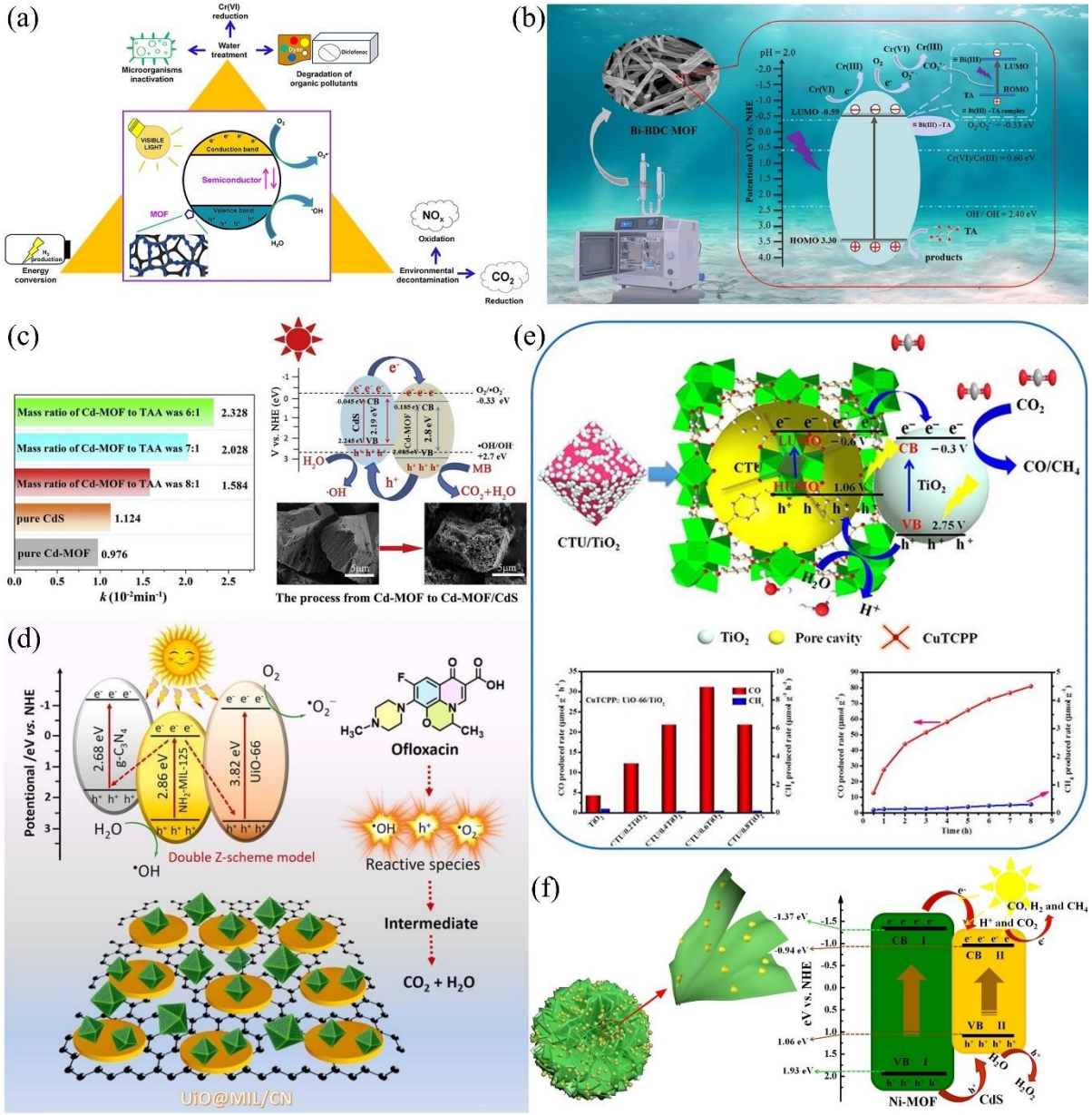

Fig. 9. (a) Composite materials featuring metal-organic frameworks for heterogeneous photocatalysis driven by visible light. MOF-based composites have potential applications in the

degradation of organic compounds, reduction of Cr(VI), inactivation of microorganisms, oxidation of NOx, reduction of CO_2, and production of H_2. Adopted from Ref. [192] with permission. (b) Microwave-assisted synthesis of Bi-BDC MOF photocatalyst and its efficient reduction of Cr(VI) within 6.0 min under low-power LED UV light. Adopted from Ref. [193] with permission. (c) Visible light CdS/Cd-MOF photocatalyst with enhanced photodegradation of methylene blue (91.9% in 100 minutes under simulated sunlight irradiation). Adopted from Ref. [194] with permission. (d) Double Z-scheme heterojunction based on UiO/MIL/CN for the photocatalytic degradation of ofloxacin under visible light irradiation. Adopted from Ref. [195] with permission. (e) CuTCPP-functionalized zirconium MOF and TiO_2 for photocatalytic CO_2 reduction to CO under simulated solar illumination. The figure contains the dependence of total CO/CH_4 evolution on the amount of TiO_2 and various CTU/TiO_2 ratios under Xe lamp irradiation (λ > 300 nm) within 1 hour, total CO/CH_4 evolution amount produced by $CTU/0.6TiO_2$ under Xe lamp irradiation within 8 hours, and a proposed photocatalytic CO_2 reduction pathway over CTU/TiO_2. Adopted from Ref. [196] with permission. (f) 3D hierarchical structure of CdS/Ni-MOF and schematic diagram illustrating the electron transfer process and photocatalytic mechanism involved in the reduction of CO_2. Adopted from Ref. [197] with permission.

Regarding the elimination of Cr(VI) from water, Gao et al. [193] have synthesized a high-throughput MOF composed of Bi-benzene-1,4-dicarboxylic acid (Bi-BDC) and featuring a consistent rod-like structure using a microwave-assisted technique (**Fig. 9(b)**). This MOF demonstrated the capability to achieve a complete photocatalytic reduction of Cr(VI) in just 6.0 minutes when exposed to low-power LED UV light [193]. Furthermore, the degradation of contaminant was also reported using MOFs photocatalyst. Jing et al. [194] constructed a binary CdS-Cd-MOF nanocomposite by an *in-situ* sulfurization of Cd-MOF. When exposed to simulated sunlight, the degradation rate of methylene blue using 10 mg of the material reached 91.9% within 100 minutes [194]. The mechanism of the photocatalytic degradation is described based on the difference in the band gap between the CdS (2.29 eV) and Cd-MOF (2.8 eV) (**Fig. 9(c)**). In a similar context, a recent study investigates the photocatalytic degradation of ofloxacin using UiO/MIL/CN [195]. In this work, the synthesis involved growing UiO-66 on the surface of NH_2-MIL-125 using the solvothermal method to create MOF-on-MOF architectures. Following that, the authors achieved the successful deposition of g-C_3N_4 nanosheets onto the surface of UiO-66/NH_2-MIL-125, resulting in the development of a novel double Z-scheme heterojunction photocatalyst (**Fig. 9(d)**). When exposed to visible light, this double Z-scheme

View Article Online
DOI: 10.1039/D4TA03877K

heterojunction serves as an exceptionally efficient photocatalyst for the degradation of ofloxacin, exhibiting a rate constant of 0.07 min^{-1} [195].

Furthermore, the photocatalytic reduction of carbon dioxide into valuable chemicals stands as an appealing technique, addressing both environmental concerns and energy scarcity simultaneously. Interestingly, MOFs have garnered significant interest in this field due to their remarkable chemical and structural diversity. Wang et al. [196] employed an in-situ hydrothermal process to combine TiO_2 nanoparticles with a mixed ligand-based MOF structure consisting of CuTCPP and BDC (CTU). This integration resulted in the formation of CTU/TiO_2 nanocomposites, which effectively merge MOFs with inorganic semiconductors (**Fig. 9(e)**). When employed as photocatalysts for CO_2 conversion under simulated solar light ($\lambda > 300$ nm), the optimized CTU/TiO_2 heterostructure demonstrated significantly enhanced performance [196]. The rate of CO_2 reduction into CO reached 31.32 μmol/g h, approximately seven times higher than that achieved with bare TiO_2. In another study conducted by Xu et al. [197], they explored the development of 3D hierarchical CdS/Ni-MOF photocatalysts. These photocatalysts exhibited a notably CO yield, surpassing the yields achieved by both Ni-MOF and CdS individually by 16 and 7 times, respectively. The researchers proposed a preliminary mechanism for the CO_2 conversion process (**Fig. 9(f)**). Upon exposure to UV-Vis light, both Ni-MOF and CdS become excited, generating electrons (e-) and holes (h+). Their intimate interface facilitates the efficient transfer of excited electrons from Ni-MOF to CdS, which boasts a more positive conduction band [197]. Consequently, CdS, acting as the active site, proficiently reduces CO_2 to CO. Concurrently, the holes in the valence bands of Ni-MOF and CdS engage in oxidation reactions, yielding oxygen and hydrogen peroxide, effectively eliminating the holes. This well-coordinated charge separation and electron-hole pair transfer contribute to the enhanced photocatalytic activity of the system.

View Article Online
DOI: 10.1039/D4TA03877K

Because the careful selection of linkers/metal clusters or the addition of catalysts can significantly increase light adsorption, reactant adsorption, charge separation, and reactant activation, the modification of MOF elements is especially crucial for photocatalyst applications [23]. As a result, photocatalytic performance will be enhanced. Sensitiser addition is one example of modulating ligand and metal clusters. MOFs can incorporate sensitisers (metal complexes or organic dyes) to increase the amount of visible-light-driven photocatalysis [167]. In their study, Furukawa et al. [24] successfully introduced dyes and encapsulated precious metals into a series of MOF photocatalysts, producing an enhanced photocatalytic performance for almost all MOFs tested as well as a slightly increased spectrum region for photoactivity. In a similar vein, Pt/ NH_2-MIL-125(Ti) was used in visible light for CO_2 reduction [23]. The results of this were also positive with the material showing an improvement in photocatalytic performance when compared to the plain NH_2-MIL-125(Ti). Pt/NH_2-MIL-125(Ti) exhibited a remarkable boost in its photocatalytic efficiency for CO_2 reduction into formate. Over the course of 8 hours of irradiation, Pt/NH_2-MIL-125(Ti) yielded approximately 12.96 mmol of formate, representing a notable 21% increase in activity when compared to the performance of pure NH_2-MIL-125(Ti). These experiments suggest that the use of precious metals in MOFs to improve photocatalytic behaviour has great potential.

Furthermore, studies indicate that MOFs' thermal and chemical stabilities are a bonus and contribute to their appeal as catalysts and catalytic hosts. Zhao et al. [22] posit that MOF photocatalysts should be stable under service conditions, including water. In addition to this, MOF photocatalysts have shown resistance to moderately acidic and basic solutions [22]. An example of an aquatically stable MOF can be found in Drache et al. [198] report in which they investigated a series of Zr-based MOFs and found they exhibited excellent stability in water.

The authors suggest that this is a result of the strong coordination between the organic ligands and the Zr nodes. Howarth et al. [199] recommend another method to improve the stability of MOFs in water, involving decorating the MOF organic linkers with sulphonic, fluorinated, or phosphonate substituents. Metal oxide encapsulation within MOF photocatalysts is an additional line of inquiry. POMs, or polyoxometalates, have attracted a lot of interest because of their exceptional redox capacity, highly negative charges, and structural characteristics [22]. When POM $[(PW_9O_{34})_2Co_4(H_2O)_2]$ was encapsulated in MOF-545 the product was able to endure reversible electron transfer reactions with negligible structural degradation [200]. This material was also successfully used for water oxidation under visible light. As demonstrated, recent advancements have introduced numerous new MOFs and MOF-based composites specifically designed for the photocatalytic reduction of CO_2. MOFs are recognized as state-of-the-art photocatalysts due to their exceptional coordination between active metal centers and organic linkers. Their unique structural features such as vast surface areas, well-ordered frameworks, high porosity, and significant structural tunability contribute to their effectiveness [201]. Compared to traditional catalysts, MOF-based photocatalysts present several advantages, including ultra-high specific surface areas, adjustable pore structures that enhance CO_2 adsorption and reduction and unlike homogenous photocatalysts, they are easily separated from the reaction products and can therefore be reused many times [22]. As such, MOF photocatalysts will have a longer lifetime, contributing to a decrease in waste, end-of-life process costs, and pollution. Additionally, the metal nodes and organic ligands in MOFs can be selectively functionalized, and the abundant pores allow for the accommodation of various functional guest substances.

Despite these benefits, challenges persist in the use of MOFs composites as photocatalysts. These include low visible light utilization efficiency, poor stability with rapid loss of activity

View Article Online
DOI: 10.1039/D4TA03877K

and structural integrity after several cycles, and reliance on organic sacrificial reagents and solvents that pose environmental concerns. Furthermore, not much research has been done on how MOFs employed in photocatalytic applications affect the environment. An LCA could be performed to more accurately assess the possible impact of MOF photocatalysts. On the other hand, as previously noted, the synthesised MOFs continue to be costly because of the intricate synthesis procedures and the absence of mass production processes, even though the component linkers and ions are frequently quite affordable [18]. However, MOFs improved efficiency compared to TiO_2 photocatalysts and their potential for an extended lifetime will likely reduce their long-term costs.

5. Evaluation and comparison

Investigating potential MOF as sorbents, SCs electrodes or photocatalysts is a difficult endeavour due to the vast number available, with over 90,000 synthesized MOFs in the public domain [202]. However, the creation of software with these capabilities is yet to be achieved [35]. To increase the TRL level of MOF sorbents, pilot-scale MOF production needs to be investigated. Methods of bulk-producing structured MOFs are imperative if they are to be used for industrial use. **Table 3** shows a summary of the advantages and disadvantages of MOFs, liquid amine, activated carbon, as well as titanium dioxide for application in various technologies identified from a review of recent literature.

Table 3. Advantages and disadvantages of MOFs, liquid-amine, activated carbon, and TiO_2 technologies for uses in CCS, SCs electrodes and photocatalysis.

	Advantages	Disadvantages
	• Controllable morphology (pore size). • MOFs are used for CCS at lower temperatures compared to amines [52]. • CO_2 capture capacity ≥ amine scrubber under the same dry working conditions [32]. • Solid sorbents have a much lower heat capacity compared to liquid-amine solutions [32]. • Suitable for DAC processes [33].	• Still in early developmental stages – further research is required [191]. • Poor stability under CCS operational conditions [18]. • Prone to decompose when exposed to moisture [18]. • Poor thermal conductivity (leading to higher regeneration costs and slower regeneration processes) [36].

MOFs	• Some MOFs can provide a greater CO_2 uptake capacity, good SCN, and acceptable regeneration energy requirements [50]. • Reduced effect on power plant efficiencies [203]. • High capacitance compared to ACs. • Some MOFs show exceptional cyclic stability [22]. • High power densities. • Possibility of using waste PET for production [113]. • Light harvesting range can be extended to include visible/NIR light through the inclusion of long-wavelength-light-responsive units within the MOF. • Can reduce recombination of the photogenerated electrons and holes. • Some MOFs have shown improved photocatalytic behaviour. • Reported successful application under mild conditions.	• CO_2 capture capacity can be reduced in the presence of moisture [18]. • Lack of processes to convert MOF powders into devices [18]. • Low CO_2 capacity in the presence of water [27]. • Reports of poor stability over multiple cycles of absorption/desorption [27]. • Can have high production costs [27]. • All the feasible methods to modify MOFs for DAC currently rely on amine doping [62]. • Little known about MOF toxicity. • Suitability for widescale deployment not well established • Comparatively complex synthesis process. • The stability of MOFs under photocatalytic reaction conditions requires more research – some reports of low stability.
Liquid amines	• Proven success in bulk scale CCS [18]. • The most developed method of CCS [25]. • MEA has a high CO_2-carrying capacity [27]. • MEA has a fast absorption rate [27]. • Amines can provide high separation/purification performance [18]. • Some liquid amines like MEA are low-cost [26]. • MEA is readily biodegradable [26].	• Energy intensive - High solvent regeneration energies (>140 °C) [31]. • Requires large equipment [31]. • Prone to equipment corrosion and requires inhibitors to prevent it [31]. • Prone to degradation [25]. • Can reduce the overall efficiency of a powerplant [18]. • Limited potential for performance improvement [19]. • High cost, and levels of sorbent loss [33,35]. • Highly toxic and environmentally harmful, not suitable for DAC [33]. • Insufficient CO_2 capacity for industrial-scale emissions mitigation [25].
Coconut shell activated carbon	• Low cost [80]. • Raw material readily available [80]. • High thermal and electrochemical stability [204]. • Renewable and non-toxic [204]. • Low net GHG emissions over the lifespan [96].	• Low power densities. • Capacitive performance is not as high as that offered by some MOFs • Low specific capacitance [83].
Titanium dioxide	• Showed great promise for commercial use [170]. • Non-toxic [170]. • Environmentally benign [181]. • Suitably efficient photoactivity [205]. • High stability [205]. • Low cost [205].	• Complex separation process [206]. • Prone to aggregation [206]. • Rapid rate recombination of the photogenerated electron-hole pairs [206].

- Photocatalytic activity is restricted to the UV region (low photocatalytic efficiency) [207].

5.1 Carbon capture

Metal-organic frameworks (MOFs) present numerous advantages over non-MOF materials for applications in carbon capture. MOFs such as MOF-5 and HKUST-1 exhibit exceptional surface areas and porosity, exceeding 1000 m²/g, which translates to higher CO_2 adsorption capacities up to 33.5 wt% and 31.0 wt% respectively under standard conditions [208]. This is significantly better than traditional materials like zeolites and activated carbons, which have lower surface areas and CO_2 adsorption capacities. The tunability of MOFs allows for precise control over pore size and functionality, enhancing selectivity towards CO_2, as demonstrated by ZIF-8's CO_2/N_2 selectivity of 25 at room temperature. However, MOFs generally show high sensitivity toward moisture and high structural degradation, such as MOF-5, which can lose as much as 90% of its CO_2 adsorption capacity under humid conditions. Moreover, high synthesis and processing costs, along with difficulties in the production of defect-free membranes, are of vital importance against scalability. Carbon capture performance metrics are important. Although MOFs showed an upper CO_2-carrying capacity compared to liquid amines in the laboratory tests, both materials showed a suitable level of CO_2 selectivity with excellent selectivity shown by MOFs doped with amines. MOFs doped with amine dopants also had lower regeneration energies compared to liquid amines. The possibility of development is higher for MOFs due to their tunable structure and number of available MOFs. While MOFs are under development, liquid amines find industrial applications. Both materials have stability problems under CCS conditions, and as far as reported there was no problem of corrosion observed with MOF, unlike liquid amines which in addition to being corrosive are volatile. On performance, MOF scores 128 against liquid amine's 93. The three broad factors were further allocated relative weightings based on the findings of the literature review and summed up to

View Article Online
DOI: 10.1039/D4TA03877K

100. For C-capture, the weights were distributed as performance 34/100, environmental impact 25/100 and cost implications 41/100. The factors, along with weightings for the evaluation of carbon capture materials, are shown in **Table 4**, and the comparison matrix showing the scoring of liquid-amine and MOF-based materials against these factors is presented in **Table 5**.

Table 4. C-capture factors and corresponding suggested weighting along with the justifications.

Subject	Factor	Weighting	Justification
Performance	CO_2-carrying capacity	3	This affects the efficiency of the material and influences the amount of sorbet required for a CCS application [18].
	CO_2 selectivity	3	This affects the purity of adsorbed CO_2 and the concentration of CO_2 in the emitted flue gases [18].
	Regenerability	3	This affects the energy efficiency of the C-capture process [31].
	Potential for development	1	All current technologies (both liquid amine and MOF sorbents) require further improvement before they can be deployed on an industrial scale. Therefore, the material must offer enough scope/potential for these changes [31].
	Current successful application	2	CCS technology takes a considerable period of time to test and validate, very few materials make it to trials and even fewer are successful in reaching real-world applications [19]. Successful small-scale trials or real-world trials are good indications of the material's suitability.
	Stability under service conditions	3	The material used in CCS applications must be able to withstand the operating conditions and regeneration conditions to perform well.
	Corrosivity and volatility	2	Ideally, materials used should not be volatile as that can lead to high levels of sorbent loss and reduced levels of performance over time [33]. Corrosive materials can also cause performance issues as they may damage equipment, thus reducing its efficiency [33].
	Material recyclability	3	For the technology to be "future-proof" it needs to be sustainable.
	Toxicity	2	A toxic material is detrimental to the environment, it can also result in

Environmental impact			higher costs for disposal at the end of the products life.
	Production methods	2	Energy-intensive production methods may negate some of the benefits of the technology use.
	Functional energy requirements	3	Literature suggests that the application of post-combustion CCS can lead to an overall reduction of a power plant's efficiency [19].
Cost	Raw material cost	2	Influences the overall cost of a material. It is also important to consider the likelihood of a significant change in the price of a material.
	Usage costs (equipment, temperature/pressure requirements)	3	If a technology is excessively expensive then it will likely never be suitable for wide-scale deployment. Furthermore, if the costs of using the technology outweigh the benefits then it is likely the technology will fail or be superseded and become obsolete.
	Synthesis/manufacturing costs	3	High production costs can act as a barrier to wide-scale technology deployment. It is also important to consider if the production costs are likely to reduce when the technology develops further/becomes more mainstream.

1771

1772 **Table 5.** Comparison matrix between liquid amines and MOFs for C-capture applications.

Factor	**Weighting**	**Material score**		**Justification**
		Liquid-amines	**MOFs**	
CO_2-carrying capacity	6	3	5	MOFs have shown higher CO_2-carrying capacities in laboratory tests [52].
CO_2 selectivity	5	3	3	Both materials have shown suitable levels of CO_2 selectivity [52]. While pristine MOF sorbents have shown SCN values below those of liquid-amine sorbents, amine-doped MOF sorbents have shown excellent SCN values exceeding those of liquid-amine sorbents [18].
Regenerability	5	3	4	While both materials have shown acceptable (albeit high) results for required regenerability energy, some amine-doped MOF sorbents have exhibited lower regeneration energies [18,31].

Potential for development	4	1	5	Liquid amine technology provides little potential for further development whereas MOF sorbents provide vast potential due to their customisable structure and the number of available MOFs [19,25]. Furthermore, MOFs have shown potential for DAC [62].
Current successful application	5	4	2	Liquid amines are already used in industry but are yet to be rolled out on a wide scale [25]. MOFs for CCS are still in their developmental stages and are a long way from real-world trials [52].
Stability under service conditions	6	3	3	Both pristine MOF sorbents and liquid-amine sorbents have issues with stability under CCS conditions [18,25]. Whilst, amine-doped MOFs have shown improved stability under regeneration and service conditions, they are still mildly affected by the presence of moisture [18].
Corrosivity and volatility	3	1	5	Liquid amines are shown to be very corrosive and can cause damage to equipment if it has not been given a protective coating [25]. Liquid amines are also very volatile and therefore the process can be subject to high levels of sorbent loss [33]. There are currently no reported issues with MOF sorbents and corrosion.
Performance score:		93	128	
Recyclability	4	3	3	Recycling prospects for both materials are reasonably poor [18,26].
Toxicity	8	1	4	Liquid amines are toxic [33]. There is limited research into the toxicity of MOFs however, the literature suggests that some may be toxic when they start to decompose [125].
Production methods	7	3	3	The production of both materials is both complex and reasonably energy-intensive.
Functional Energy requirements	6	3	4	MOFs have shown potential for CCS at a lower temperature than those used for liquid-amine CCS [52]. Furthermore, amine-doped MOF sorbents have a lower regeneration energy requirement compared to liquid-amine sorbents [18].
Environmental impact score:		59	89	
Raw material cost	14	3	2	The cost of the MOFs constituent linkers and metal clusters is relatively cheap [18]. However, pre-synthesised MOFs are expensive due to complex production processes [18]. Some liquid-

				amines like MEA are relatively low-cost [26].
Usage costs (equipment, temperature/pressure requirements)	15	3	4	MOFs have demonstrated the potential for CCS at lower temperatures [52]. Liquid-amine scrubbers have also been shown to reduce the overall efficiency of a power plant to a greater degree than the predicted effects of MOF sorbents [18,203].
Production costs	12	3	2	As previously discussed, MOFs are expensive due to complex production processes. Liquid-amine technology is comparatively well-developed, and processing costs are cheaper [26].
Cost score:		123	112	
Overall scores:		275	329	

Note: All materials were evaluated for each factor using a scale ranging from 1 to 5 (where 1 corresponds to "very bad," 2 to "bad," 3 to "suitable," 4 to "good," and 5 to "very good").

Carbon capture technology stands as one of the most important strategies for mitigating climate change through the reduction of CO_2 emissions from industrial sources. There are three major parameters used that express a comparison among the different carbon capture methods: their cost, efficiency, and environmental impact. Cost means the financial expenditure incurred to capture, transport, and store CO_2, including capital, operational, and maintenance costs. Advanced carbon capture methods using MOFs reduce this cost to a large extent. For example, conventional amine-based capture processes may range between \$40–\$100 per ton of CO_2 captured while advanced materials, such as MOFs, are expected to drop these costs down to \$20–\$50 per ton by the increase in efficiency and reduction in energy requirements [209]. Efficiency is the percentage of CO_2 that can be captured from the sources of emission relative to the total amount of emissions produced. Traditional methods have efficiencies of 85–90%, while MOFs and other advanced materials could theoretically be as high as 95–99% according to the study on 2D MOFs for the reduction of CO_2, where $Cu_3(C_{12}N_6S_6)_2$ demonstrated very high activity with small overpotentials, which reflects high efficiency in the processes of capture and conversion of CO_2 [210]. Environmental impact looks at the bigger picture of how carbon capture affects the environment in general, such as the probable risks associated with

View Article Online
DOI: 10.1039/D4TA03877K

the leakage of CO_2 during storage, the energy used by capture and sequestration, and the net reduction of GHG emissions. While traditional methods may leave room for a capture process that is 10–20% more energy-intensive, advanced MOF-based methods can reduce this extra energy requirement to under 10%, making the process more sustainable. Moreover, according to the researchers in this study, 2D MOFs showed improved selectivity toward CO_2 reduction relative to competing reactions, such as hydrogen evolution, which further minimizes unwanted environmental impacts. The utilization of 2D MOF as an advanced material in carbon capture technology shows a very promising avenue toward cost-effective, efficient, and environmentally sustainable processes.

5.2 Photocatalysis

Given the very high porosity of the MOFs, the surface area can reach more than 3000 m^2/g. Such high values raise the adsorption and reduction rates of CO_2 in photocatalysis. Furthermore, their tunable structure provides conditions for the introduction of different metals, increasing active sites, and enhancing photocatalytic properties. Also, the MOFs exhibit enhanced light harvesting and photostability, which is very critical in efficient photocatalysis [211]. However, these materials have low stability in an aqueous/high-temperature environment and poor light absorption, thereby mostly limiting their application to only the ultraviolet regime, with the added need for sophisticated and expensive synthesis methods. MOFs demonstrated lower recombination rates and higher resistance to aggregation compared to titanium dioxide, which, although highly stable, is prone to aggregation. While titanium dioxide is restricted to UV light, MOFs can be active in a broader spectrum that includes visible light. Moreover, the MOFs provide larger surface areas with increased resistance to photo-corrosion. MOFs score 176 while titanium dioxide scores 116, hence superior efficiency for performance evaluation. The evaluation parameters are weighted as performance, which is efficiency, at 45/100, environmental impact at 18/100 and cost implications at 37/100. Performance factors include

View Article Online
DOI: 10.1039/D4TA03877K

photostability, the extent of light absorption and recombination rates 180. Environmental impact factors include stability of materials in various environments and resistance to photo-corrosion. These are, among others, the complexity and cost of the synthesis methods. **Table 6** presents the evaluation criteria in the case of photocatalysis, and **Table 7** presents a detailed comparison between titanium dioxide and MOFs in photocatalytic applications.

Table 6. Photocatalysis factors and the corresponding suggested weighting along with the justifications.

Subject	Factor	Weighting	Justification
Performance	Recombination rate	3	Low recombination rates are desirable as it directly effects the efficiency of the photocatalyst.
	Stability under photocatalytic conditions	3	The photocatalytic material must be able to withstand the operating conditions to perform well.
	Level of current development	2	Successful small-scale trials or real-world trials are good indications of the material's suitability.
	Resistance to Aggregation	2	Material aggregation can block the active sites of a material and therefore reduce the effective surface area of the material and consequently reduce its efficiency.
	Photocatalytic activity under Visible light	3	In order to maximise the efficiency of a photocatalyst, ideally it should be photoactive in a wide region of the light spectrum as possible. Most current photocatalysts are only active in the UV region of the spectrum.
	Material morphology	3	This has been shown to greatly influence the efficiency of photocatalysts [206].
	Resistance to photo corrosion	2	High resistance to photo corrosion is desirable as photo corrosion can lead to a reduction in performance over time.
Environmental impact	Toxicity	3	A toxic material is detrimental to the environment, it can also result in higher costs for disposal at the end of the product's life.
	Energy requirements for processing raw materials	2	Energy-intensive processing methods can be detrimental to the environment. This is an important consideration for technologies with a wide-scale deployment aim.
	End of life outlook	2	For the technology to be "future-proof" it needs to be sustainable.

			Consequently, the option for recycling or safe disposal is very important.
Cost	Raw material cost	3	This greatly influences the overall cost of a material. It is also important to consider the likelihood of a significant change in the price of a material.
	Production costs	3	High production costs can act as a barrier to wide-scale technology deployment. It is also important to consider if the production costs are likely to reduce when the technology develops further or becomes more mainstream.

1824

1825 **Table 7.** Comparison matrix for titanium dioxide and MOFs for photocatalytic applications.

Factor	Weighting	Material Score		Justification
		TiO_2	MOFs	
Recombination rate	7	2	4	MOFs have shown reduced recombination rates.
Stability under photocatalytic conditions	8	4	3	Titanium dioxide has shown high stability under photocatalytic conditions [205]. MOFs however, have shown some degradation under these conditions [23].
Level of current development	4	5	4	Titanium dioxide has shown issues with aggregation [206] unlike MOFs.
Resistance to Aggregation	5	1	3	ACs are prone to aggregation and therefore often have to be used as a gel suspension, this often limits the reduction of the device size.
Photocatalytic activity under Visible light	9	1	5	Titanium dioxide's photoactivity is restricted to the UV region of the light spectrum (only 5% of available light) [206]. However, some MOFs have shown photoactivity in an extended region of the spectrum.
Material morphology	7	3	4	MOFs can provide a significantly larger surface area [121]. Furthermore, titanium dioxide is prone to aggregation which reduces its effective surface area [206].
Resistance to photo corrosion	5	3	4	MOFs have shown increased resistance to photo corrosion [206]. Titanium dioxide has mild difficulty with photo corrosion [170].
Performance score:		116	176	
Toxicity	6	5	4	Some MOFs used for this application (such as MILMIL-100(Fe)) are non-toxic [121]. Titanium dioxide is non-toxic [170].
Processing raw materials	6	3	4	The production of both materials is both complex and reasonably energy-intensive. However, due to the novelty of MOFs,

				their production costs remain prohibitively high [206].
End of life outlook	6	2	2	Methods for recycling both materials remain largely unsearched.
Environmental impact score:		60	54	
Raw material costs	17	5	2	Titanium Dioxide is a low-cost material whereas MOFs for this application are high-cost [205].
Processing costs	20	3	3	MOFs have a significantly higher processing cost [191].
Cost score:		145	94	
Overall scores:		341	304	

Note: All materials were evaluated for each factor using a scale ranging from 1 to 5 (where 1 corresponds to "very bad," 2 to "bad," 3 to "suitable," 4 to "good," and 5 to "very good").

5.3 Supercapacitors

Supercapacitors, being next-generation energy storage devices, are assessed based on the metrics of specific capacitance, energy density, power density, and cycling stability. The presence of high specific surface areas and porosity contributes to really good electrochemical performance in metal-organic framework materials such as Cu-MOF, Zr-MOF, and Ti-MOF. For example, Cu-MOF showed a specific capacitance of 104.8 F/g with an energy density of 18.2 Wh/kg, greatly outperforming all other materials because of increased ionic transport and charge storage capabilities [212]. Moreover, Ni-DMOF-ADC gave a specific capacitance of 552 F/g and over 98% retention after 16,000 cycles, indicating its excellent cycling stability. Similarly, $Ni_3(HITP)_2$ tends to be 117 F/g and 90% after 10,000 cycles. For instance, MnOx-MHCF has reached as high as 1200 F/g with 94.7% retention after 10,000 cycles in composite materials, whereas rGO/ZIF-8 has reached 336 F/g with 96% retention [213]. While these methods could enhance the capacity, the poor intrinsic conductivity of pristine MOFs remains a large problem and needs conductive additives or hybridization with conductive materials like graphene and conductive polymers. Although this composite approach has improved the conductivity and overall performance, it adds complexities in synthesis and possible trade-offs in mechanical stability [214]. Therefore, innovation in design and optimization of electrode

View Article Online
DOI: 10.1039/D4TA03877K

materials remains the key to unlocking the full potential of supercapacitors so that high power and long-life energy storage applications are fully satisfied.

However, the complex and rather pricey synthesis processes of MOFs, combined with the fact that long-term stability and durability under real conditions is still a topic of research, representt major handicaps. On the other hand, non-MOF materials are normally much more stable and less expensive but do not offer such high tunability and selectivity as MOFs do. For overall performance, MOFs score 173, while activated carbon scores 126. The supercapacitors could therefore have evaluation parameters that are weighted at 40/100 for performance, 15/100 for environmental impact, and 45/100 for cost implications. Parameters for performance include those for cyclic stability, capacitance, energy and power densities; parameters in environmental impact include the stability of the materials and their impact on the environment; those in cost implication involve the complexity of the methods of synthesis and expenses incurred. The evaluation criteria for supercapacitors are summarized in **Table 8**, while **Table 9** presents the comparison matrix between AC and MOFs as electrodes of supercapacitors.

Table 8. Supercapacitor factors and corresponding suggested weighting along with justifications.

Subject	Factor	Weighting	Justification
Performance	Cycle life	3	The electrode's lifespan is very important as it affects which applications the electrode can be used for as well as the level of performance over its lifespan [74].
	Capacitance	3	A poor capacitance can limit an SC's potential applications. A high capacitance is desirable.
	Current successful application	2	Successful laboratory results or real-world trials are good indications of the material's suitability.
	Size and weight	2	Literature suggests that for most applications, weight and size are not a key consideration, as the systems they would be used in are already

			very large and packaging space will likely not be an issue [80].
	Integrity under service conditions (e.g. thermal stability)	3	This is important as it affects the lifespan of the electrode as well as its performance (including issues with charge leakage) and overall suitability for this application [119].
	Energy and power densities	3	High energy and power densities are desirable for SCs. High power density would optimise their charging speeds and therefore make the SC an attractive option for electric vehicle charging equipment. A high energy density would increase the number of potential applications of the SC (as it would be able to hold more energy).
	Raw material renewability	3	For the technology to be "future-proof" it needs to be environmentally sustainable. A renewable raw material is desirable as it means the raw material cost is less likely to increase in the future (unlike non-renewable finite resources)
Environmental impact	Toxicity	3	A toxic material is detrimental to the environment, it can also result in higher costs for disposal at the end of the product's life.
	Recyclability	2	For the technology to be "future-proof" it needs to be sustainable.
	Production impacts (e.g. energy use)	2	Energy-intensive processing methods can be detrimental to the environment. This is an important consideration for technologies with a wide-scale deployment aim.
	Material cost	3	Manufacturers want to keep costs low even at the expense of performance. Literature suggests that price is one of the key factors for the material choice of SC electrodes [80].
Cost	Ease of production/ production cost	2	Simple, low-energy production processes are often cheaper. If the production method can be used for bulk production, it also means the cost of the product is likely going to be lower.

Table 9. Comparison matrix for AC and MOFs as SC electrodes.

View Article Online
DOI: 10.1039/D4TA03877K

Factor	Weighting	Material Score		Justification
		Activated carbon	MOFs	
Cycle life	8	3	4	MOFs have exhibited higher cyclic stabilities in both beakers and constructed SC laboratory tests [75]. ACs have shown suitable performances for this application [80].
Capacitance	9	3	5	Secondary data suggests that MOFs are able to achieve higher values for capacitance compared to ACs [106].
Current successful application	6	4	3	ACs have proven to be successful and are currently used by electrode manufacturers [80]. While MOFs have shown success in laboratory tests, there have been not extensive real-life application trials.
Size and weight	7	3	4	ACs are prone to aggregation and therefore often have to be used as a gel suspension, this often limits the reduction of the device size.
Energy and power densities	10	3	5	AC electrodes have shown limited power output due to the device's charge delivery rate [84]. Laboratory testing of MOFs has shown improved power densities [119].
Performance score:		126	173	
Raw material renewability	3	4	3	While ACs can be produced from renewable sources, the majority of commercially available ACs are produced from non-renewable precursors [79]. Many MOFs used for this application involved non-renewable materials for their synthesis [75].
Non-toxicity	4	5	3	ACs are environmentally benign [204]. The toxicity of MOFs is not well understood and there is some suggestion that some may be toxic, especially when they begin to degrade [125].
Recyclability	5	4	3	AC electrodes show great recycling potential, with research suggesting processes and promising results from laboratory tests [97]. While there is little research available on the recycling of MOF SC electrodes, there is research focused on the synthesis of MOFs using waste PET plastics [113].
Production impacts (e.g. energy use)	3	3	4	AC Production is simple and chemical activation requires relatively little energy [80]. It is important to note that bulk production of MOFs is largely unresearched and consequently an accurate assessment of this factor is difficult.
Environmental impact score:		61	48	
Material cost	35	4	2	AC is very cheap [80]. MOFs are prohibitively expensive [74].

Ease of production/ production cost	10	5	4	ACs production process is well-developed and relatively inexpensive [80]. Bulk production of MOFs requires further research as the process is often complex and expensive [74].
Cost score:		190	110	
Overall scores:		383	350	

Note: All materials were evaluated for each factor using a scale ranging from 1 to 5 (where 1 corresponds to "very bad," 2 to "bad," 3 to "suitable," 4 to "good," and 5 to "very good").

Overall, MOFs score higher than liquid amines for CCS applications despite their poor cost score (52 compared to 60 for liquid amines) and the high weighting assigned to cost factors. As the radar graph (**Fig. 10(a)**) shows, the MOFs score considerably better for environmental impact due to liquid-amines toxicity and environmental harmfulness. Notwithstanding their relatively modest stage of development, MOFs have a high-performance grade because they also have the potential to provide considerable performance improvements over liquid amines. According to the graph, MOFs' performance score gives them the greatest advantage over liquid amines. In contrast, ACs receive a slightly better rating for SC electrode applications than MOFs. However, the radar graph (**Fig. 10(b)**) shows that MOFs score considerably better for performance and their score for environmental impact is only slightly less than that of AC. It is apparent from **Fig. 10** that this evaluation suggests that the factor preventing the wide-scale use of MOF electrodes is cost. Literature suggests that the incredibly low price of AC is acting as a barrier to the entrance of any other material to the SC electrode market [80], despite the potential for improved performance. Consequently, further research into the cost-effective synthesis of MOF electrodes may be beneficial. Regarding photocatalytic application, titanium dioxide achieved the highest overall score, suggesting that, based on these factors, it provides the most benefits despite MOFs achieving a considerably higher performance score of 70 (as seen in **Fig. 10(c)**). Because of the high weighting of the cost elements, MOFs' cost score was significantly lower than titanium dioxide's, which is probably what prevents MOFs from being used in this application. In summary, the cost of MOFs can vary considerably, influenced by factors such

View Article Online
DOI: 10.1039/D4TA03877K

as the specific MOF material, the synthesis method, the production scale, and the purity of the final product. It's important to note that while some MOFs may be relatively expensive to produce, they can offer unique properties and advantages in various applications, which can justify their cost in certain contexts. As research and development in MOFs continue to advance, there may be efforts to optimize synthesis methods and reduce production costs, making MOFs more accessible for a broader range of applications.

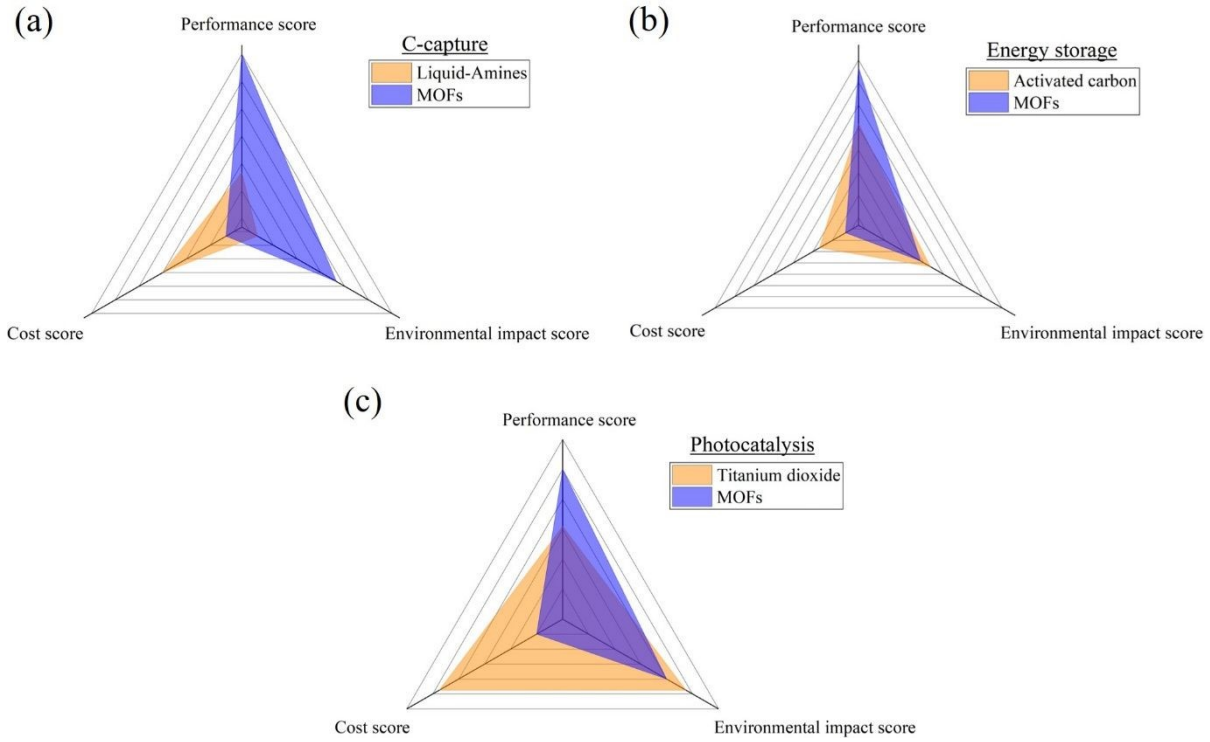

Fig. 10. Radar graph showing 3 factor comparison between MOFs and other conventional materials for; (a) C-capture, (b) Energy storage, and (c) Photocatalysis applications.

6. Limitations and future research directions

6.1 Current MOF technologies

Probably the most stressed limitation of the existing technologies behind MOFs is their poor thermal stability. The span in the thermal decomposition temperatures (Td) of MOFs is very large, which is the result of inconsistencies in the experimental conditions that include the heating rates and atmospheres. As an example, the reported Td values for MOF-5 range from

400 to 500 °C, whereas normally UiO-66 decomposes within the temperature range of 425–500°C, and HKUST-1 shows Td values between 250–300°C. These are some of the factors that influence the nature and location of functional groups, the hardness of metal ions, and coordinated solvent molecules [215]. MOFs with harder metal ions, such as lithium-based UL-MOF-1, showed the highest stability with Td values as high as about 600 °C due to an increased ionic character of the metal-oxygen bonds compared to Zn or Zr-based MOFs. For example, Mg-MOF-74 has extremely high thermal stability with a Td of ca. 400°C under nitrogen atmosphere [215].

Another large problem is their chemical stability, which is easily influenced by moisture and, therefore, significantly limits their usability for industrial processes. Many MOFs have been reported to decompose above 300 °C or under humid conditions, which thus bounds their practical applications. Their syntheses are often complicated, requiring pricey reagents; large-scale production is economically challenging. For instance, the price for the production of MOFs can be as high as $50 per gram, which is very expensive compared with conventional porous materials like activated carbon with a price of around $1 per kilogram [216]. Moreover, while some MOFs have very high methane storage capacities, for example, HKUST-1, impurities can reduce their actual performance by a large extent, significantly diminishing real application.

Another challenge is that it is somehow difficult to scale up the production of MOFs sustainably. Traditional methods of synthesis typically utilize highly toxic solvents under harsh conditions, therefore posing associated environmental and health risks, but usually at high production costs. With more than 99,075 synthetic variants, the enormous number of possible MOF structures makes it challenging and cumbersome to identify and optimize MOFs for a

View Article Online
DOI: 10.1039/D4TA03877K

given application with certain desired properties. This leads to long experimental cycles and a high R&D cost [217]. Even for very promising materials like CALF-20 and MIL-100(Fe), multi-ton scale syntheses were achieved only recently, which clearly shows the slow transformation from lab scale to industrial scale production [218]. This is further frustrated by raw material costs and synthesis processes, which themselves are costly, often using highly toxic solvents like DMF that add to the cost and energy requirement of purification methods necessary to maintain the quality of the MOF product.

6.2 Future research directions

Future research in MOF technologies has to be directed toward the enhancement of stability, precise characterization of catalytic sites, effective regeneration techniques, and controlled defect engineering. Current MOFs typically show stability up to 300 °C, but future developments must take it further beyond 500°C through the incorporation of more thermally stable inorganic components and improvement of the node-linker bonds [219]. Improvement in chemical stability to less than 10% degradation in catalytic activity over 100 hours in an aqueous environment must also be attained. Advanced spectroscopic techniques and computational modelling shall quantify active catalytic sites with an error margin of less than 5% and predict reaction rates to within 10% accuracy of the experimental values. Effective regeneration protocols restore at least 90% of the original catalytic activity upon deactivation cycles; long-term studies. This type of controlled defect synthesis thus should give a standard deviation of less than 10% in defect concentration from batch to batch, while for defect-free MOFs it has to be below 1% of total sites [219].

One major challenge lies in the naturally very low ionic conductivity of most MOFs, typically much below the level of 10^{-10} S/cm. Nearly liquid electrolyte conductivities are hard to attain with solid electrolytes because of the limited carrier mobility and lack of low-energy pathways

View Article Online
DOI: 10.1039/D4TA03877K

for ionic conduction [220]. Future efforts, therefore, need to build on these limitations and focus on strategies that involve improved density of mobile ions and uninterrupted ionic conduction pathways. Additionally, it requires the development of MOFs with stable and high ionic conductivities toward changes in both temperature and humidity. Advancement in synthesis and functionalization approaches with the design of corresponding theoretical models is highly imperative for bringing solutions to the above challenges. The inclusion of flexible frameworks and phase transition mechanisms may yield MOFs with conductivities above 10^{-2} S/cm and may thus render them applicable in the new class of the next-generation energy storage and conversion devices [220].

Critical is the reduction in the number of steps involved in the synthesis process to reduce production costs to less than $10 per gram. This can be realized by developing more efficient and up-scaled synthesis methods where applicability is maximally enhanced, such as solvent-free synthesis or the adoption of cheaper and more abundant raw materials [221]. In the future, research should also focus on green synthesis methods with non-toxic, biocompatible linking agents and eco-friendly solvents, along with techniques that apply either no use of solvents at all or solid-state synthesis. High-throughput computation screening and data mining will greatly accelerate the assessment of MOF properties to find promising candidates more efficiently [222]. Separation and recovery processes relating to vacuum filtration and continuous centrifugation, for example, need to be optimized in the scale-up of production. It may potentially also provide more sustainable and cost-effective solutions with respect to reduced energy use and improvement in scalability [223]. This could provide more sustainable and cost-effective solutions due to less energy consumption and efficient scaling of microwave-assisted and mechanochemical synthesis methods.

View Article Online
DOI: 10.1039/D4TA03877K

It is with strategies in creative structural modification and composite material preparation that finally, such MOF materials could be fabricated with enhanced stability and durability to real-world working conditions. Comprehensive techno-economic analyses and life cycle assessment (LCA) are required concerning an evaluation of the feasibility and environmental impact of large-scale production of MOFs [224]. These assessments will set targets for the development of green and sustainable economically viable MOF technologies whose industrial applications would not contradict their environmental benefits. By taking into consideration these points, there will be a chance for the synthesization of MOFs with improved thermal and chemical stability, reduced production cost, increased scalability, and finally making them practical in much more extended temperature range applications and industrial uses [225].

7. Conclusion

In conclusion, this study provides a comprehensive comparative assessment of Metal-Organic Frameworks (MOFs) and conventional materials across the domains of energy storage, environmental remediation, and photocatalysis. The results underscore the remarkable potential of MOFs as versatile and innovative materials in these critical areas, backed by empirical data. In energy storage, MOFs consistently outperform conventional activated carbons (ACs) with a performance score of 128, significantly surpassing them. Their exceptional specific surface areas, often exceeding 3,000 m^2/g, enable efficient charge adsorption, rapid charge transfer, and easy ion diffusion within their porous structures. These characteristics, along with their chemical, thermal, and mechanical stability, and the ability to be hybridized with conductive materials, position MOFs as promising contenders for advanced energy storage devices like supercapacitors. Regarding environmental concerns, MOFs excel as effective carbon capture agents, scoring 329 compared to 275 for liquid amines. Exposed surface areas and high pore volumes further increase their potential for the adsorption capacity toward pollutants. Additionally, besides the presence of functional groups that act specifically toward interactions

View Article Online
DOI: 10.1039/D4TA03877K

with the contaminants, the stability under environmental conditions and recyclability underline their effectiveness for environmental clean-up and, therefore, in the promotion of environmental sustainability. In the field of photocatalysis, MOFs exhibit substantial potential with a total score of 304. They showcase extended light harvesting capabilities into the visible and near-infrared regions due to their tunable bandgap, allowing for effective utilization of visible light. They have high surface areas that offer high active sites, while the mechanisms of charge separation do provide a platform for the prevention of recombination of electron-hole pairs, therefore enhancing the catalytic activity. Moreover, their photochemical stability and surface functionalization further enhance their applicability as efficient photocatalysts. However, it's crucial to acknowledge the cost challenges faced by MOFs, with an overall cost score of 110 for supercapacitors and 94 for photocatalysis. High production costs due to complex synthesis processes can act as barriers to widespread technology deployment in these domains. Some challenges, however, remain, such as stability issues, conductivity, and very high production costs. It is a problem of stability and poor electrical conductivity that hampers their potency in energy storage and photocatalysis. Future research should focus on the development of MOF structures with improved stability and conductivity, integration of MOFs with other materials to enhance their performance, and expansion of their applications in environmental remediation. This would have to be supplemented by enhanced environmental adaptability, low-toxicity development of variants to avoid secondary pollution and a deeper study of the pathways and kinetics of charge transfer. Computation design of more effective photocatalysts is probably going to provide the answer. Hence, these issues will be resolved through focused research and innovative solutions for MOFs to achieve their full potential. This empirical data underscores MOFs' promising future in energy storage, environmental remediation, and photocatalysis, showcasing their adaptability and high performance. As the

View Article Online
DOI: 10.1039/D4TA03877K

world seeks sustainable technologies, MOFs emerge as pivotal materials, paving the way for a more eco-conscious future.

Acknowledgement

The authors are grateful to the International Society of Engineering Science and Technology (ISEST) UK. This research is also supported by "Pioneer" and "Leading Goose" R&D Program of Zhejiang (2024C04049), China. The authors are also thankful for financial support from the Ministry of Research, Innovation and Digitalization (MCID) under Romanian National Core Program LAPLAS VII-Contract No. 30N/2023.

View Article Online
DOI: 10.1039/D4TA03877K

Reference

1 A. Maghfirah, M. M. Ilmi, A. T. N. Fajar and G. T. M. Kadja, *Mater Today Chem*, 2020, **17**, 100348.

2 A. El Guerraf, W. Zeng, A. Mantel, E. Benhsina, J. M. Chin and H. Shiozawa, *Adv Electron Mater*, 2024, 2300854.

3 M. Ding, X. Cai and H.-L. Jiang, *Chem Sci*, 2019, **10**, 10209–10230.

4 H. C. J. Zhou and S. Kitagawa, *Chem Soc Rev*, 2014, 43, 5415–5418.

5 S. Akhtar, P. Singha, A. De, K. S. Das, S. Saha, S. Bala and R. Mondal, *New Journal of Chemistry*, 2021, **45**, 6438–6449.

6 L. R. Redfern and O. K. Farha, *Chem Sci*, 2019, **10**, 10666–10679.

7 C. Yue, L. Wu, Y. Lin, Y. Lu, C. Shang, R. Ma, X. Zhang, X. Wang, W. D. Wu and X. D. Chen, *ACS Appl Mater Interfaces*, 2021, **13**, 26264–26277.

8 R. Shah, S. Ali, F. Raziq, S. Ali, P. M. Ismail, S. Shah, R. Iqbal, X. Wu, W. He and X. Zu, *Coord Chem Rev*, 2023, **477**, 214968.

9 G. Song, Y. Shi, S. Jiang and H. Pang, *Adv Funct Mater*, 2023, **33**, 2303121.

10 N. F. Suremann, B. D. McCarthy, W. Gschwind, A. Kumar, B. A. Johnson, L. Hammarström and S. Ott, *Chem Rev*, 2023, **123**, 6545–6611.

11 J. Chen and Y. Li, *The Chemical Record*, 2016, **16**, 1456–1476.

12 M. U. Shahid, T. Najam, M. H. Helal, I. Hossain, S. M. El-Bahy, Z. M. El-Bahy, A. ur Rehman, S. S. A. Shah and M. A. Nazir, *Int J Hydrogen Energy*, 2024, **62**, 1113–1138.

13 T. Wu, X. Liu, Y. Liu, M. Cheng, Z. Liu, G. Zeng, B. Shao, Q. Liang, W. Zhang, Q. He and W. Zhang, *Coord Chem Rev*, 2020, **403**, 213097.

14 N. C. Burtch, J. Heinen, T. D. Bennett, D. Dubbeldam and M. D. Allendorf, *Advanced materials*, 2018, **30**, 1704124.

15 D. Senthil Raja and D.-H. Tsai, *Chemical Communications*, 2024.

16 C. Lamiel, I. Hussain, H. Rabiee, O. R. Ogunsakin and K. Zhang, *Coord Chem Rev*, 2023, **480**, 215030.

17 L. Zhang and Y. Hou, *Adv Energy Mater*, 2023, **13**, 2204378.

18 A. Mukherjee, J. A. Okolie, A. Abdelrasoul, C. Niu and A. K. Dalai, *Journal of Environmental Sciences*, 2019, **83**, 46–63.

19 S. Ghosh, *Metal-organic frameworks (MOFs) for environmental applications*, 2019.

20 S. Horike, S. Shimomura and S. Kitagawa, *Nat Chem*, 2009, **1**, 695–704.

21 T. Ghanbari, F. Abnisa and W. M. A. Wan Daud, *Science of The Total Environment*, 2020, **707**, 135090.

22 Y. Zhao, Z. Song, X. Li, Q. Sun, N. Cheng, S. Lawes and X. Sun, *Energy Storage Mater*, 2016, **2**, 35–62.

23 Y. Li, H. Xu, S. Ouyang and J. Ye, *Physical Chemistry Chemical Physics*, 2016, **18**, 7563–7572.

24 H. Furukawa, K. E. Cordova, M. O'Keeffe and O. M. Yaghi, *Science (1979)*, , DOI:10.1126/science.1230444.

25 F. Vega, M. Cano, S. Camino, L. M. G. Fernández, E. Portillo and B. Navarrete, *Carbon Dioxide Chemistry, Capture and Oil Recovery*, , DOI:10.5772/INTECHOPEN.71443.

26 M. Bui, C. S. Adjiman, A. Bardow, E. J. Anthony, A. Boston, S. Brown, P. S. Fennell, S. Fuss, A. Galindo, L. A. Hackett, J. P. Hallett, H. J. Herzog, G. Jackson, J. Kemper, S. Krevor, G. C. Maitland, M. Matuszewski, I. S. Metcalfe, C. Petit, G. Puxty, J. Reimer, D. M. Reiner, E. S. Rubin, S. A. Scott, N. Shah, B. Smit, J. P. M. Trusler, P. Webley, J. Wilcox and N. Mac Dowell, *Energy Environ Sci*, 2018, **11**, 1062–1176.

27 J. J. Vericella, S. E. Baker, J. K. Stolaroff, E. B. Duoss, J. O. Hardin, J. Lewicki, E. Glogowski, W. C. Floyd, C. A. Valdez, W. L. Smith, J. H. Satcher, W. L. Bourcier, C. M. Spadaccini, J. A. Lewis and R. D. Aines, *Nat Commun*, 2015, **6**, 6124.

28 A. I. Osman, M. Hefny, M. I. A. Abdel Maksoud, A. M. Elgarahy and D. W. Rooney, *Environ Chem Lett*, 2021, **19**, 797–849.

29 X. Li, X. Zhou, J. Wei, Y. Fan, L. Liao and H. Wang, *Sep Purif Technol*, 2021, **265**, 118481.

30 M. Stec, A. Tatarczuk, L. Więcław-Solny, A. Krótki, T. Spietz, A. Wilk and D. Śpiewak, *Clean Technol Environ Policy*, 2016, **18**, 151–160.

31 C. A. Grande, R. Blom, A. Spjelkavik, V. Moreau and J. Payet, *Sustainable Materials and Technologies*, 2017, **14**, 11–18.

32 Z. Zhang, Z.-Z. Yao, S. Xiang and B. Chen, *Energy Environ Sci*, 2014, **7**, 2868.

33 N. Williams, R. C.-C. C. Journal and undefined 2019, *osti.govNJ Williams, R CustelceanCarbon Capture Journal, 2019•osti.gov*.

34 Energy technologies Institute, *Reducing the cost of CCS developments in capture plant technology*, 2016.

35 S. Budinis, S. Krevor, N. Mac Dowell, N. Brandon and A. Hawkes, *Energy Strategy Reviews*, 2018, **22**, 61–81.

36 A. Andersen, S. Divekar, S. Dasgupta, J. H. Cavka, Aarti, A. Nanoti, A. Spjelkavik, A. N. Goswami, M. O. Garg and R. Blom, *Energy Procedia*, 2013, **37**, 33–39.

37 B. L. Huang, Z. Ni, A. Millward, A. J. H. McGaughey, C. Uher, M. Kaviany and O. Yaghi, *Int J Heat Mass Transf*, 2007, **50**, 405–411.

38 N. Iqbal, X. Wang, J. Yu and B. Ding, *Adv Sustain Syst*, 2017, **1**, 1600028.

39 Y. Lin, C. Kong, Q. Zhang and L. Chen, *Adv Energy Mater*, 2017, **7**, 1601296.

40 H. R. Khan, Z. Jahan, M. B. Khan Niazi, T. Noor, H. Hou and S. Rafiq, *Carbon Capture Science & Technology*, 2022, **3**, 100048.

41 P. M. Bhatt, Y. Belmabkhout, A. Cadiau, K. Adil, O. Shekhah, A. Shkurenko, L. J. Barbour and M. Eddaoudi, *J Am Chem Soc*, 2016, **138**, 9301–9307.

42 L. Hu, W. Wu, L. Jiang, M. Hu, H. Zhu, L. Gong, J. Yang, D. Lin and K. Yang, *ACS Appl Mater Interfaces*, 2023, **15**, 43925–43932.

43 G. Greene-Diniz, D. Z. Manrique, W. Sennane, Y. Magnin, E. Shishenina, P. Cordier, P. Llewellyn, M. Krompiec, M. J. Rančić and D. Muñoz Ramo, *EPJ Quantum Technol*, 2022, **9**, 37.

44 T. Zurrer, K. Wong, J. Horlyck, E. C. Lovell, J. Wright, N. M. Bedford, Z. Han, K. Liang, J. Scott and R. Amal, *Adv Funct Mater*, , DOI:10.1002/adfm.202007624.

45 A. S. Palakkal and R. S. Pillai, *Sep Purif Technol*, 2022, **295**, 121298.

46 L. Lei, Y. Cheng, C. Chen, M. Kosari, Z. Jiang and C. He, *J Colloid Interface Sci*, 2022, **612**, 132–145.

47 H. An, W. Tian, X. Lu, H. Yuan, L. Yang, H. Zhang, H. Shen and H. Bai, *Chemical Engineering Journal*, 2023, **469**, 144052.

48 T.-H. Bae, M. R. Hudson, J. A. Mason, W. L. Queen, J. J. Dutton, K. Sumida, K. J. Micklash, S. S. Kaye, C. M. Brown and J. R. Long, *Energy Environ. Sci.*, 2013, **6**, 128–138.

49 D. Bahamon and L. F. Vega, *Chemical Engineering Journal*, 2016, **284**, 438–447.

50 H. Li, K. Wang, Y. Sun, C. T. Lollar, J. Li and H.-C. Zhou, *Materials Today*, 2018, **21**, 108–121.

51 Y. He, W. Zhou, G. Qian and B. Chen, *Chem. Soc. Rev.*, 2014, **43**, 5657–5678.

52 E. J. Kim, R. L. Siegelman, H. Z. H. Jiang, A. C. Forse, J.-H. Lee, J. D. Martell, P. J. Milner, J. M. Falkowski, J. B. Neaton, J. A. Reimer, S. C. Weston and J. R. Long, *Science (1979)*, 2020, **369**, 392–396.

53 T. M. McDonald, J. A. Mason, X. Kong, E. D. Bloch, D. Gygi, A. Dani, V. Crocellà, F. Giordanino, S. O. Odoh, W. S. Drisdell, B. Vlaisavljevich, A. L. Dzubak, R. Poloni, S.

K. Schnell, N. Planas, K. Lee, T. Pascal, L. F. Wan, D. Prendergast, J. B. Neaton, B. Smit, J. B. Kortright, L. Gagliardi, S. Bordiga, J. A. Reimer and J. R. Long, *Nature*, 2015, **519**, 303–308.

54 Y. Huang, W. Qin, Z. Li and Y. Li, *Dalton Transactions*, 2012, **41**, 9283.

55 T. M. McDonald, W. R. Lee, J. A. Mason, B. M. Wiers, C. S. Hong and J. R. Long, *J Am Chem Soc*, 2012, **134**, 7056–7065.

56 P.-Q. Liao, X.-W. Chen, S.-Y. Liu, X.-Y. Li, Y.-T. Xu, M. Tang, Z. Rui, H. Ji, J.-P. Zhang and X.-M. Chen, *Chem Sci*, 2016, **7**, 6528–6533.

57 D. Saha, Z. Bao, F. Jia and S. Deng, *Environ Sci Technol*, 2010, **44**, 1820–1826.

58 M. Mazaj, N. Z. Logar, E. Žagar and S. Kovačič, *J Mater Chem A Mater*, 2017, **5**, 1967–1971.

59 J. Liu, Y. Wang, A. I. Benin, P. Jakubczak, R. R. Willis and M. D. LeVan, *Langmuir*, 2010, **26**, 14301–14307.

60 G. W. Peterson, J. B. DeCoste, T. G. Glover, Y. Huang, H. Jasuja and K. S. Walton, *Microporous and Mesoporous Materials*, 2013, **179**, 48–53.

61 T. Asadi, M. R. Ehsani, A. M. Ribeiro, J. M. Loureiro and A. E. Rodrigues, *Chem Eng Technol*, 2013, **36**, 1231–1239.

62 Z. Hu, Y. Wang, B. B. Shah and D. Zhao, *Adv Sustain Syst*, , DOI:10.1002/adsu.201800080.

63 P. J. Milner, R. L. Siegelman, A. C. Forse, M. I. Gonzalez, T. Runčevski, J. D. Martell, J. A. Reimer and J. R. Long, *J Am Chem Soc*, 2017, **139**, 13541–13553.

64 V. H. Dalvi and P. J. Rossky, *Proceedings of the National Academy of Sciences*, 2010, **107**, 13603–13607.

65 A. H. Valekar, K.-H. Cho, U.-H. Lee, J. S. Lee, J. W. Yoon, Y. K. Hwang, S. G. Lee, S. J. Cho and J.-S. Chang, *RSC Adv*, 2017, **7**, 55767–55777.

66 R. Das, D. Muthukumar, R. S. Pillai and C. M. Nagaraja, *Chemistry – A European Journal*, 2020, **26**, 17445–17454.

67 J. Yan, Y. Sun, T. Ji, Y. Liu, N. Zhang, B. Sun, S. Meng, B. H. Yin, M. Wu, H. Hu and Y. Liu, *Ind Eng Chem Res*, 2023, **62**, 5973–5983.

68 M. R. Abdul Hamid, Y. Qian, R. Wei, Z. Li, Y. Pan, Z. Lai and H.-K. Jeong, *J Memb Sci*, 2021, **640**, 119802.

69 F. Yang, T. Ge, X. Zhu, J. Wu and R. Wang, *Sep Purif Technol*, 2022, **287**, 120535.

70 J. M. Park, D. K. Yoo and S. H. Jhung, *Chemical Engineering Journal*, 2020, **402**, 126254.

71 Y. Liu, Z. Ng, E. A. Khan, H.-K. Jeong, C. Ching and Z. Lai, *Microporous and Mesoporous Materials*, 2009, **118**, 296–301.

72 C. R. Groom, I. J. Bruno, M. P. Lightfoot and S. C. Ward, *Acta Crystallogr B Struct Sci Cryst Eng Mater*, 2016, **72**, 171–179.

73 S. Huang, X.-R. Shi, C. Sun, Z. Duan, P. Ma and S. Xu, *Nanomaterials*, 2020, **10**, 2268.

74 S. Sundriyal, H. Kaur, S. K. Bhardwaj, S. Mishra, K.-H. Kim and A. Deep, *Coord Chem Rev*, 2018, **369**, 15–38.

75 P. Forouzandeh, V. Kumaravel and S. C. Pillai, *Catalysts*, 2020, **10**, 969.

76 A. C. Forse, C. Merlet, J. M. Griffin and C. P. Grey, *J Am Chem Soc*, 2016, **138**, 5731–5744.

77 Y. Wu and C. Cao, *Sci China Mater*, 2018, **61**, 1517–1526.

78 S. Kumar, G. Saeed, L. Zhu, K. N. Hui, N. H. Kim and J. H. Lee, *Chemical Engineering Journal*, 2021, **403**, 126352.

79 J. Phiri, J. Dou, T. Vuorinen, P. A. C. Gane and T. C. Maloney, *ACS Omega*, 2019, **4**, 18108–18117.

80 L. Weinstein and R. Dash, *Materials Today*, 2013, **16**, 356–357.

81 P. Pongprayoon and A. Chaimanatsakun, *Acta Mechanica Solida Sinica*, 2019, **32**, 81–92.

82 A. Gitipour, A. El Badawy, M. Arambewela, B. Miller, K. Scheckel, M. Elk, H. Ryu, V. Gomez-Alvarez, J. Santo Domingo, S. Thiel and T. Tolaymat, *Environ Sci Technol*, 2013, **47**, 14385–14393.

83 L. Li, X. Wang, S. Wang, Z. Cao, Z. Wu, H. Wang, Y. Gao and J. Liu, *Electroanalysis*, 2016, **28**, 243–248.

84 M. Cossutta, V. Vretenar, T. A. Centeno, P. Kotrusz, J. McKechnie and S. J. Pickering, *J Clean Prod*, 2020, **242**, 118468.

85 K. M. Ajay and M. N. Dinesh, *IOP Conf Ser Mater Sci Eng*, 2018, **310**, 012083.

86 M. Karnan, A. G. K. Raj, K. Subramani, S. Santhoshkumar and M. Sathish, *Sustain Energy Fuels*, 2020, **4**, 3029–3041.

87 S. Breitenbach, A. Lumetzberger, M. A. Hobisch, C. Unterweger, S. Spirk, D. Stifter, C. Fürst and A. W. Hassel, *C — Journal of Carbon Research*, 2020, **6**, 17.

88 A. Arenillas, J. A. Menéndez, G. Reichenauer, A. Celzard, V. Fierro, F. J. Maldonado Hodar, E. Bailón-Garcia and N. Job, 2019, pp. 1–26.

89 Z. S. Iro, C. Subramani and S. S. Dash, *Int J Electrochem Sci*, 2016, **11**, 10628–10643.

90 I. I. G. Inal, S. M. Holmes, E. Yagmur, N. Ermumcu, A. Banford and Z. Aktas, *Journal of industrial and engineering chemistry*, 2018, **61**, 124–132.

91 J. Chen, J. Xie, C. Q. Jia, C. Song, J. Hu and H. Li, *Chemical Engineering Journal*, 2022, **450**, 137938.

92 X. Li, Y. Tang, J. Song, W. Yang, M. Wang, C. Zhu, W. Zhao, J. Zheng and Y. Lin, *Carbon N Y*, 2018, **129**, 236–244.

93 F. Ma, S. Ding, H. Ren and Y. Liu, *RSC Adv*, 2019, **9**, 2474–2483.

94 R. Mehdi, S. R. Naqvi, A. H. Khoja and R. Hussain, *Fuel*, 2023, **348**, 128529.

95 S. Bhat, U. T. Uthappa, T. Sadhasivam, T. Altalhi, S. Soo Han and M. D. Kurkuri, *Chemical Engineering Journal*, 2023, **459**, 141577.

96 Y.-P. Gao, Z.-B. Zhai, K.-J. Huang and Y.-Y. Zhang, *New Journal of Chemistry*, 2017, **41**, 11456–11470.

97 G. Jiang and S. J. Pickering, *Waste Management*, 2016, **48**, 465–470.

98 Q. Ke and J. Wang, *Journal of Materiomics*, 2016, **2**, 37–54.

99 V. Ntuli, I. H.-S. A. J. of Science and undefined 2013, *journals.co.zaV Ntuli, I HapazariSouth African Journal of Science, 2013•journals.co.za*, , DOI:10.1590/sajs.2013/1077.

100 E. Glogic, A. K. Kamali, N. M. Keppetipola, B. Alonge, G. R. A. Kumara, G. Sonnemann, T. Toupance and L. Cojocaru, *ACS Sustain Chem Eng*, 2022, **10**, 15025–15034.

101 Z. Jiang, Y. Zou, Y. Li, F. Kong and D. Yang, *Biochar*, 2021, **3**, 701–714.

102 V. Ruiz, C. Blanco, M. Granda and R. Santamaría, *Electrochim Acta*, 2008, **54**, 305–310.

103 C. Li, W. Wu, P. Wang, W. Zhou, J. Wang, Y. Chen, L. Fu, Y. Zhu, Y. Wu and W. Huang, *Advanced Science*, 2019, **6**, 1801665.

104 D. Dong and Y. Xiao, *Chemical Engineering Journal*, 2023, 144441.

105 L. M. Grishchenko, G. G. Tsapyuk, M. Ricco, V. E. Diyuk, O. Yu. Boldyrieva, R. Mariychuk, I. P. Matushko, D. Pontiroli, V. V. Lisnyak and S. Scaravonati, in *2020 IEEE 40th International Conference on Electronics and Nanotechnology (ELNANO)*, IEEE, 2020, pp. 173–177.

106 F. Cheng, X. Yang, S. Zhang and W. Lu, *J Power Sources*, 2020, **450**, 227678.

107 L.-H. Tseng, W.-C. Li and T.-C. Wen, *J Taiwan Inst Chem Eng*, 2023, **143**, 104684.

108 G. Dhakal, D. R. Kumar, S. Sahoo and J.-J. Shim, *Carbon N Y*, 2023, **208**, 277–289.

109 I. Bordun, V. Pohrebennyk, M. Sadowa, V. Ptashnyk, A. Klos-Witkowska and V. Martsenyuk, in *2017 9th IEEE International Conference on Intelligent Data Acquisition and Advanced Computing Systems: Technology and Applications (IDAACS)*, IEEE, 2017, pp. 86–90.

110 F. R. Maria Sundar Raj, N. V. Jaya, G. Boopathi, D. Kalpana and A. Pandurangan, *Mater Chem Phys*, 2020, **240**, 122151.

111 I. I. G. Inal, Y. Gokce and Z. Aktas, in *2016 IEEE International Conference on Renewable Energy Research and Applications (ICRERA)*, IEEE, 2016, pp. 458–462.

112 M. A. Yahya, Z. Al-Qodah and C. W. Z. Ngah, *Renewable and Sustainable Energy Reviews*, 2015, **46**, 218–235.

113 A. M. Al-Enizi, M. Ubaidullah, J. Ahmed, T. Ahamad, T. Ahmad, S. F. Shaikh and Mu. Naushad, *Compos B Eng*, 2020, **183**, 107655.

114 M. K. Sahoo, P. Mane, B. Chakraborty and J. N. Behera, *Inorg Chem*, 2024, **63**, 6383–6395.

115 B. Ramasubramanian, C. Chinglenthoiba, X. Huiqing, N. Xiping, H. K. Hui, S. Valiyaveettil, S. Ramakrishna and V. Chellappan, *Surfaces and Interfaces*, 2022, **34**, 102397.

116 S. Xiong, S. Jiang, J. Wang, H. Lin, M. Lin, S. Weng, S. Liu, Y. Jiao, Y. Xu and J. Chen, *Electrochim Acta*, 2020, **340**, 135956.

117 M. Shaheen, M. Z. Iqbal, M. W. Khan, S. Siddique, S. Aftab and S. M. Wabaidur, *Energy & Fuels*, 2023, **37**, 4000–4009.

118 F. Yi, R. Zhang, H. Wang, L. Chen, L. Han, H. Jiang and Q. Xu, *Small Methods*, , DOI:10.1002/smtd.201700187.

119 M. Gu, M. Wu, S.-C. Wang, C. Chen, D. Xiong and F.-Y. Yi, *Electrochim Acta*, 2020, **343**, 135617.

120 N. Campagnol, R. Romero-Vara, W. Deleu, L. Stappers, K. Binnemans, D. E. De Vos and J. Fransaer, *ChemElectroChem*, 2014, **1**, 1182–1188.

121 L. Wang, Y. Han, X. Feng, J. Zhou, P. Qi and B. Wang, *Coord Chem Rev*, 2016, **307**, 361–381.

122 R. Ramachandran, W. Xuan, C. Zhao, X. Leng, D. Sun, D. Luo and F. Wang, *RSC Adv*, 2018, **8**, 3462–3469.

123 D. Y. Lee, S. J. Yoon, N. K. Shrestha, S.-H. Lee, H. Ahn and S.-H. Han, *Microporous and Mesoporous Materials*, 2012, **153**, 163–165.

124 Y. Tan, W. Zhang, Y. Gao, J. Wu and B. Tang, *RSC Adv*, 2015, **5**, 17601–17605.

125 P. Kumar, B. Anand, Y. F. Tsang, K.-H. Kim, S. Khullar and B. Wang, *Environ Res*, 2019, **176**, 108488.

126 Y. Yan, P. Gu, S. Zheng, M. Zheng, H. Pang and H. Xue, *J Mater Chem A Mater*, 2016, **4**, 19078–19085.

127 J. Yang, P. Xiong, C. Zheng, H. Qiu and M. Wei, *J. Mater. Chem. A*, 2014, **2**, 16640–16644.

128 M. S. Rahmanifar, H. Hesari, A. Noori, M. Y. Masoomi, A. Morsali and M. F. Mousavi, *Electrochim Acta*, 2018, **275**, 76–86.

129 G. Li, H. Cai, X. Li, J. Zhang, D. Zhang, Y. Yang and J. Xiong, *ACS Appl Mater Interfaces*, 2019, **11**, 37675–37684.

130 Q. Yang, R. Song, Y. Wang, X. Hu, Z. Chen, Z. Li and W. Tan, *Colloids Surf A Physicochem Eng Asp*, 2021, **631**, 127665.

131 R. Sahoo, S. Ghosh, S. Chand, S. Chand Pal, T. Kuila and M. C. Das, *Compos B Eng*, 2022, **245**, 110174.

132 Y.-L. Chang, M.-D. Tsai, C.-H. Shen, C.-W. Huang, Y.-C. Wang and C.-W. Kung, *Materials Today Sustainability*, 2023, **23**, 100449.

133 S. C. Wechsler and F. Z. Amir, *ChemSusChem*, 2020, **13**, 1491–1495.

134 H. S. Kim, M. S. Kang and W. C. Yoo, *J Mater Chem A Mater*, 2019, **7**, 5561–5574.

135 K. M. Choi, H. M. Jeong, J. H. Park, Y.-B. Zhang, J. K. Kang and O. M. Yaghi, *ACS Nano*, 2014, **8**, 7451–7457.

136 D. Sheberla, L. Sun, M. A. Blood-Forsythe, S. Er, C. R. Wade, C. K. Brozek, A. Aspuru-Guzik and M. Dincă, *J Am Chem Soc*, 2014, **136**, 8859–8862.

137 M. G. Campbell, D. Sheberla, S. F. Liu, T. M. Swager and M. Dincă, *Angewandte Chemie International Edition*, 2015, **54**, 4349–4352.

138 D. Feng, W. Sun and W. Hu, *Optical Switching and Networking*, 2018, **29**, 1–14.

139 M. Sajid, *Environmental Science and Pollution Research*, 2016, **23**, 14805–14807.

140 K. M. Choi, H. M. Jeong, J. H. Park, Y.-B. Zhang, J. K. Kang and O. M. Yaghi, *ACS Nano*, 2014, **8**, 7451–7457.

141 T. N. Tu, M. V Nguyen, H. L. Nguyen, B. Yuliarto, K. E. Cordova and S. Demir, *Coord Chem Rev*, 2018, **364**, 33–50.

142 H. Luo, F. Cheng, L. Huelsenbeck and N. Smith, *J Environ Chem Eng*, 2021, **9**, 105159.

143 M. Mon, R. Bruno, J. Ferrando-Soria, D. Armentano and E. Pardo, *J Mater Chem A Mater*, 2018, **6**, 4912–4947.

144 Y. Zhao, J. Peng, K. Chen, L. Luo, H. Chen, H. Zhang, S. Chou, X. Feng, W. Chen and R. Cao, *Sci China Chem*, 2023, **66**, 3154–3160.

145 Y. Fang, Y. Zeng, Q. Jin, X. F. Lu, D. Luan, X. Zhang and X. W. Lou, *Angewandte Chemie International Edition*, 2021, **60**, 8515–8520.

146 J. Du, J. Chai, Q. Li, W. Zhang and B. Tang, *Colloids Surf A Physicochem Eng Asp*, 2022, **632**, 127810.

147 J.-G. Zhao, H.-Y. Zhou, Z. Hu, Y.-W. Wu, H. Jia and X.-M. Liu, *Rare Metals*, 2022, **41**, 1504–1511.

148 Y. Fang, D. Luan, Y. Chen, S. Gao and X. W. Lou, *Angewandte Chemie International Edition*, 2020, **59**, 2644–2648.

149 S. Bibi, S. S. A. Shah, M. A. Nazir, M. H. Helal, S. M. El-Bahy, Z. M. El-Bahy, S. Ullah, M. A. Wattoo and A. ur Rehman, *Adv Sustain Syst*, 2024, 2400011.

150 X.-Y. Dao, J.-H. Guo, Y.-P. Wei, F. Guo, Y. Liu and W.-Y. Sun, *Inorg Chem*, 2019, **58**, 8517–8524.

151 Y. Wang, Y. Pan, L. Zhu, H. Yu, B. Duan, R. Wang, Z. Zhang and S. Qiu, *Carbon N Y*, 2019, **146**, 671–679.

152 K.-S. Lin, A. K. Adhikari, C.-N. Ku, C.-L. Chiang and H. Kuo, *Int J Hydrogen Energy*, 2012, **37**, 13865–13871.

153 M. Y. Zorainy, M. G. Alalm, S. Kaliaguine and D. C. Boffito, *J Mater Chem A Mater*, 2021, **9**, 22159–22217.

154 Q. Zhao, W. Yuan, J. Liang and J. Li, *Int J Hydrogen Energy*, 2013, **38**, 13104–13109.

155 Z. Yin, Y.-L. Zhou, M.-H. Zeng and M. Kurmoo, *Dalton Transactions*, 2015, **44**, 5258–5275.

156 T.-H. Chen, I. Popov, W. Kaveevivitchai and O. Š. Miljanić, *Chemistry of Materials*, 2014, **26**, 4322–4325.

157 K.-S. Lin, A. K. Adhikari, C.-N. Ku, C.-L. Chiang and H. Kuo, *Int J Hydrogen Energy*, 2012, **37**, 13865–13871.

158 Z. Mai and D. Liu, *Cryst Growth Des*, 2019, **19**, 7439–7462.

159 M. A. Mohamud and A. B. Yurtcan, *Int J Hydrogen Energy*, 2021, **46**, 33782–33800.

160 S. Bibi, S. S. A. Shah, M. A. Nazir, M. H. Helal, S. M. El-Bahy, Z. M. El-Bahy, S. Ullah, M. A. Wattoo and A. ur Rehman, *Adv Sustain Syst*, 2024, 2400011.

161 Z. Hu, Y. Peng, Z. Kang, Y. Qian and D. Zhao, *Inorg Chem*, 2015, **54**, 4862–4868.

162 E. M. C. Morales, M. A. Méndez-Rojas, L. M. Torres-Martínez, L. F. Garay-Rodríguez, I. López, I. E. Uflyand and B. I. Kharisov, *Polyhedron*, 2021, **210**, 115517.

2339 163 S. Bibi, S. S. A. Shah, M. A. Nazir, M. H. Helal, S. M. El-Bahy, Z. M. El-Bahy, S. Ullah,
2340 M. A. Wattoo and A. ur Rehman, *Adv Sustain Syst*, 2024, 2400011.
2341 164 A. Al Obeidli, H. Ben Salah, M. Al Murisi and R. Sabouni, *Int J Hydrogen Energy*, 2022,
2342 **47**, 2561–2593.
2343 165 M. Safaei, M. M. Foroughi, N. Ebrahimpoor, S. Jahani, A. Omidi and M. Khatami, *TrAC*
2344 *Trends in Analytical Chemistry*, 2019, **118**, 401–425.
2345 166 A. FUJISHIMA and K. HONDA, *Nature*, 1972, **238**, 37–38.
2346 167 A. B. Djurišić, Y. He and A. M. C. Ng, *APL Mater*, , DOI:10.1063/1.5140497.
2347 168 S. R. Shanmugham, G. B. Jegadeesan and V. Ponnusami, in *Nanotechnology in the*
2348 *Beverage Industry*, Elsevier, 2020, pp. 25–49.
2349 169 A. Dhakshinamoorthy, Z. Li and H. Garcia, *Chem Soc Rev*, 2018, **47**, 8134–8172.
2350 170 M. Pawar, S. Topcu Sendoğdular and P. Gouma, *J Nanomater*, 2018, **2018**, 1–13.
2351 171 S. Peiris, H. B. de Silva, K. N. Ranasinghe, S. V. Bandara and I. R. Perera, *Journal of*
2352 *the Chinese Chemical Society*, 2021, **68**, 738–769.
2353 172 S.-N. Zhao, G. Wang, D. Poelman and P. Van Der Voort, *Molecules*, 2018, **23**, 2947.
2354 173 J. Moma and J. Baloyi, *Photocatalysts-Applications and Attributes*.
2355 174 S. Higashimoto, *Catalysts*, 2019, **9**, 201.
2356 175 Z. Li, S. Wang, J. Wu and W. Zhou, *Renewable and Sustainable Energy Reviews*, 2022,
2357 **156**, 111980.
2358 176 F. Li, G. Liu, F. Liu, J. Wu and S. Yang, *J Hazard Mater*, 2023, **452**, 131237.
2359 177 Y. Jin, W. Tang, J. Wang, F. Ren, Z. Chen, Z. Sun and P.-G. Ren, *J Alloys Compd*, 2023,
2360 **932**, 167627.
2361 178 A. Meng, L. Zhang, B. Cheng and J. Yu, *Advanced Materials*, ,
2362 DOI:10.1002/adma.201807660.
2363 179 S.-Y. Lee and S.-J. Park, *Journal of Industrial and Engineering Chemistry*, 2013, **19**,
2364 1761–1769.
2365 180 S. Higashimoto, *Catalysts*, 2019, **9**, 201.
2366 181 X. Chen, S. Shen, L. Guo and S. S. Mao, *Chem Rev*, 2010, **110**, 6503–6570.
2367 182 M. Skocaj, M. Filipic, J. Petkovic and S. Novak, *Radiol Oncol*, , DOI:10.2478/v10019-
2368 011-0037-0.
2369 183 F. Wu, Z. Zhou and A. L. Hicks, *Environ Sci Technol*, 2019, **53**, 4078–4087.
2370 184 A.-I. Gopalan, J.-C. Lee, G. Saianand, K.-P. Lee, W.-Y. Chun, Y. Hou, V. Kannan, S.-
2371 S. Park and W.-J. Kim, *Materials*, 2020, **13**, 5072.

185 T. Sansenya, N. Masri, T. Chankhanittha, T. Senasu, J. Piriyanon, S. Mukdasai and S. Nanan, *Journal of Physics and Chemistry of Solids*, 2022, **160**, 110353.

186 T. Chankhanittha, N. Komchoo, T. Senasu, J. Piriyanon, S. Youngme, K. Hemavibool and S. Nanan, *Colloids Surf A Physicochem Eng Asp*, 2021, **626**, 127034.

187 D. Kim and K. Yong, *Appl Catal B*, 2021, **282**, 119538.

188 Z. Li, R. Li, H. Jing, J. Xiao, H. Xie, F. Hong, N. Ta, X. Zhang, J. Zhu and C. Li, *Nat Catal*, 2023, **6**, 80–88.

189 N. A. F. Al-Rawashdeh, O. Allabadi and M. T. Aljarrah, *ACS Omega*, 2020, **5**, 28046–28055.

190 K. Chaudhary, M. Aadil, S. Zulfiqar, S. Ullah, S. Haider, P. O. Agboola, M. F. Warsi and I. Shakir, *Fullerenes, Nanotubes and Carbon Nanostructures*, 2021, **29**, 915–928.

191 A. Alshammari, Z. Jiang and K. E. Cordova, in *Semiconductor Photocatalysis - Materials, Mechanisms and Applications*, InTech, 2016.

192 V. García-Salcido, P. Mercado-Oliva, J. L. Guzmán-Mar, B. I. Kharisov and L. Hinojosa-Reyes, *J Solid State Chem*, 2022, **307**, 122801.

193 Y. Gao, X.-H. Yi, C.-C. Wang, F. Wang and P. Wang, *Mater Res Bull*, 2023, **158**, 112072.

194 C. Jing, Y. Zhang, J. Zheng, S. Ge, J. Lin, D. Pan, N. Naik and Z. Guo, *Particuology*, 2022, **69**, 111–122.

195 H. Sepehrmansourie, H. Alamgholiloo, N. Noroozi Pesyan and M. A. Zolfigol, *Appl Catal B*, 2023, **321**, 122082.

196 L. Wang, P. Jin, S. Duan, H. She, J. Huang and Q. Wang, *Sci Bull (Beijing)*, 2019, **64**, 926–933.

197 M. Xu, C. Sun, X. Zhao, H. Jiang, H. Wang and P. Huo, *Appl Surf Sci*, 2022, **576**, 151792.

198 F. Drache, V. Bon, I. Senkovska, C. Marschelke, A. Synytska and S. Kaskel, *Inorg Chem*, 2016, **55**, 7206–7213.

199 A. J. Howarth, Y. Liu, P. Li, Z. Li, T. C. Wang, J. T. Hupp and O. K. Farha, *Nat Rev Mater*, 2016, **1**, 15018.

200 G. Paille, M. Gomez-Mingot, C. Roch-Marchal, B. Lassalle-Kaiser, P. Mialane, M. Fontecave, C. Mellot-Draznieks and A. Dolbecq, *J Am Chem Soc*, 2018, **140**, 3613–3618.

201 S. S. A. Shah, M. A. Nazir, K. Khan, I. Hussain, M. Tayyab, S. S. Alarfaji, A. M. Hassan, M. Sohail, M. S. Javed and T. Najam, *J Energy Storage*, 2024, **75**, 109725.

202 D. Crawford, J. Casaban, R. Haydon, N. Giri, T. McNally and S. L. James, *Chem Sci*, 2015, **6**, 1645–1649.

203 J. C. Glier and E. S. Rubin, *Energy Procedia*, 2013, **37**, 65–72.

204 M. Karnan, A. G. K. Raj, K. Subramani, S. Santhoshkumar and M. Sathish, *Sustain Energy Fuels*, 2020, **4**, 3029–3041.

205 J. Moma and J. Baloyi, in *Photocatalysts - Applications and Attributes*, IntechOpen, 2019.

206 S.-N. Zhao, G. Wang, D. Poelman and P. Van Der Voort, *Molecules*, 2018, **23**, 2947.

207 R. Asahi, T. Morikawa, T. Ohwaki, K. Aoki and Y. Taga, *Science (1979)*, 2001, **293**, 269–271.

208 H. Demir, G. O. Aksu, H. C. Gulbalkan and S. Keskin, *Carbon Capture Science and Technology*, , DOI:10.1016/j.ccst.2021.100026.

209 S. Ali, P. M. Ismail, F. Wahid, A. Kumar, M. Haneef, F. Raziq, S. Ali, M. Javed, R. U. Khan and X. Wu, *Fuel Processing Technology*, 2022, **236**, 107427.

210 S. Ali, P. M. Ismail, M. Humayun, M. Bououdina and L. Qiao, *Fuel Processing Technology*, 2024, **255**, 108049.

211 M. Khan, Z. Akmal, M. Tayyab, S. Mansoor, A. Zeb, Z. Ye, J. Zhang, S. Wu and L. Wang, *Carbon Capture Science and Technology*, , DOI:10.1016/j.ccst.2024.100191.

212 P. Dubey, V. Shrivastav, P. H. Maheshwari, M. Hołdyński, A. Krawczyńska and S. Sundriyal, *J Energy Storage*, , DOI:10.1016/j.est.2023.107828.

213 Y. Cao, W. Yang, M. Wang, N. Wu, L. Zhang, Q. Guan and H. Guo, *Int J Hydrogen Energy*, 2021, **46**, 18179–18206.

214 J. Khan, A. Khan, B. Rubab, F. Jamshaid, A. A. Al-Kahtani and A. Dahshan, *Appl Mater Today*, 2023, **34**, 101906.

215 C. Healy, K. M. Patil, B. H. Wilson, L. Hermanspahn, N. C. Harvey-Reid, B. I. Howard, C. Kleinjan, J. Kolien, F. Payet and S. G. Telfer, *Coord Chem Rev*, 2020, **419**, 213388.

216 S. Bhattacharyya and T. K. Maji, *Coord Chem Rev*, 2022, **469**, 214645.

217 Q. He, F. Zhan, H. Wang, W. Xu, H. Wang and L. Chen, *Materials Today Sustainability*, 2022, **17**, 100104.

218 D. Chakraborty, A. Yurdusen, G. Mouchaham, F. Nouar and C. Serre, *Adv Funct Mater*, 2023, 2309089.

219 D. Yang and B. C. Gates, *ACS Catal*, 2019, **9**, 1779–1798.

220 W. Xue, C. D. Sewell, Q. Zhou and Z. Lin, *Angewandte Chemie International Edition*, 2022, **61**, e202206512.

221 R. Freund, O. Zaremba, G. Arnauts, R. Ameloot, G. Skorupskii, M. Dincă, A. Bavykina, J. Gascon, A. Ejsmont and J. Goscianska, *Angewandte Chemie International Edition*, 2021, **60**, 23975–24001.

222 A. Bavykina, N. Kolobov, I. S. Khan, J. A. Bau, A. Ramirez and J. Gascon, *Chem Rev*, 2020, **120**, 8468–8535.

223 P. Falcaro, R. Ricco, C. M. Doherty, K. Liang, A. J. Hill and M. J. Styles, *Chem Soc Rev*, 2014, **43**, 5513–5560.

224 E.-S. M. El-Sayed and D. Yuan, *Green Chemistry*, 2020, **22**, 4082–4104.

225 X. Song, Y. Wang, C. Wang, D. Wang, G. Zhuang, K. O. Kirlikovali, P. Li and O. K. Farha, *J Am Chem Soc*, 2022, **144**, 10663–10687.

View Article Online
DOI: 10.1039/D4TA03877K

Data availability statement

The data that support the findings of this study are available from the corresponding author, upon reasonable request.